CISTER

PhD Thesis

Aerial Multi-hop Sensor Networks

Luis Ramos Pinto

CISTER-TR-181003

Aerial Multi-hop Sensor Networks

Luis Ramos Pinto

*CISTER Research Centre

Polytechnic Institute of Porto (ISEP-IPP)

Rua Dr. António Bernardino de Almeida, 431

4200-072 Porto

Portugal

Tel.: +351.22.8340509, Fax: +351.22.8321159

E-mail:

http://www.cister.isep.ipp.pt

Abstract

Unmanned Aerial Vehicles (UAVs) recently enabled a myriad of new applications spanningdomains from personal entertainment and industrial inspection, to criminal surveillanceand forest monitoring. A combination of sensor collection, wireless communicationand path planning between multiple distributed agents is the natural way tosupport applications. Several small UAVs working collaboratively can rapidly provideextended reach, at low cost, and efficiently stream sensor information to operators ona ground station. A significant amount of previous work has addressed each of thesetopics independently, but in this dissertation we propose a holistic approach for joint coordinationof networking and topology (placement of mobile nodes). Our thesis is thatthis approach improves user-interactive control of UAVs for live-streaming applicationsin terms of throughput, delay and reliability.In order to defend these claims, this dissertation begins by experimentally evaluatingand modeling the wireless link between two UAVs, under different conditions. Dueto limited link range, and the need for wide-area operation, the model is extended toencompass a multi-hop topology. We show that the performance of such networks usingCOTS devices is typically poor, and solutions must rely on coordination of networkprotocol and topology, simultaneously.At the network layer, we introduce a novel Time-division Multiple Access (TDMA)scheme called Distributed Variable Slot Protocol that relies on adaptive slot-length. Weprove its convergence as well as its meliorated performance experimentally validated,namely 50% higher packet delivery. In terms of network topology, we show that withoutnode placement control overall performance of the network is severely penalized, dueto natural link asymmetries. We propose a novel protocol, named Dynamic Relay Placement, that is able to do both online link quality model-estimation and in a distributedfashion decide the best location for each network node, increasing throughput by 300%.Finally, we demonstrate the end-to-end system in a multi-vehicle monitoring mission.We show that coordination of multiple UAVs increases the sensor sampling rateup to 7 times in wide areas when compared to a naive approach. This work considersenvironmental constraints such as wind, as well as the intrinsic limitations of the vehiclessuch as maximum acceleration.

U.PORTO

FEUP FACULDADE DE ENGENHARIA
UNIVERSIDADE DO PORTO

Aerial Multi-hop Sensor Networks

Luis Ramos Pinto

Programa Doutoral em Engenharia Electrotécnica e de Computadores

Co-advisor: Prof. Doutor Luís Miguel Pinho de Almeida

Co-advisor: Prof. Doutor Anthony Rowe

May, 2018

Aerial Multi-hop Sensor Networks

Luis Ramos Pinto

Programa Doutoral em Engenharia Electrotécnica e de Computadores

Dissertation submitted in partial fulfilment of the requirements for the

degree of Doctor of Philosophy in Electrical and Computer Engineering at the Faculty of Engineering, University of Porto

Approved by:

Co-advisor: Prof. Anthony Rowe, PhD

Referee: Prof. Pedro Ferreira do Souto, PhD

Referee: Prof. Mário Jorge Rodrigues de Sousa, PhD

Referee: Prof. Bruno Sinopoli, PhD

Referee: Prof. Patrick Tague, PhD

April 10, 2018

To my family,

Mafalda

and my daughters

À minha família,

à Mafalda

e às minhas filhas

Acknowledgements

Abstract

Unmanned Aerial Vehicles (UAVs) recently enabled a myriad of new applications spanning domains from personal entertainment and industrial inspection, to criminal surveillance and forest monitoring. A combination of sensor collection, wireless communication and path planning between multiple distributed agents is the natural way to support applications. Several small UAVs working collaboratively can rapidly provide extended reach, at low cost, and efficiently stream sensor information to operators on a ground station. A significant amount of previous work has addressed each of these topics independently, but in this dissertation we propose a holistic approach for joint coordination of networking and topology (placement of mobile nodes). Our thesis is that this approach improves user-interactive control of UAVs for live-streaming applications in terms of throughput, delay and reliability.

In order to defend these claims, this dissertation begins by experimentally evaluating and modeling the wireless link between two UAVs, under different conditions. Due to limited link range, and the need for wide-area operation, the model is extended to encompass a multi-hop topology. We show that the performance of such networks using COTS devices is typically poor, and solutions must rely on coordination of network protocol and topology, simultaneously.

At the network layer, we introduce a novel Time-division Multiple Access (TDMA) scheme called Distributed Variable Slot Protocol that relies on adaptive slot-length. We prove its convergence as well as its meliorated performance experimentally validated, namely 50% higher packet delivery. In terms of network topology, we show that without node placement control overall performance of the network is severely penalized, due to natural link asymmetries. We propose a novel protocol, named Dynamic Relay Place-

ment, that is able to do both online link quality model-estimation and in a distributed fashion decide the best location for each network node, increasing throughput by 300%.

Finally, we demonstrate the end-to-end system in a multi-vehicle monitoring mission. We show that coordination of multiple UAVs increases the sensor sampling rate up to 7 times in wide areas when compared to a naive approach. This work considers environmental constraints such as wind, as well as the intrinsic limitations of the vehicles such as maximum acceleration.

Keywords: 802.11, ad hoc networks, channel models, monitoring, relay placement, relay networks, time division multiple access, unmanned aerial vehicle, wireless communication.

Resumo

Avanços recentes em veículos aéreos não tripulados (UAVs) têm vindo a permitir uma miríade de novas aplicações, espalhando-se por domínios do entretenimento pessoal à inspeção industrial, da vigilância criminal à monitorização florestal. Uma combinação de sensores, comunicação sem fios e planeamento de rotas entre múltiplos agentes distribuídos é a forma natural de realizar tais aplicações. Vários UAVs trabalhando colaborativamente podem rapidamente fornecer maior alcance, a baixo custo, e eficientemente transmitir ao vivo informação sensorial para operadores numa estação base, no solo. Uma parte significativa do estado-de-arte relacionado visa cada um destes tópicos independentemente, por isso nós nesta dissertação propomos uma abordagem holística para uma coordenação conjunta do protocolo da rede e da topologia (colocação de nós). A nossa tese é que esta abordagem melhora a interactividade do utilizador no controlo de UAVs em aplicações de transmissão ao vivo em termos de velocidade, latência e confiabilidade.

De forma a defender esta tese, esta dissertação começa por experimentalmente avaliar e modelar o canal sem fio entre dois UAVs, sob diferentes condições. Devido ao limitado alcance da ligação, e à necessidade de operação a larga escala, o modelo é completado considerando para isso topologias multi-salto. Mostramos que o desempenho destas redes usando dispositivos COTS é tipicamente pobre, e que pode ser melhorado com uma coordenação simultânea da rede e da topologia.

A nível da rede, propomos um novo sistema de melhoria da comunicação baseado em TDMA (Acesso Múltiplo por Divisão de Tempo). Este novo protocolo chamado Distributed Variable Slots Protocol funciona com base na adaptação do tamanho das *slots* atribuídas a cada transmissor. A sua convergência é provada, assim como validada experimentalmente no desempenho melhorado do sistema, nomeadamente 50% mais

entrega de pacotes. A nível da topologia, mostramos que sem controlo de posiciona-
mento de nós o desempenho da rede é severamente penalizado devido a assimetrias
naturais dos links. Propomos um novo protocolo, chamado Dynamic Relay Placement
que é capaz de estimar a qualidade das ligações em tempo-real assim como de forma
distribuída decidir a melhor localização para cada um dos nós da rede, aumentando as
taxas de transferência em 300%.

Para finalizar, desenhamos uma missão de monitorização multi-veículo. Mostramos
que com uma cordenação adequada de vários veiculos aumenta em 7 vezes a taxa de
sensorização de áreas extensas quando comparada com uma abordagem mais simples.
Este trabalho considera restrições ambientais tais como o vento, assim como as limi-
tações intrínsecas dos veículos tais como aceleração máxima.

Palavras-chave: 802.11, ad hoc, modelo canal, monitorização, redes sem fio, repetidores,
TDMA, UAV.

Table of Contents

List of Tables

List of Figures

Notation

Technical abbreviations and acronyms

- 3D: three-dimensional

- AL: application layer

- AoI: area of interest

- BS: base station

- ID: identification number

- COTS: commercial of the shelf

- CSMA/CA: carrier sense multiple access with collision avoidance

- DVSP: distributed variable slot-length protocol

- DRP: dynamic relay placement

- E2E: end-to-end

- FoV: field of view

- FPV: first person view

- GPS: global positioning system

- GS: ground station; same as BS

- LIDAR: light detection and ranging

- MAC: medium access control

- OSI: open systems interconnection

- PID: proportional, integrator and differential controller

- PDR: packet delivery ratio

- PDU: protocol data unit

- PHY: physical layer of the OSI model

- PM: packet manager

- PoI: point of interest

- QoS: quality-of-service

- RA-TDMA: reconfigurable and adaptive TDMA

- RCVM: remote control and video-monitoring

- RMSE: root mean square error

- Rx: receiver

- SI: international system of units

- SNR: signal-to-noise ratio

- TCP: transmission control protocol

- Tx: transmitter

- TDMA: time-division multiple access

- UAV: unmanned aerial vehicle

- UDP: user datagram protocol

- wc: worst case

- WSN: wireless sensor network

Units

- bit/s: bps, bits per second

- B/s: bytes per second

- dBm: power decibel

- k: kilo multiplier (a thousand)

- M: mega multiplier (a million)

- pps: packets per second

Math Expressions

Unless explicitly stated, referred quantities use SI units.

- $\lfloor \cdot \rfloor$: floor operator

- $\lceil \cdot \rceil$: ceiling operator

- $\text{frac}(\cdot)$: fractional part of a number

- Π - the product operator

- $\mathbb{R}$: set of real numbers

- $\mathbb{R}^+$: set of positive real numbers

- $\mathbb{R}^{0+}$: set of non-negative real numbers

- d: network E2E length

- $B_{i,j}$: bandwidth from node i to node j

- d_{wc}: worst case delay

- d_{tx}: transmission delay

- d_w: waiting delay

- h: number of hops

- iff: if and only if

- l_i: length of link i

- p_l: link PDR

- p_n: network E2E PDR

- RMSE_e: exponential model's RMSE

- RMSE_σ: sigmoid model's RMSE

- s_i: time duration of TDMA slot attributed to node i

- T: TDMA round period

- ζ_l: link throughput

- ζ_n: network E2E throughput

- ζ_{max}: maximum ζ_n, when using optimal number of relays.

Definitions

- affine: functions of the form $f(x_1, ..., x_n) = A_1 x_1 + ... + A_n x_n + b$

- bandwidth: maximum throughput a node is capable of achieving

- goodput: similar to throughput where only useful payload is considered as transferred data.

- sink: in sensor networks, it is the node receiving the main flow of data from all sensor-nodes.

- PDR: percentage of packets successfully transferred from source to destination.

- throughput: speed of data being successfully transferred from source to destination.

Other

- aka: also known as

- CMU-ECE: Carnegie Mellon University, Electrical and Computer Engineering (Dept.)

- cf.: latin *confer/conferatur*, both meaning "compare"

- DEEC: Departamento de Engenharia Eletrotécnica e Computadores

- e.g.: latin *exempli gratia*, meaning "for example"

- et al.: latin *et alia*, meaning "and others"

- FEUP: Faculdade Engenharia da Universidade do Porto

- i.e.: latin *id est*, meaning "that is"

- vs.: versus

Chapter 1

Introduction

1.1 Unmanned Aerial Vehicles

An Unmanned Aerial Vehicle (UAV) is an aircraft that is able to fly and be controlled without the presence of a human pilot on board. These vehicles date back as early as the Great War, from balloons to miniatured versions of traditional airplanes. Also around this time, a different category of aerial vehicle – the man-piloted helicopter – made its debut. It rapidly became a resourceful vehicle due to its ability to take off and land vertically as well as hover. In recent years, improvements in micro electromechanical systems such as inertial sensors and low-cost high-speed micro-controllers have made remotely piloted helicopters increasingly smaller and extremely accessible. Especially in small vehicles, the main throttle rotor with a smaller tail-rotor design was replaced by multiple equally-powered rotors on a single plane. This ends up being a simpler design and producing a more agile vehicle. These vehicles are named multirotors in the literature and commonly known nowadays as drones due to their noise sounding similar to a male bee. Throughout this document we will refer to multirotors as UAVs or drones, since the vast majority of times the terms are interchangeable.

Figure 1.1: Parrot AR Drone 2.0 quadrotor is controlled by a smartphone.

Figure 1.2: DJI Mavic Pro does obstacle avoidance and allows insertion of external cameras.

1.2 Context

Commercial-off-the-shelf (COTS) drones, in particular the four-rotor design known as a quadrotor, have seen their popularity expanded tremendously in the recent years. Agile maneuverability and hovering capabilities at small scales are highly relevant features in urban scenarios, but its popularity can mainly be justified by three others factors.

The first is their simplified (remote) user control. Even without aeronautical knowledge or previous flight-time, users can rapidly gain skills, and fly smoothly in a matter of hours. Vehicle stabilization is typically guaranteed by a local automatic controller. This means the vehicle maintains vertical and horizontal position, as well as pose, even without providing user input. Primarily, drones resort to accelerometers, compasses and gyroscopes for navigation; precision may be enhanced by encompassing ultrasound sensors and barometers to maintain vertical position, and by cameras running optical flow algorithms for the horizontal position. UAVs such as Parrot (2012) AR.Drone 2.0 (cf. Figure 1.1) allow the operator to use a smartphone and its embedded touch interface to move the UAV forward/backwards or left/right with one finger, and simultaneously spin or move up/down the vehicle with another finger.

The second driver for drone popularity is the fact that these devices are now carrying high-quality cameras on-board. Inclusively, high-end COTS drones (eg. DJI (2017)

Mavic Pro, in Figure 1.2) allow the operator to insert a professional camera that records on-board movie-grade video from the surroundings; some include additional camera stabilizers (a gimbal). For flight control, a low-resolution, low-delay alternative camera is included that streams video to the operator on the ground.

The third justification is simply their reduced price. Low-end drones without cameras are available for as low as USD$20, and have cheap replacement parts on-sale. Going up the scale, depending on the added features, we find racing drones with First Person View (FPV) head-screens for USD$70, such as the Banggood (2017) Eachine E013 (cf. Figure 1.3). Research drones that include GPS and 3D cameras such as Intel (2017) Aero are recently available for USD$1000 (cf. Figure 1.4).

1.3 Team of UAVs

Drones typically have two communication flows. Upstream, from user to drone, for control and downstream, from drone to user, for acknowledgment and sensor data. Currently, the dominant data path is from user to drone, but this is rapidly changing with the advent of high resolution cameras and other external sensors. Streaming from the environment opens a new course of operation, namely using such flying devices

Figure 1.3: Eachine E013 is a low-cost micro quadrotor equipped with camera and FPV headset.

Figure 1.4: Intel Aero research platform comes with a vast set of external sensors.

as mobile and agile sensors in a cooperative swarm (cf. Figure 1.5). A network that considers all of these aspects is what we define as an **aerial multi-hop sensor network**.

The four main requirements to create a UAV team are 1) (on-board) sensors to collect data, 2) communication for cooperation and sensor streaming, 3) computational power to process data, 4) world-perception for obstacle avoidance and flight-formation. Due to technology advances, it is now possible to equip drones to fulfill these requirements. A good example is the Intel (2017) Aero with a 8 megapixel camera, a 802.11ac WiFi card (that goes up to 3466.8Mb/s), a Intel Atom quad-core processor with 2.56Ghz of maximum clock-speed and 4GB of RAM, and it also includes a depth-camera for obstacle avoidance (Intel RealSense) as well as GPS. Other companies also include ultrasound (eg. Mavic Pro) and LIDAR technologies in their platforms (eg. Tech (2017) LeddarOne, shown in Figure 1.6) for improved obstacle avoidance;

1.4 Applications

Small and semi-autonomous multirotor aircraft is enabling a myriad of new applications. To date the focus has been primarily on single devices and not swarms. Companies have found applications in advertising due to the relative low investment cost and interesting bird-eye perspective. Media crews are now able to report events such as the
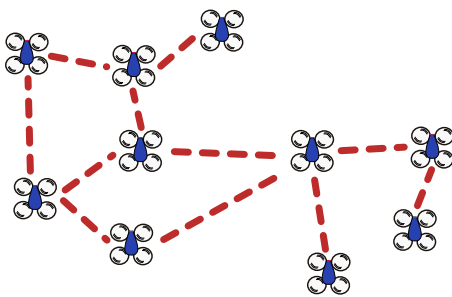
Figure 1.5: A quadrotor swarm and communication links (red dashed-lines).

Figure 1.6: LeddarOne is a LIDAR sensor designed for small UAVs.

aftermath devastation caused by wild forest fires on a remarkably unfamiliar way such as in Santa Rosa, California (cf. Figure 1.8, Fortune (2017)) and Pedrogão, Portugal (cf. Figure 1.7, SIC (2017)). We now find multirotors also being used by law enforcement agencies to track people and their movements during crowded and chaotic events (cf. Figure 1.9, CNN (2015)).

On a different context, UAVs are an excellent option for monitoring, inspection and surveillance of large-scale facilities, such as industrial plants or large factories, and even big infrastructures such as bridges and buildings. On one hand, sites such as high chimneys, electrical poles, large petrol tanks, pillars and long pipelines typically demand labor-intensive, dangerous and expensive manual inspections. On the other hand, drones are *disposable* and can become remote *eyes on the ground*; a swarm of multiple vehicles can inclusively increase the speed of such work many folds. Search-and-rescue in areas affected by disasters can benefit tremendously from remotely operated multi-

Figure 1.7: Pedrogão, Portugal

Figure 1.8: Santa Rosa, California

Figure 1.9: Indian authorities are considering drones for crowd control.

Figure 1.10: Swarms of drones can be used for monitoring and inspection of large-scale facilities. Search-and-rescue is another application.

rotors. Such scenarios, as depicted in Figure 1.10, cannot assume an ubiquitous radio communication infrastructure in place such as cellular, or clear roads for transportation of human-resources. Therefore, it is natural that multirotors taking off vertically and a swarm generating its own ad-hoc network are viewed as potential problem solvers.

All these scenarios have two common requirements. First, they need to collect images, video or other sensor information over large areas. Second, they often need to stream this data live to a base station to support interactive control by an operator. In these scenarios an operator located at a ground station often needs to fine-tune the position of drones and sensors in order to improve sensing resolution in certain areas of interest.

Unfortunately, video streaming on standard WiFi performs poorly, particularly with relays, resulting in long delays and lost frames. Currently, the vast majority of live-stream video from drones, such as the use in FPV systems, uses analog channels, due to its low latency. However, these are not only more susceptible to noise, but also harder to multiplex among several transmitters, as in swarms. Ad-hoc communication between drones may offer a viable alternative compared to infrastructure networks, e.g., cellular,
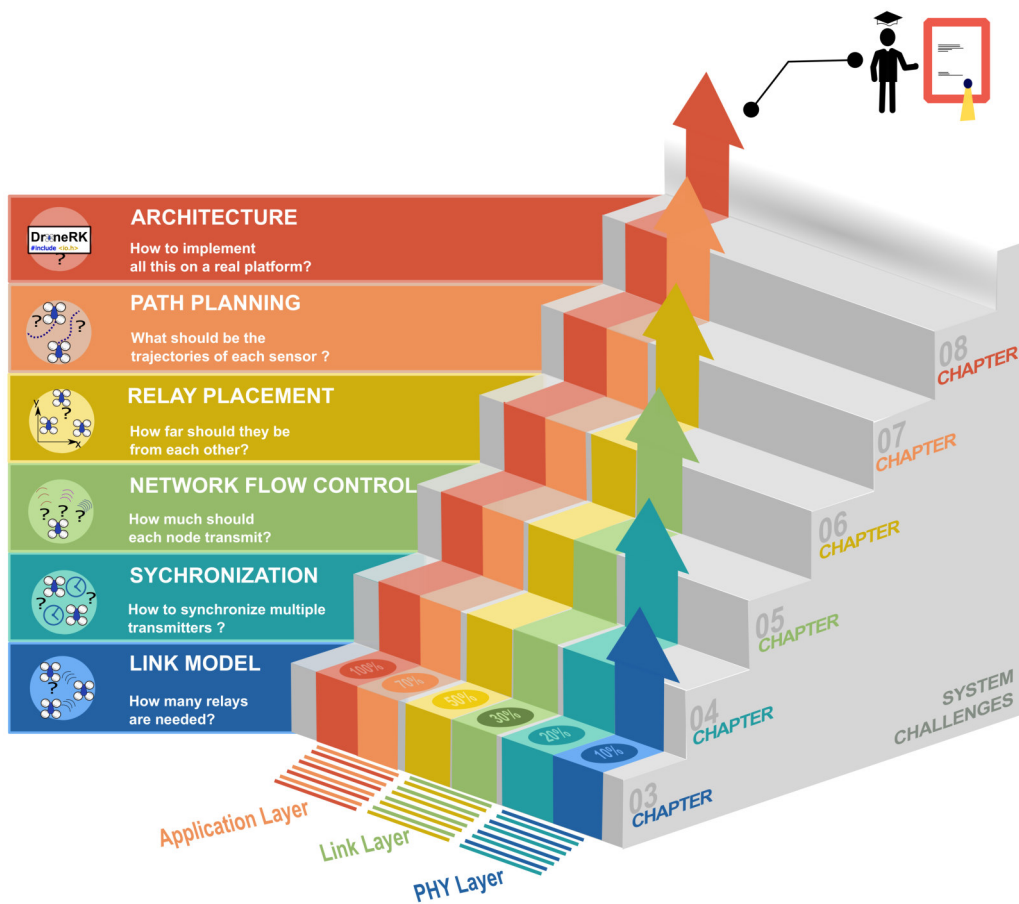
Figure 1.11: List of challenges designing aerial multi-hop sensor networks span across three networking layers, and are covered in the next six chapters.

in terms of availability, reliability and/or cost but such solution will come attached to multiple challenges.

1.5 System Challenges

From potential problem solvers to a fully-fledged system that copes with such scenarios, there is a long road of challenges that swarms have to overcome, summarized in the diagram of Figure 1.11. To begin, it is hard to establish a reliable communication link to convey remote sensing information. The wireless medium is well known to be

inherently unreliable. A receiver has to translate an electromagnetic signal into meaningful information, the received **s**ignal needs to stand above the background **n**oise, (cf. signal to noise ratio – SNR). Such signal is time-variant, dependent on other radio transmissions taking place in the surroundings (interference), whether these are generated by unknown sources or some other network nodes. Furthermore, on aerial networks it is expected that nodes change both location and pose, continually. This means distance and angle of the receiver-transmitter antennas will vary. It is known the quality of wireless communication, or more precisely, the channel capacity, degrades sharply with distance between receiver (Rx) and transmitter (Tx), and varies with respect to antennas orientation.

Typically in video stream applications, losses are compensated for by automatically changing the physical layer modulation scheme (PHY), lowering the bit rate or using complementary Internet-based technologies, such as TCP/IP, at the cost of a severe and unpredictable impact on delays.

Nevertheless, we know that for a given set of antennas and transmission power, eventually there is a distance above which the SNR will be lower than needed for actual communication no matter the orientation between a sensor node and the operator. The communication link is said to be broken at that point. We will show that assigning UAVs to relay data can fix this condition between far-neighboring nodes, by decreasing the Tx-Rx distance. From top to bottom, this creates a new set of challenges shown in Figure 1.11.

The first challenge regards the optimal number of relays to use. If all nodes operate on the same wireless channel, they will have to share it. Note that typically, wireless cards can only listen to or transmit packets one at the time. Without coordination, too many simultaneous transmitters create interference and packet loss, in consequence. More relays mean shorter Tx-Rx distances, and consequently more reliability. However, more relays imply more elements sharing the medium and less available throughput for

each one.

The second challenge regards the actual coordination among UAVs to avoid simultaneous transmissions. Synchronizing transmissions on a wide distributed, multi-agent, wireless system is inherently a hard problem. To synchronize nodes, clock information needs to be shared. The problem is that on a wide network, especially a not fully connected one, information takes several hops and a non-trivial time to travel through the nodes. Associated jitter and delay make clock adjustments imprecise. The challenge is to synchronize tightly enough that simultaneous transmissions are minimized. This first set of challenges is represented by the blue layer of Figure 1.11, and treated in Chapters 3 and 4.

The third and fourth challenges regard the relays placement and their transmission rate. When data is flowing through multiple nodes, a multi-hop network, each intermediate node is in charge of receiving incoming packets, and retransmitting them at a later moment. When inbound packets arrive at a higher rate than they can leave, we have a backlog problem. Under this condition, packets have to enter a buffer and wait to be delivered. This is one of the major roots of end-to-end delay; if the buffer reaches its limit, it creates losses, too. Unless the channel characteristics of the outbound link are at least as good as those of the inbound link, we can not guarantee that under heavy load, there will be no backlog. Having control of UAVs gives us conditions to change the inbound/outbound link characteristics. On a slower time scale, moving UAVs change links capacity directly at the physical level. The challenge is to measure such capacities (unbalances), and act accordingly. On a faster time scale, deciding the rate of transmission at every node changes link utilization at the link level. The challenge here is to measure and react fast enough before the channel changes. These are the core of the challenges on optimizing an aerial multi-hop network. They are represented by the yellow and green middle layer of Figure 1.11, and treated in Chapters 5 and 6.

The last two challenges relate to the application programming. Monitoring an area

periodically means sensor data (i.e. video) is being collected and streamed back to a Base Station (BS). The problem is to assign UAV roles to a given team of UAVs. With too many UAVs assigned for sensing and few for relaying, the system can sweep the Area of Interest (AoI) faster than it can deliver data to the BS. In opposition, with plenty of relays and few sensors, the communication backbone from AoI to BS has now potentially more capacity than the effective data the system is generating. Therefore, one challenge is to resolve this tradeoff, and the other is to strategically design trajectories that allow n-sensor UAVs collect data n-times faster than a single one. This last set of challenges is represented by the red layer of Figure 1.11, and treated in Chapter 7.

1.6   Vision and thesis

This dissertation and its underlying research was carried out with the vision that *Unmanned Aerial Vehicles (UAVs), in particular multirotors, can become a powerful tool for live (interactive) remote inspection of large-scale structures.* Instead of manual, local and labor-intensive inspections, we envision one human operator working together with semi-autonomous UAVs on four stages. Firstly, the operator at a ground Base Station (BS) defines an remote Area-of-interest (AoI) and instructs a group of semi-autonomous sensor-capable UAVs to navigate there; secondly, interactive control of the fine position and pose of UAVs is initiated to focus on features of interest; concurrently, a live stream of sensor data from the AoI is initiated; finally, the necessary communication backbone is established, by means of a complementary autonomous group of UAVs, linking sensor UAVs to the BS. This vision, illustrated by Figure 1.12, is accompanied with the perception that the current state-of-the-art in UAVs still does not focus enough on solutions for creating and maintaining a reliable network.

We claim that user-interactive coverage and inspection applications resorting to UAVs and without the presence of an external infrastructure need a reliable, long-range, high-
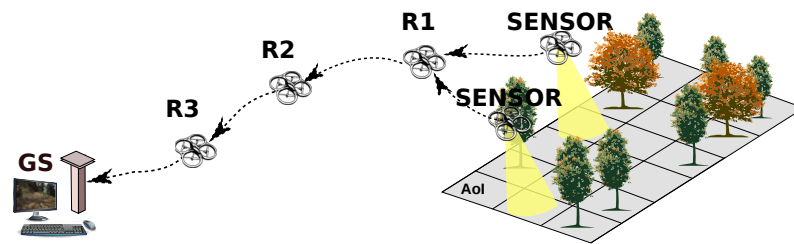
Figure 1.12: Our vision of an aerial multi-hop sensor network, streaming to a base station, resorting to UAVs to relay data.

throughput and low-delay communication backbone properly setup. As a result, this dissertation presents the following thesis:

Joint coordination of network protocol and topology (placement of nodes) will improve user-interactive control of UAVs for streaming applications in terms of throughput, delay and reliability.

1.7 Goals

This dissertation was designed to meet five main goals, namely:

1. Understand in detail a UAV-to-UAV link.

2. Understand in detail a multi-hop network of UAVs.

3. Uncover major issues in these networks when transporting delay-sensitive high-throughput data.

4. Provide a systems solution tailored to swarm operations.

5. Prove these concepts through a monitoring/inspection application.

1.8   Contributions

The contributions are organized along two categories: conceptual and technical. Under the former, this dissertation introduces several new models and algorithms. First, a new model for packet delivery ratio (PDR) as a function of link length, packet size, and node orientation has been identified; later, extended for multi-hop networks. Then, we present a new algorithm for distributed slot synchronization to optimize TDMA communication. Building from the slot synchronization, we introduce a new algorithm called Dynamic Variable-length Sloted Protocol (DVSP) has been designed, and its own convergence proved. An online, distributed algorithm named dynamic relay placement (DRP) has been designed. It is able to assess the quality of the medium online, and also seek the best location for each relay to achieve maximum network performance. Finally, this dissertation provides and evaluates a new persistent multi-vehicle monitoring algorithm with communication constraints. A model is designed that is able to identify the minimum sweeping period of an Area of Interest given UAV and network conditions.

Under technical contributions, this dissertation presents the implementation of the software library for our embedded GNU/Linux drone platform as well as a reference implementation of each algorithm with supporting protocols. It was organized into several modules, each with its own functionality as part of the Drone-RK platform. Drone-RK is a dynamic library written in C that contains 13 main modules, namely: 1) *Navdata* and 2) *GPS* to read sensor data; 3) *Actuator* and 4) *Flight Control* to send motion commands; 5) *ARConfig* to setup the vehicle; 6) *Autonomous Flight* to do waypoint flights; 7) *TDMA* and 8) *Packet Manager* to provide multi-hop communication and run DVSP protocol; 9) *PDR* to estimate PDR and run DRP protocol; 10) *Video* and 11) *Image Processing* to collect video and process its content; 12) *Utils* to provide a generic set of tools to all modules; 13) *Keyboard* to allow user-input. User-level applications are able to dynamically load Drone-RK and easily access these functions.

This dissertation validates by experimentation all concepts referred above, namely validation of link and multi-hop models, DVSP and DRP. Last but not least, a simulator was created. It is able to run and test multiple Drone-RK applications in a single machine.

Most of these contributions have been published under the following references:

- L. Pinto, A. Moreira, L. Almeida and A. Rowe, "Aerial multi-hop network characterisation using COTS multi-rotors," 2016 IEEE World Conference on Factory Communication Systems (WFCS), Aveiro, 2016, pp. 1-4 – (Pinto et al., 2016a)

- L. R. Pinto, L. Oliveira, L. Almeida and A. Rowe, "Extendable Matrix Camera Using Aerial Networks," 2016 International Conference on Autonomous Robot Systems and Competitions (ICARSC), Braganca, 2016, pp. 181-187 – (Pinto et al., 2016b)

- L. R. Pinto, L. Almeida and A. Rowe, "Demo Abstract: Video Streaming in Multi-hop Aerial Networks," 2017 16th ACM/IEEE International Conference on Information Processing in Sensor Networks (IPSN), Pittsburgh, PA, 2017, pp. 283-284 – (Pinto et al., 2017c)

- L. R. Pinto, A. Moreira, L. Almeida and A. Rowe, "Characterizing Multihop Aerial Networks of COTS Multirotors," in IEEE Transactions on Industrial Informatics, vol. 13, no. 2, pp. 898-906, April 2017 – (Pinto et al., 2017d)

- L. R. Pinto , L. Almeida and A. Rowe, "Balancing Packet Delivery to Improve End-to-End Multi-hop Aerial Video Streaming," in ROBOT 2017: Third Iberian Robotics Conference. Advances in Intelligent Systems and Computing, Seville, 2017, vol 694 – (Pinto et al., 2017b)

- L. R. Pinto, L. Almeida, H. Alizadeh and A. Rowe, "Aerial Video Stream over Multi-hop Using Adaptive TDMA Slots," 2017 IEEE Real-Time Systems Symposium (RTSS), Paris, 2017, pp. 157-166 – (Pinto et al., 2017a)

1.9   Organization

The remainder of this dissertation is organized as follows. Chapter 2 discusses relevant background knowledge for this dissertation. Chapter 3 studies the communication link between two multirotors. Chapter 4 describes an extension to multi-hop operation and the node synchronization problem. We identify the major sources of inefficiencies on such networks, and we dedicate the following two chapters to solving them. Chapter 5 proposes a new technique based on adaptive TDMA slots to optimize data traffic in the network. Chapter 6 presents a complementary and also novel technique for relay placement to optimize the multi-hop network. An application scenario and its idiosyncrasies are explored in Chapter 7, revolving around coordinated monitoring using several sensor-UAVs. Chapter 8 describes the implementation effort to run the experiments necessary to test all the concepts explored in the other chapters. Chapter 9 summarizes the main conclusions along the mentioned topics, and inclusively revisits initial claims to provide necessary closure. Potential future work is discussed as well.

Chapter 2

Background

In this chapter, we present some background that allows the reader to be acquainted with the topics referred along this dissertation. Furthermore, we include state-of-the-art research work that provided the driving force for this work, by identifying tried solutions and *lacunae* in the literature.

2.1 UAV

UAVs are generally composed by flying chassis and its actuators, sensors , a central processing unit and a battery pack. Figure 2.1 depicts a multirotor with four rotors, the most common design found. To counteract the angular acceleration, the rotors rotate in two different directions. To hover, all the rotors move at the same speed, while to move up/down thrust is increased/decreased equally on all rotors. In order to move forward/backwards, pitch is changed by increasing thrust on the rear/front pair of propellers, respectively. In the
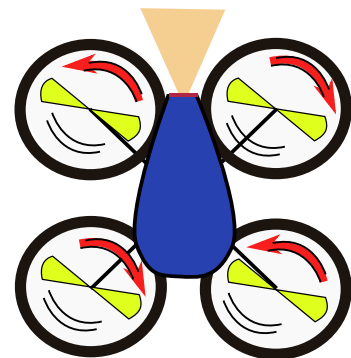
Figure 2.1: Drone with four rotors. Propellers rotate in different directions to counteract angular acceleration.

same way, to move left/right, roll is changed by in-
creasing thrust on the right/left pair of propellers, re-
spectively. By merging controls, the vehicle is able to
move in any combinations of these directions. Most vehicles can also spin around their
own center by changing the spin on the same-rotation pair of propellers, and creating
a non-null angular acceleration. In order to guarantee vehicle stabilization, accelerom-
eters and gyroscopes are constantly measuring the pose of the vehicle, and feeding it
to the auto-pilot, the controller of the vehicle. These vehicles have typically low energy
autonomy when compared to airplanes. Under operation, this type of vehicles is either
hovering or flying; in both states, the motors are running. In fact, energy consumption
is mainly drawn at the motors. Communication and computation power is typically
minimal in comparison. Therefore, autonomy is majorly dependent on the time in the
air, battery capacity, total vehicle weight, and also on the number of rotors and area of
the propellers. As rule of thumb, smaller quadrotors have less autonomy than bigger
ones.

Numerous UAV test-beds have been developed for commercial, military and re-
search purposes, some of which explored using UAVs as flying wireless sensor net-
works, especially image/video sensing. In many works, such as (Forster et al., 2013),
UAVs are used to collect aerial imagery for mapping and localization. This can be
performed locally if UAVs have enough computing power or remotely using a cloud
infrastructure if a connection is available. In tasks such as monitoring or target track-
ing, a human operator is often the end user that takes final decisions. Local storage of
sensor data is often not an option. In disaster scenarios, drones might be destroyed any
second. In military scenarios, drones might be captured and stored data is sensitive.
This means that the UAVs should be able to form a network and stream *live* video/data
from a remote location.
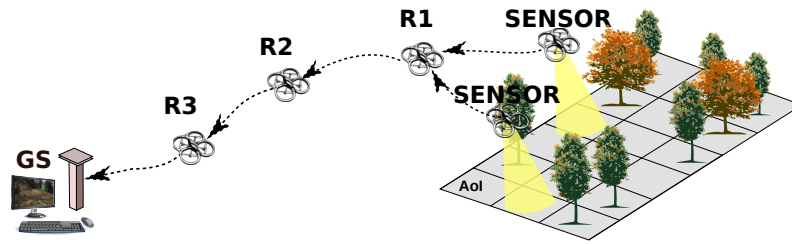
Figure 2.2: A UAV wireless sensor network, with two sources and three relays.

2.2 UAV Wireless Sensor Networks

A wireless sensor network (WSN) is a broad name for the set of networks that comprise sensor nodes, i.e. devices, that are capable of measuring environmental metrics such as temperature, noise or pollution. These devices have wireless capabilities to share this data remotely among themselves and/or with other nodes such as a base station.

A UAV WSN is such network where the sensing devices in use are UAVs. Some authors have explored these networks, resorting to UAVs to construct flying wireless sensor networks, as seen in (Goddemeier et al., 2012); here authors describe multiple ways to organize UAVs to form a sensor network, whether the sensors can be disconnected from the base station for sometime, whether sensors are all directly connected to the ground station, or if relays are allowed to be used in order to increase the range of communication, while maintaining the communication streams.

The latter is what is labeled as a *relay network* or *multi-hop network*, which is a type of wireless network characterized by the use of relay nodes, i.e., nodes that are in charge of interconnecting source and destination nodes, when these are not in direct reach of each other. Generically, relays might also generate their own data. We say there is a wireless link when two nodes can communicate directly. A hop is each one of the links a packet utilizes to reach its intended (final) destination;

A particular case of such network is depicted in Figure 2.2, entailing several interesting aspects. In this example, there are two sensor UAVs – the sources sensing/gener-

ating information from the surroundings; there are three relay UAVs – passing packets along the route; there is one ground Base Station (BS) – the final data destination, sometimes also named sink. We can say this is a 4-hop network, since sensor packets use four links to reach the sink. There is no central node of coordination. Each node is responsible to relay data that it receives to another neighbor that is closer to the packet destination. This holds the advantage of allowing information to travel longer distances, at the cost of increased number of nodes and therefore complexity. Guaranteeing good link quality is now paramount to build a solid network. For that, it is necessary to assess the characteristics of the wireless channel on a UAV-UAV link.

2.3   Network Performance

There are three main metrics to assess the quality of a network, in particular the wireless channel, namely throughput, packet delivery ratio and delay

Definition 2.1 (Packet delivery ratio - PDR)**.** *The PDR is the percentage of packets that are being successfully transmitted from one node to another – denoted as p_l.*

The PDR can be computed by considering a small window of time and dividing the number of packets received during that time with the total number of packets actually sent. Packet loss ratio (PLR) measures the opposite, i.e., the percentage of packets lost in the link. Assuming packets lost at any given point are not recovered, the product of all link-PDRs along the network chain gives us the end-to-end packet delivery ratio, since there is no data generated at the relays. It depends on several factors, such as distance, packet size and antenna orientation, number of retries at PHY level, and selected PHY bitrate. It is expected that as bitrate and packet size increase, PDR decreases for the same distance. This issue of packet delivery ratio (PDR) has been addressed by several works. For example, Zhao and Govindan (2003) and Jia et al. (2010) clearly identified distance as the main factor of PDR, in fixed sensor networks. The work in (Basagni et al.,

2010), on the other hand, shows the impact of packet size on PDR (and throughput), in underwater networks. Antenna orientation is studied in (Ahmed et al., 2013), where IEEE802.15.4 radios are used to test its impact on PDR. In the field of vehicular networks, one can also find work bearing similar results. For example, in (Bohm et al., 2010) the authors present an experimental characterization of the 802.11p channel focusing on the effects of relative speed between ground vehicles, including the effects of speed on the PDR.

The second paramount metric is throughput.

Definition 2.2 (Link Throughput). *The link throughput, or data rate, is the average number of packets successfully transmitted per second between two nodes that are directly linked – denoted as ζ_l.*

A distinction should be done between link-throughput and network throughput. The former regards two direct neighbor nodes. The latter, regards two nodes connected through several relay nodes, i.e., a multi-hop network;

Link throughput depends directly on two main variables: one regarding the transmitter, and one regarding the receiver. The former is the packet transmission speed B, i.e., the number of packets sent from the transmitter per second (pps). The latter is the probability of receiving a packet $p_l(d)$, which we approximate with the PDR (defined above).

Note that throughput is not the same as transmission data rate, because data might be lost along the route. Some authors prefer to use the term goodput when they are considering just the payload, and ignoring associated packet headers. Typically both are measured in bits per second (bit/s), and their multiples. We can convert B into bit/s multiplying it by the size of the packets being transmitted L (in bits), leading to Equation 2.1.

$$\zeta_l = B \times L \times p_l \tag{2.1}$$

This is upper bounded by the PHY bitrate in operation. For IEEE802.11g, bitrate ranges from 1Mbit/s to 56Mbit/s, and with newer versions such as IEEE802.11n it can go up to 300Mbit/s.

Definition 2.3 (Network Throughput). *Assuming there is a flow or stream of data from a source node to the sink node along a relay chain, the network throughput or the end-to-end (E2E) throughput is the rate of data effectively being received at the destination – denoted ζ_n.*

Network throughput actually corresponds to the throughput on the last hop, i.e., the link closest to the sink node, the intended final receiver. Its value is also technically given by the slowest link of the network, since the links are organized in series, as we will explore further in Chapter 3. It can be computed by considering a small window of time, and dividing the number of packets received during that time by such time span.

Asadpour et al. (2013) show that in a UAV network throughput depend on distance between UAVs. They provide extensive experimental data for UDP over WiFi throughput, testing for different PHY bit-rates and distances, and relative velocities. They inclusively show that WiFi bit-rate can and should be set manually, disabling automatic adaptation mechanisms designed for static machines such as computers, for improved throughput. Initially such mechanisms were designed to cope with signal fading due to distance or with interference from other sources. However, they argue UAV nodes have typically faster dynamics than the time taken to find the best bit-rate. Knowing the position and distances between UAVs, can provide means to develop a faster algorithm. However, they do not present PDR results neither information is given on the effect of packet size on throughput. They also assume an isotropic medium behaviour, which is not always the case, as we will see, particularly with COTS multirotors. Asadpour et al. (2014) go further and analyze factors such relative orientation and UAV relative speed. Conversely, the authors of (Muzaffar et al., 2016) propose a UAV wireless multi-source video streaming system in which transmitters adapt their PHY rate according to the

network load and link conditions, thus improving performance. Such results will help us developing a more complete idea of the typical UAV-to-UAV channel. However, it is clear the lack of results in the literature on multiple hop metrics.

Definition 2.4 (Network Delay)**.** *Network delay, or end-to-end delay is the time a packet takes to travel from source (when it is generated) to sink (when it is received).*

We can also consider relay delay as the time span from the moment a packet is received at a relay until it is resent to the next node. Delay is relevant in real-time applications, where it is vital to known in advance an upper bound for the time a packet will take to transverse the network. It should be as predictable as possible. Most literature found on UAV communication does not consider such metric; neither explores the impact on delay of buffering packets at intermediate relays in a loaded network. Most applications rely on sensor collection for later dissemination – data muling, or rely on a direct link to the base station. Therefore, the vast majority of related work found rely on the standard IEEE 802.11 medium access mechanism – CSMA/CA, which as is stochastic by design.

2.4 Medium Access

Video monitoring as presented in our vision section is a soft-real time application. To perform drone control with video feedback, delay has to be bounded. However, as we have discussed so far links are unstable, asymmetric, i.e., different from each other, and under high traffic backlogs arise due to accumulated traffic. As such, coordination of transmission among several nodes despite complex is vital to prevent backlogs and their associated long delays.

Using Time-division Multiple Access (TDMA) to guarantee timeliness has been studied extensively as it is a technique that grants all nodes a periodic transmission window, called a slot, thus preventing phenomena like starvation.
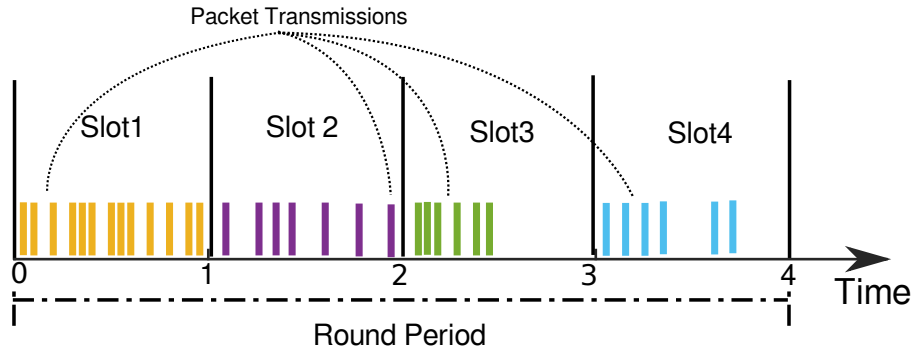
Figure 2.3: TDMA allows each node to send packets in their own slots.

TDMA is contention-free scheme, that typically provides an exclusive (collision-free) slot to every transmitter in the network, preventing mutual interference. It grants a fixed length to the slots of all nodes ($s_1 = s_2 = \cdots = s_N = T/N$) as Figure 2.3 illustrates. The round period T is constant and represents the periodicity that each node has to transmit. The set of all slots times (s_i) in a time period is called TDMA frame. Each vertical colored-bar in the figure represents a packet transmission. Each color belongs to a different node. We can see that some nodes can transmit more packets than others, during the same time period.

Most wireless sensor networks using TDMA focus on guaranteeing that all nodes can communicate their own data. The fact that, in our work, middle nodes are solely relaying data, but their links can present variable throughput, makes the system prone to inefficiencies when using traditional TDMA approaches. Relays in our network only require a time slot long enough to relay incoming data while minimizing in-network queuing; hence slots should adapt to overall network throughput. Changing slot size to improve network metrics has been studied before, as in (Wandeler and Thiele, 2006), but not applied to a multi-hop aerial line network, where data is generated at one tip of the network, only, and relayed through the other nodes, over links that present variable throughput. Our work is the first to propose an adaptive overlay TDMA framework on-

top of CSMA/CA links in a mobile line relay network, that keeps TDMA cycles constant, but adjusts slots dynamically in a distributed fashion in order to minimize end-to-end delay.

The work in (Wang et al., 2017) also shows relationship to ours since it analyzes the behavior of multi-hop networks under TDMA versus CSMA/CA. This work addresses networks in general, focusing on a small scale case, and the authors conclude that, depending on payload size and slot length, both medium access control techniques can dominate one another in terms of worst-case network delay. However, in most such works, there is no on-line stream of sensor data; packets are sent scarcely, not generating queuing issues. When streaming data intensely, as in our case, buffer overflow becomes a strong problem and a potential cause of PDR degradation, requiring adequate traffic management to avoid stalling the network. For that reason, we intend to use TDMA implemented over CSMA/CA, which allows achieving the best of both techniques.

Therefore, to the best of our knowledge, we still miss a thorough comparison on delay, packet delivery and goodput on a multi-hop WiFi UAV network when using the native CSMA/CA vs. a TDMA overlay, specially regarding live video stream applications.

It is important to clarify that there are many other RF solutions and protocols that can improve communication on a multi-hop network, such as slot re-utilization, nodes with multiple NICs on orthogonal channels, directional antennas for SNR improvement, among others. Nevertheless, those are orthogonal to the solutions we propose. Those other solutions can be applied simultaneously on top of ours to further improve network performance.

2.5   Relay Placement

Besides controlling the traffic, multi-hop wireless network improvements are generally done at management level, improving routing (IEEE802.11s, AODV, DSDV, BATMAN, and their variants) and/or coping with unreliable links using redundancy.

Routing it not really a problem in line networks. Redundancy mechanisms can be employed generically in any network, at the application level inclusively. We focus our effort on the coordination of relay placement, since it is a novel approach in UAV networks. We found some related work in ground robotic networks. For example, Lindhe and Johansson (2009) investigate how robots motion can be controlled in order to maintain high throughput for streaming data to a base-station using a multi-hop network. They conclude that, instead of transmitting from every point directly to a gateway, it is better to concentrate transmissions in areas where/when the channel is good, slowing the robot, and then moving faster in areas with poor channel characteristics. The paper does highlight the variability and asymmetry of wireless links, which we will take into account.

Henkel and Brown (2008) analyze mobile robotic networks performance as a function of distance from a base station and required data-rate/delay requested by users. They also consider the implications of using relay nodes. When robots move far from the base, the authors propose swapping to a data mule model that leverages delay tolerant networking, giving away the live connection to the base. Although other researchers have also explored different UAV network operation modes, most tolerate breaking base connectivity, which is incompatible with the live streaming scenarios we consider under our initial vision.

Flushing et al. (2014) create a method to predict link quality based on an off-line learning phase. This predictor provides the robot network with a map of expected communication quality at any point in space. They do not measure channel performance

on a real world system, and therefore our work is likely to be useful to feed real data into learning phases of tools like this.

In (Goddemeier et al., 2012), links are maintained by measuring radio-signal strength indicator (RSSI), and forcing nodes to approach it other when that value falls below a given threshold. No explicit analysis on multi-hop networks is done.

In contrast, none of the above approaches explores moving relay nodes dynamically to gain an advantage, since some applications use uncontrollable or fixed nodes or their applications do not allow it to happen. In turn, online PDR analysis on mobile networks has been addressed by several works but mostly with low throughput scenarios with static nodes (Zhao and Govindan, 2003; Jia et al., 2010). Thus, in-network buffer overflow is not necessarily a problem, unlike our case where the video streaming needs high throughput, requiring adequate traffic management. On the other hand, the work in (Bohm et al., 2010) addresses the effect of relative speed in a vehicular network, including PDR during data streaming, but it does not address multi-hop communication.

As seen in this brief survey, existing works in the literature address related but different aspects of wireless ad-hoc communication with respect to our work. Again, most of current solutions in this field are orthogonal to our proposed solution. Hence, to the best of our knowledge, we still miss a thorough packet delivery and throughput analysis of multi-hop WiFi UAV networks using relay location to improve end-to-end network performance for live video streaming.

2.6 Applications

Area monitoring problem is widely studied in the literature. There are several related projects that address sensing and coverage in robot data collection. However, there are important variations of the same main problem. Some authors consider the coverage problem with the purpose of spreading sensors as efficiently as possible to cover a given

Area of Interest (AoI), under some constraints such as communication. Others, consider the problem of monitoring a given set of points, each with a different periodicity. Nigam et al. (2012) propose that the UAVs move based on a mixed policy between closest point to visit and age of the point, i.e., how long ago it was visited. It is seen that deciding the next point to visit is of great importance, if we want to minimize the overall maximum data-age. We will focus on the problem of periodically sweeping an AoI as fast as possible, using multiple vehicles as sensors themselves, while maintaining a communication link to the GS. In (Cheng et al., 2008), the authors consider a similar problem, they propose periodic coverage to gather information from ground sensors. Their solution for multiple UAVs is to partition the route that includes all Points of Interest (PoI) into N parts and assign one part per vehicle, that will periodically visit each segment. In (Gorain and Mandal, 2013), the authors propose a solution where the space is divided into N parts and the UAVs move along the same route, where they follow each other with a certain separation. Neither of these approaches require that the UAVs are streaming data, and that they need to reduce their speed at each PoI to sense data. They also do not consider external disturbances that could eventually move the UAVs out of place.

Huang (2001) studies the shortest paths that cover a given AoI with minimum overlap and minimum number of turns. This can be particularly interesting to consider when using airplanes. However, with a regular AoI and multirotor UAVs we can provide a better (optimal in terms of distance and time) covering path. The closest work to ours that we found is that in (Franco and Buttazzo, 2015), where pictures are to be taken from an AoI. However, they do not consider periodic visits or even streaming. Their main focus is to obtain the path that minimizes energy, given a non regular AoI shape. The authors in (Yanmaz, 2012) evaluate connectivity versus area coverage in UAV networks. They propose a distributed algorithm that spreads the UAVs without breaking the network links among them, which allows streaming to be maintained. This

algorithm might be suitable during the deployment of the UAVs at the AoI, but does not help in the case of periodic coverage. Finally, Tuna et al. (2012) show that UAV dynamics are complex and important to be considered when simulating their path to their targets, if we want to obtain accurate results. For this reason, in this dissertation we will consider a more complete motion model by including non-fixed velocities, unlike the majority of coverage work.

Thus, our work contributes to the state of the art by considering the periodic coverage problem with a controlled team of multirotor UAVs that creates a streaming connection to a ground station while tolerating physical and radio interference of environmental factors.

In sensing applications, monitoring an area is usually referred as coverage. As Gorain and Mandal (2014) define within the sensor networks field, coverage is classified in two main types. The first is *continuous coverage*, where a set or all of the points inside a AoI are to be monitored continuously by fixed sensors nodes. The second is *sweep coverage* where periodic monitoring of the points inside the AoI is enough to fulfill the needs of the application. Instead of static nodes, mobile sensors are used to periodically collect data and refresh the information at the sink. Sweep coverage is now accessible due to the rapid development of mobile robotics, despite the fact that the available energy in these systems is still the main limitation and source of concern (Toksoz et al., 2011; Suzuki et al., 2012; Yang et al., 2013; Franco and Buttazzo, 2015) – robot motion represents the majority of the consumed energy. Some other authors focus less on the energy consumption of the UAVs during flight, and more on the sweeping period and the minimum number of nodes needed to monitor the whole AoI (a NP-hard problem (Li et al., 2009)). Detecting unusual activities quickly enough in a wide area, such as a leak in a pipe or an intruder in a facility are good examples where the aforementioned goals are relevant.

Typical solutions (Cheng et al., 2008; Gorain and Mandal, 2013) for sweep coverage

using multiple UAV is to discretize the AoI into Points of Interest (PoI), and then create a single route that includes all of the PoI. As in (Huang, 2001), routes are typically divided into multiple parts and each part is assigned to a single vehicle. Another possibility authors in (Nigam et al., 2012) propose is that the UAVs move based on a mixed policy between closest point to visit and data-age of the point, i.e., how long ago it was visited. Alternatively, the UAVs can move along the same route and they follow each other with a certain separation.

Besides some of the assumptions usually provided in sweep coverage, works are often unrealistic. Most current approaches do not consider practical features such as adapting UAV's velocity to stream buffered data to a sink (both buffers and wireless channel are limited), or reducing speed when reaching a PoI to sense undamaged data (eg. taking a camera snapshot without blur). We also realized that during some preliminary tests that flights are usually affected by external disturbances such as wind, and localization errors that can eventually modify velocity and position of the UAVs along their trajectories. Synchronizing the whole fleet is therefore another practical challenge since these conditions are often disregarded in more theoretical approaches. Correct estimation and simulation of the UAV dynamics are essential to predict the fleet performance in the real world (Tuna et al., 2012).

Most coverage scenarios regard mobile robots that collect data from a set of PoI, and upload it at a later moment to one or more sinks, by what we call data muling. This typically implies the robots move in a completely autonomous manner, disconnected from a ground station, and define their trajectories either offline, or online based on the information they receive from their sensors. However, when interactive applications are to be implemented, information must constantly be exchanged between operator and sensors. If for instance a factory or mall are being monitored and some target is detected, the operator can receive this information rapidly enough to perform remote sensor position control. An operator can opt for reassigning the AoI in order to track the

target manually, or to increase the number of robots over the area to improve sensing data refresh rate. Some decisions can be autonomous, but many other are complex and still very likely dependent on human assessment of the current situation. This rationale leads us to believe that interactive monitoring systems resorting to such agile robots as multirotors and a human operator are promising and applicable in many different ways. We now see how information typically flows from an AoI to an operator.

Chapter 3

Building an Aerial Multi-hop Network

Building a UAV-based on-line stream embraces several challenges, such as establishing a reliable communication link, potentially several of them in a multi-hop fashion, to convey sensing information. In fact, it is well known that the quality of wireless communications degrades sharply with distance. Adding relays can improve the reliability between neighboring nodes giving them relative shorter distances. On the other hand, relays typically share the wireless channel imposing a cost on the overall throughput.

These results are particularly useful for designing networks of multirotors since in these networks we can control the position of the nodes to improve the communication links. This is not possible in typical mobile ad-hoc networks, such as networks of personal devices or vehicular networks. In other cases, such as networks of ground robots, position control would still be possible, but the propagation characteristics in those cases are rather different due to obstacles, multi-path, close-range and near the floor environment. In this work, we seek to provide novel insight into outdoor aerial networks of COTS multirotors, specially in characterizing and modeling their links.

This chapter we will discuss building a multi-hop line aerial network, comprised of a sensor-UAV and a variable number of relay-UAVs. We address the problem of deciding the optimal number of relays in order to optimize its performance. This work has been

reported preliminary in (Pinto et al., 2016a), and later extended in (Pinto et al., 2017d).

We start by collecting data on packet delivery ratio (PDR) of one aerial link based on extensive measurements (1st contribution). In this work, we use those measurements to introduce an adequate modeling approach that allows deducing the PDR as a function of link length (2nd contribution). Furthermore, we provide the formal support to deduce the optimal placement and number of relay nodes that maximizes PDR and throughput (3rd contribution). This is then validated with experimental data using multiple relays (4th contribution).

The organization of this chapter is as follows. In Section 3.1, we expose the problem of communication as a function of distance. The link performance of the platform is explained in Section 3.2, and we model this channel in Section 3.3. Section 3.4 describes our concept of multi-hop network, and we prove its properties. Section 3.5 details the experiments and their results carried out to validate the network model. Finally, Section 3.6 provides conclusions and remarks on the open problems and the ones we will treat further along this dissertation.

3.1   Problem Statement

Using a single UAV with sensing capabilities (sensor-UAV) that collects information to deliver to a fixed remote point (Ground **B**ase **S**tation – BS), what is the network topology that allows the highest throughput in a relatively wide range of distances? Note that assuming an arbitrary distance between the sensor-UAV and the BS, direct communication may be unfeasible. To overcome this issue, we consider that additional UAVs may be deployed to act as relays and help increase individual link quality, forming a line-network. However, more nodes in the network decreases the available time each node has to transmit since multiple nodes are sharing the same radio channel. Therefore, we aim at solving the problem of finding the number and optimal placement of relay-

Figure 3.1: AR Drone 2.0 platform, a common COTS quadrotor, used for the experiments.

ing COTS multirotors that maximize throughput in a line network, given an arbitrary distance between the sensor-UAV and the BS.

In the following sections, we will solve this problem by characterizing the communication channel in our system. We start by studying the link layer, i.e., the node to node direct communication, by performing multiple experiments on COTS multirotors as well as developing a model for it. Then, we extend this model to the network layer, i.e., end-to-end communication using different number of relaying nodes in a line topology. We then validate our model by performing experiments and measuring the end-to-end throughput under different conditions.

3.2 Link Layer – Experiments

In this section we describe the experiments characterizing the UAV-to-UAV communication, using the AR Drone 2.0 platform Parrot (2012), shown in Figure 3.1. It is a common programmable quadrotor available in the market. It comes with on-board camera and wireless WiFi interface.

We used two UAVs at a time, one as the sender, and the other one as the receiver. In each experiment, the sender transmitted 1000 packets, and the receiver recorded the relevant part of the received packets' payload together with the reception time-stamp into a log file. We also carried out experiments with different configurations of distance,

packet size and relative vehicle orientation to evaluate how these affected the packet delivery ratio (PDR), and ultimately the throughput. In particular, we used three distinct packet sizes as well as two different relative orientations at each distance.

More than 5600 experiments were carried out with the UAVs at 3m height, far from interfering sources in the same RF band. The transmitter was set to send packets as fast as possible. Each experiment took between 1 and 2s to complete. In total, the experiments resulted in more than 950MB of gathered data from multiple distances, packet sizes and vehicle orientations. Table 3.1 summarizes all settings used in the experiments.

The top of Figure 3.2 shows the PDR evolution over time, performed for a given orientation, distance and packet size. Each point represents the average of 1000 packets. Since the variations between consecutive points do not exhibit significant visible correlation, we conjecture that the probability of successful delivery of each packet is also independent of each other and can be characterized by its average p alone, i.e., a

Table 3.1: Experiment setup for the two AR Drone 2.0 vehicles in the single-link channel characterization

PHY layer	802.11g, fixed to 54 Mbit/s, Tx power 15dBm
Wireless mode	Ad-hoc
Max retry	2 (minimum allowed by the platform)
# of packets	1000 per experiment
Packet type	UDP (78 bytes header)
Location	Open field with low external interference
Height	3 meters above the ground.
Distance	$0, 5, 10, 15, 25, 35, 45, 55, 65, 75$m
Payload size	200, 500, 1000 bytes
Orientation	Parallel, Collinear
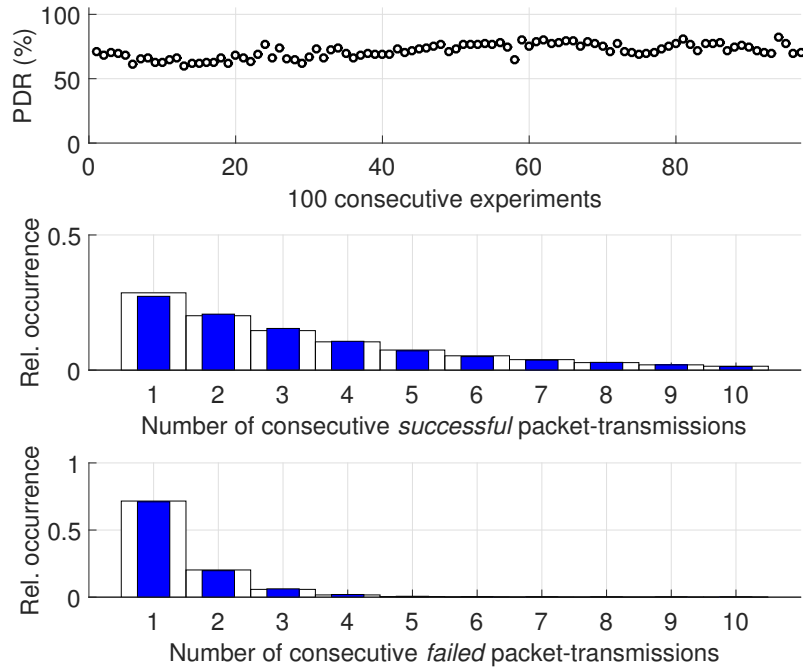
Figure 3.2: Top figure shows typical PDR values of multiple consecutive experiments performed over time, under a given condition of orientation, distance and packet size. Its variation and relative occurrence of consecutive successful/failed packets (colored bars) follows the same trend as a pure Bernoulli experiment (white bars). These plots correspond to the probability mass function (pmf) of geometric random variables.

Bernoulli process. To test our conjecture, we analyzed the histograms of the number of consecutive successfully transmitted packets and number of consecutive failed packets (colored bars in the middle and bottom part of Figure 3.2, respectively). Then, we generated a synthetic Bernoulli process with trial success probability p and 100000 trials, and we overlapped the corresponding histograms with those of the PDR measurements in Figure 3.2 (wider white bars behind the corresponding colored bars). Given the visibly good match between the histograms, we claim that our conjecture is true, and that our PDR experiment does follow a Bernoulli distribution.

The results of the link layer experiments are shown in Figure 3.3. Here, we characterize the two relative orientations that generated the strongest differences, only. Namely, the vehicles were positioned in parallel (solid line) or co-linearly (dashed) to each other
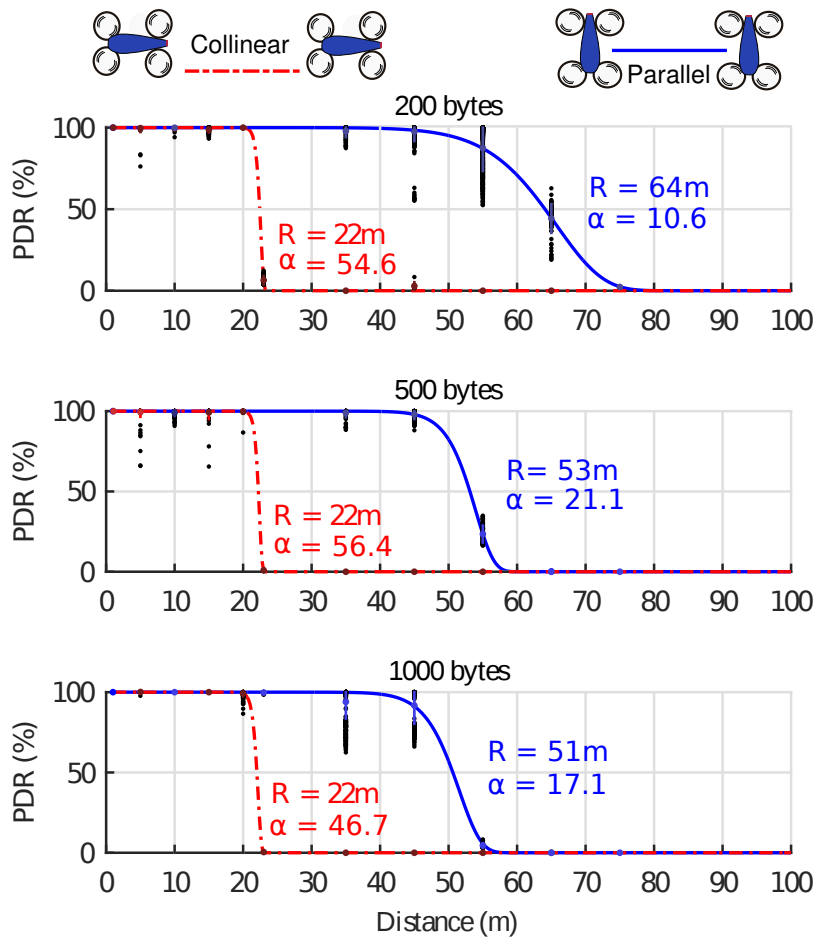
Figure 3.3:   Packet Delivery Ratio in a single link as a function of distance between sender and receiver. Packet size and relative orientation of the vehicles affect the ratio. Dots represent experimental data. Solid and dashed lines are fitting curves, based on the model developed in Section 3.3.

while transmitting packets. An immediate observation is that the relative orientation of the vehicles has a striking impact on the performance of the network.

The observed differences result from the non-omni-directionality of the antennas in the plane of flight. We believe this feature is common on COTS multirotors, since a good connection with ground controls is to be prioritized. Thus, this is an issue to consider when using communications between multiple AR Drone 2.0. Curiously, the different orientations impact not only the effective length of the link but also the steepness of the PDR reduction with distance. In fact, there is a very narrow region (about 3m) where the link suddenly changes from good to practically broken.

PDR depends also on the number of bytes being sent in a packet. More bytes mean less probability of delivery, as Figure 3.3 data shows, which is specially visible when we compare the three blue plots (parallel orientation). We can see a reasonable range difference between 200 and 1000-byte packets. The explanation is that for the same bit error rate, longer packets have more bits prone to suffer from errors. Curiously, the difference in PDR between packet sizes of 500B and 1000B is practically negligible in both orientations.

Distance is the third dimension that clearly affects the PDR. As other authors have concluded on other platforms (cf. Section 2.3), for short distances the PDR is sustainably high with negligible packet losses but, as distance grows, eventually it enters an unstable region where PDR drops, in average, almost linearly to zero where the link is considered broken.

The orientation aspect is rather relevant in a line topology as the one we are studying here. It is important to keep all vehicles' heading perpendicular to the network line itself in order to maximize the operation range of our network. Currently, we intend to use our bottom-facing camera to sense the environment (mainly ground monitoring) and so the top-end node (sensor node) as well as all other nodes can assume this optimal pose. However, when the front-camera is to be used, the worst-case orientation must

be assumed (collinear) for safety reasons, and so a multi-hop network will use shorter links.

3.3   Link Layer – Model

Analyzing the data set collected during the link experiments allows to create a mathematical channel model. This model is intended to easily predict the likely PDR value given the distance between two nodes, i.e., the link length l, for each orientation and packet size scenario. After an analysis of different family functions, we selected a negative exponential curve to fit our data which generic form is given by Equation 3.1, where $\beta = -\ln(2)/R^\alpha$ and d is link length.

$$p_l(d) = e^{-\ln(2)\cdot\left(\frac{d}{R}\right)^\alpha} = e^{\beta d^\alpha} \tag{3.1}$$

We believe this family of functions is a good fit for PDR data since it is a non-negative, strictly non-increasing function whose range matches that of our data, i.e., $[0,1] \in \mathbb{R}$. This function presents also a zero derivative at $d = 0$ and at $d \to +\infty$, which mimics collected data, namely the two plateaus at PDR=100% and 0%. A rather attractive feature of the fitting function proposed in Equation 3.1 is that it only needs two parameters. Parameter R describes the distance at which packet delivery is 50% ($R \in \mathbb{R}^+$, in meters) and the curve steepness depends directly on the parameter $\alpha \in \mathbb{R}^+_{>1}$. The model parameters were estimated using the MATLAB (2016) Curve Fitting Toolbox and are shown in Table 3.2 for different packet size and relative orientation of the vehicles. This table also shows the root mean squared error (RMSE$_e$) as an indication of the accuracy of our proposed model with respect to the raw data. We recognize that more data would improve the confidence on our model, nevertheless RMSE$_e$ values are already relatively low, generally below 2.5% with just two cases rising to near 9%, thus we consider the model accuracy to be enough for a set of envisaged applications.

Table 3.2: Parameters of the proposed PDR model for different conditions, namely packet size and orientation.

	Parallel	**Collinear**
200 bytes	$\alpha = 10.6$ $R = 64\text{m}$ $\text{RMSE}_e = 0.0911$ $(\text{RMSE}_\sigma = 0.0922)$	$\alpha = 54.6$ $R = 22\text{m}$ $\text{RMSE}_e = 0.0232$ $(\text{RMSE}_\sigma = 0.0232)$
500 bytes	$\alpha = 21.1$ $R = 53\text{m}$ $\text{RMSE}_e = 0.0256$ $(\text{RMSE}_\sigma = 0.0256)$	$\alpha = 22$ $R = 56.4\text{m}$ $\text{RMSE}_e = 0.0276$ $(\text{RMSE}_\sigma = 0.0276)$
1000 bytes	$\alpha = 17.1$ $R = 51\text{m}$ $\text{RMSE}_e = 0.0896$ $(\text{RMSE}_\sigma = 0.0898)$	$\alpha = 46.7$ $R = 22\text{m}$ $\text{RMSE}_e = 0.0105$ $(\text{RMSE}_\sigma = 0.0105)$

We also tried another fitting model, namely the well known logistic sigmoid function (Equation 3.2), which has similar basic characteristics.

$$p_l(d) = \frac{1}{1 + e^{-k(R-d)}} \tag{3.2}$$

However, it presented similar or slightly higher RMSE values, represented as RMSE_σ in Table 3.2, particularly in the cases of lower accuracy. Thus, we preferred the simple negative exponential curve model (cf. Equation 3.1). Having a model of link's PDR, we can model the corresponding throughput, by using the definition present in Equation 2.1.

Transmission speed B itself depends on two variables, namely the transmitter PHY layer bitrate and the packet size. It can be set and fixed along the course of a mission. Quite differently is PDR that is affected by several variables as we have shown. Moreover, B also depends on the maximum number of automatic retransmissions configured in the network device driver. It is well known that a higher number tends to signif-

icantly increase communication latency and consumed bandwidth when the channel conditions degrade. This may improve the PDR, but such improvement can be overridden by a degradation of the channel effective bandwidth. To minimize this undesired effect we carried out all our study with the lowest limit for retries allowed in our platforms (cf. Table 3.1).

3.4 Network – Model

Even in the best conditions, direct communication between a sensor-UAV and a ground station (GS) is severely compromised beyond 60m. To improve this range, we deploy relay-UAVs in between, on a line formation creating a network. Packets are routed from sensor to sink, passing through these relays. This way, each one of the individual links (also named hops) in the network is as short as needed to guarantee packets flow through. However, we want them to be as long as possible to minimize the total number of UAVs in use, which by consequence affects the mutual interference between nodes, and the overall end-to-end throughput.

Since we want to continuously stream as much information from the sensor-UAV as possible, we use a Time-Division Multiple Access (TDMA) scheme that guarantees higher utilization of the medium than a CSMA scheme. This way we avoid mutual interference giving each node periodic and dedicated access to the wireless medium for a different time interval – called a slot. Furthermore, as we envision the use of GPS equipped UAVs, the major concern of TDMA – synchronization – can be trivially solved by using the global clock time provided by such system. To simplify slot assignment, the network creates h distinct TDMA slots, where h is the total number of transmitter nodes in the network. For the sake of simplicity we consider the BS is not transmitting and thus h will also be the number of hops in the network. All slots have the same width, so the sensor-UAV can transmit at a maximum of one-h^{th} of its original rate. To minimize

the transport time of data from source to sink, time slots are sorted in descending order by distance to the sink.

Having these considerations, we can model the corresponding PDR throughput by using the following definition.

Definition 3.1 (Network PDR). *Network PDR – $p_n(d,h)$ – is the ratio of packets that are successfully transmitted end-to-end, and it depends on the PDR at every link used by the packets.*

Network PDR is the product of every hop's PDR, because a packet is only transmitted successfully if it is successfully transmitted on all h hops on its way. Note that hops/links are considered independent, given the TDMA scheme. If a network has h hops, and hop-i has length l_i, then the network's length (d), and network PDR ($p_n(d,h)$) are given by Equation 3.3.

$$p_n(d,h) = \prod_{i=1}^{h} p_l(l_i) \qquad d = \sum_{i=1}^{h} l_i \tag{3.3}$$

Theorem 3.1. *Network PDR – $p_n(d,h)$ – is maximized by considering that the $h-1$ relays are placed uniformly between the sensor-UAV and the BS, i.e., all h links have the same length $l = d/h$.*

Proof. Assume the network has h hops, and end-to-end length equal to d. Consider that all hops are modeled by the same PDR function. Consider also that the first hop has length $l_1 = d/h + x_1$, second hop has $l_2 = d/h + x_2$, etc., where:

$$\sum x_i = 0 \Leftrightarrow \sum l_i = d$$

Hence, the PDR product over h hops comes from Equation 3.3, and it is given by Equation 3.4.

$$\prod_{i=1}^{h} p_l(\mathbf{l_i}) = \prod_{i=1}^{h} e^{\left(\beta(d/h+\mathbf{x_i})^{\alpha}\right)} = e^{\left(\beta \sum_{i=1}^{h}(d/h+\mathbf{x_i})^{\alpha}\right)} \equiv f(\mathbf{X}) \tag{3.4}$$

To find the maximizers of this function, we use the method of Lagrange multipliers - a method that allows us to find maxima of $f(\mathbf{X})$ and its maximizers, subject to constraint of the form $g(\mathbf{X}) = 0$. For our problem:

$$f(\mathbf{X}) = f(\mathbf{x_1}, \dots, \mathbf{x_h}) = e^{\left(\beta \sum_{i=1}^{h}(d/h+\mathbf{x_i})^\alpha\right)} \tag{3.5}$$

and constraint function $g(\mathbf{X})$ is:

$$g(\mathbf{X}) = g(\mathbf{x_1}, \dots, \mathbf{x_h}) = \mathbf{x_1} + \dots + \mathbf{x_h} = 0 \tag{3.6}$$

We define the Lagrangian function $\mathcal{L}(\mathbf{X}, \lambda)$, s.t:

$$\begin{aligned}
\mathcal{L}(\mathbf{X}, \lambda) &= f(\mathbf{X}) + \lambda(g(\mathbf{X}) - 0) \\
&= f(\mathbf{X}) + \lambda(\mathbf{x_1} + \mathbf{x_2} + \dots + \mathbf{x_h})
\end{aligned} \tag{3.7}$$

Setting its gradient $\nabla_{\mathbf{X}, \lambda} \mathcal{L}(\mathbf{X}, \lambda) = 0$, we have:

$$\begin{cases}
\dfrac{\partial \mathcal{L}}{\partial \mathbf{x_1}} = \dfrac{\partial f(\mathbf{X})}{\partial \mathbf{x_1}} + \lambda = 0 & \text{(3.8a)} \\[2mm]
\dots & \text{(3.8b)} \\[2mm]
\dfrac{\partial \mathcal{L}}{\partial \mathbf{x_h}} = \dfrac{\partial f(\mathbf{X})}{\partial \mathbf{x_h}} + \lambda = 0 & \text{(3.8c)} \\[2mm]
\dfrac{\partial \mathcal{L}}{\partial \lambda} = (\mathbf{x_1} + \mathbf{x_2} + \dots + \mathbf{x_h}) = 0 & \text{(3.8d)}
\end{cases}$$

The partial derivative of $f(\mathbf{X})$ over x_i ($i \in [1, \dots, h]$) is:

$$\begin{aligned}
\frac{\partial f(\mathbf{X})}{\partial \mathbf{x_i}} &= f(\mathbf{X}) \left(\beta \sum_{i=1}^{h}(d/h+\mathbf{x_i})^\alpha \right)' \\
&= \beta \left(\sum_{i=1}^{h}(d/h+\mathbf{x_i})^\alpha \right)' f(\mathbf{X}) \\
&= \beta\alpha \, (d/h+\mathbf{x_i})^{\alpha-1} f(\mathbf{X})
\end{aligned} \tag{3.9}$$

Solving Equation 3.8a to Equation 3.8c, we see that the value of all partial derivatives is the same on the critical point. This means that, for any two partial derivatives, we

have:

$$\frac{\partial f(\mathbf{X})}{\partial \mathbf{x_i}} = \frac{\partial f(\mathbf{X})}{\partial \mathbf{x_j}}$$

$$\beta\alpha \left(d/h + \mathbf{x_i}\right)^{\alpha-1} f(\mathbf{X}) = \beta\alpha \left(d/h + \mathbf{x_j}\right)^{\alpha-1} f(\mathbf{X})$$

$$\left(d/h + \mathbf{x_i}\right) = \left(d/h + \mathbf{x_j}\right)$$

$$x_i = x_j \quad \text{note that } d/h + x > 0$$

(3.10)

We showed that all variables have the same value, and according to Equation 3.8d, it comes that $x_1 = x_2 = \ldots = x_h = 0$. Thus, the PDR is maximum when $x_i = 0, \forall i \in [1, h]$, which means that links have all the same size: $l_i = d/h + 0$.

$\square$

Definition 3.2 (Network Throughput). *Network throughput – ζ_n – is the available end-to-end throughput of a relay chain, and it depends on the end-to-end packet delivery ratio multiplied by the sender transmitted packets per second, .*

Regarding transmission, the multi-hop network has h transmitter nodes, so overall sensor node sends packets at a rate of B/h, due to the aforementioned TDMA constraints. Joining all the previous assumptions, network throughput as a function of distance and the number of hops ($\zeta_{\texttt{net}}(d, h)$) can now be computed:

$$\zeta_n(d, h) = \frac{B}{h} \cdot p_n(d, h) = \frac{B}{h} \cdot [p_l(d/h)]^h \tag{3.11}$$

For notation simplicity, we will use $\zeta_h(d)$ to refer to $\zeta_n(d, h)$ in the remainder of the document. For any given distance d, different throughput values can be achieved depending on the chosen number of hops h. The optimal number of hops (h_{opt}) for a given distance (d_0) is given by the maximizer of the throughput function, st.:

$$h_{opt} = \arg\max_{h} \left(\zeta_h(d_0)\right) \tag{3.12}$$

Choosing h appropriately, one can maximize throughput and define it solely as a function of distance (cf. solid line in e.g. of Figure 3.4), using Equation 3.13.

$$\zeta_{\text{max}}(d) = \max_{h}\left(\zeta_h(d)\right) \tag{3.13}$$

This comes from link-throughput function $\zeta_h(d)$ intrinsic properties, namely:

$$\exists^1 d_{xy} = d_{yx} : \zeta_x(d_{xy}) = \zeta_y(d_{xy}) \tag{3.14}$$

$$x < y < z \Rightarrow d_{xy} < d_{xz} < d_{yz} \tag{3.15}$$

$$x < y \Rightarrow \begin{cases} \zeta_x(d_{xy}) = \zeta_y(d_{xy}) & \text{(3.16a)} \\[2mm] \zeta_x(d) > \zeta_y(d), \forall d \in [0, d_{xy}) & \text{(3.16b)} \\[2mm] \zeta_x(d) < \zeta_y(d), \forall d \in (d_{xy}, +\infty) & \text{(3.16c)} \end{cases}$$

$$\forall x, y, z \in \mathbb{N}, \quad \forall d, d_{xy}, d_{xz}, d_{yx} \in \mathbb{R}_0^+$$

These three properties indicate that:

(i) Any two link throughput distance curves using A and B hops ($\zeta_A(d)$ and $\zeta_B(d)$, respectively), intersect only once at d_{AB} – Equation 3.14.

(ii) As the number of hops increases, intersection distance increases, too – Equation 3.15.

(iii) If $A < B$, then $\zeta_A(d)$ is higher than $\zeta_B(d)$ for all distances lower than d_{AB}, and vice-versa – Equation 3.16.

The proof of these properties is in the Annex. These properties are enough to show that maximum throughput function $\zeta_{\text{max}}(d)$ can be defined by Equation 3.17, solely as a

function of d.

$$\zeta_{\texttt{max}}(d) = \begin{cases} \zeta_1(d) & \text{if } d \in [0, d_{12}) \\ \zeta_2(d) & \text{if } d \in [d_{12}, d_{23}) \\ \dots \\ \zeta_{h_o}(d) & \text{if } d \in [d_{h_o-1,h_o}, d_{h_o,h_o+1}) \end{cases} \qquad (3.17)$$

Using Equation 3.1 and Equation 3.11 to describe $\zeta_h(d)$, frontier distances (d_{xy}) are obtained using Equation 3.18 (proof in Annex).

$$d_{xy} = \sqrt[\alpha]{\frac{\ln\left(\frac{y}{x}\right)}{\beta\left(x^{(1-\alpha)} - y^{(1-\alpha)}\right)}}, \quad \forall x, y \in \mathbb{N}, x \neq y \qquad (3.18)$$

Figure 3.4 shows the maximum network throughput function $\zeta_{\texttt{max}}(d)$, using a different colour for each section with a defined number of hops ($h \in [1, \dots, 5]$). PDR function used in the figure is defined by $\alpha = 10.6$. As this example shows, a network with a single hop would not be able to communicate when its length is around $1.5R$ or above. If hop count is incremented, throughput is maximized and communications are improved ($\approx 0.5B$).

3.5 Network – Experiments

3.5.1 Setup

We conducted several experiments to prove the multi-hop network concept. For this, we fixed some parameters across all experiments, while others such as number of relay nodes, the number of slots used in each TDMA round, and end-to-end distance were modified (cf. Table 3.3) .

In order to carry out multi-hop experiments we needed to implement the TDMA framework described before, over the IEEE802.11 standard currently installed. However, just for the sake of simplicity, and since each experiment lasted for only a few seconds,
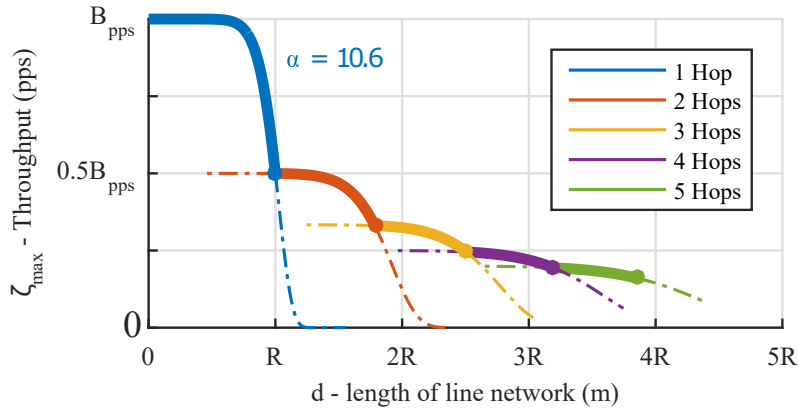
Figure 3.4: Maximum network throughput as function of distance – $\zeta_{max}(d)$, in packets per second. Each colour represents a different number of hops in use in the network, described by a different section of Equation 3.17. Number of hops $h \in [1, \ldots, 5]$, and updated at certain distances given by Equation 3.18. Link PDR assumes $\alpha = 10.6$.

Table 3.3: Experiment set-up for the AR Drone 2.0 vehicles on the multi hop network characterization.

Payload size	200 bytes
Orientation	Parallel
TX Slot time	100 ms
Number of hops	a) 1 , b) 2 , c) 3
Number of slots	a) 1 , b) 2 , c) 3
Guard interval	50ms (0ms for one hop)
Round period	a) 100ms, b) 300ms, c) 450ms
End-to-end distance	a) $0, 5, 10, 15, 35, 45, 55, 65, 75$m b) $70, 90, 110, 130, 150$m c) $105, 135, 165, 195$m

we decided to do a simplified synchronization at this point and leave the actual operational TDMA scheme for later implementation (Chapter 4). Thus, in this experiment, at the beginning of each experiment, each receiver node synchronizes its clock with the upstream routing node. The upstream node sends 10 packets containing its current clock time in the payload. The receiver node measures the difference between the time when the packet was received and the time-stamp included in the packet. The receiver computes the average difference between timestamps, and updates its clock to be the same as the transmitter. This is done once per experiment. However, this synchronization incurs in an extra error that depends essentially on jitter affecting the time of flight of each packet, from end-to-end application layer, which is not very precise. Consequently, we used large guarding windows between TDMA slots. This is orthogonal to our goal of increasing relative throughput altering the network topology. Figure 3.5 shows typical packet traces on a tree-UAV line network. These were captured by Wireshark (2016), over two TDMA rounds. Guarding windows are rather visible, during which there is no communication activity. Each colour identifies a different slot, i.e., packets sent from a each UAV. Round is 450ms long, and transmission slot is 100ms. While within a slot, rate peaks up to 400kB/s, end-to-end rate is less than $\approx$ 90kB/s.

3.5.2 Results

Network experimental results are shown in Figure 3.6. Each dot shows the throughput obtained during the experimental campaigns using different number of relays considering also different end-to-end distances. Transmission rate was set to $B \approx 800$pkts/s. No recovery, retransmissions or redundancy mechanisms were added to the network traffic, beyond the minimum number of automatic retransmissions as referred before (Table 3.1). All the experiments considered 200-byte long packets with all UAVs parallel to each other. This can be converted to a (maximum) data rate of 160kB/s Blue dots are one hop data, i.e., a single link. It comes from the the link-PDR data showed at the top
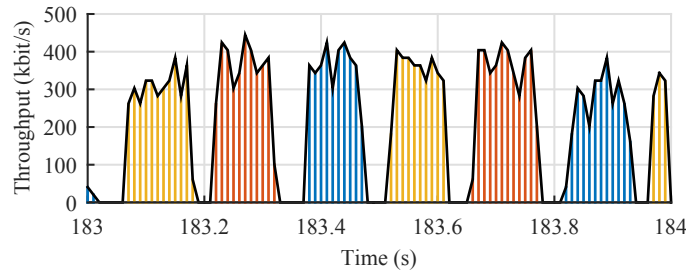
Figure 3.5:   Typical packet traces on a line network with three hops. End-to-end a rate is ≈ 90kB/s. Each colour identifies packets sent from a different UAV. Round is 450ms long, and transmission slot is 100ms. These packet traces were captured by a monitor node, using Wireshark (2016).
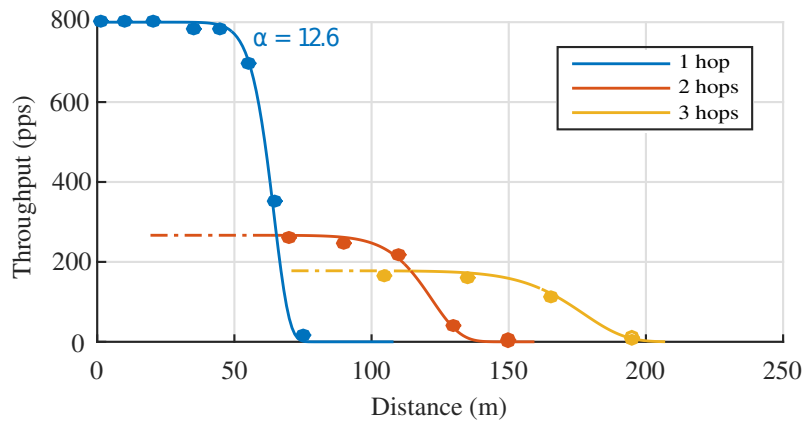
Figure 3.6:   Measured throughput at different end-to-end network lengths, using distinct number of hops. Inside their slots, nodes transmit 200-byte packets at a rate of $B \approx 800$ pkts/s. UAVs are all oriented parallel to each other.

of Figure 3.3. In red and yellow, we see the multi-hop throughput. The network maintains its throughput above 200pkts/s until 110m, which is unfeasible with a single hop. With an extra hop, the network continues to communicate to ≈ 170m, at ≈ 100pkts/s. This represents around one-eighth of the maximum speed (at 1m). The red and yellow curves from Figure 3.3, regarding two and three hops, are generated using the model equations derived in the previous section. The experimental data and the model visibly match. Due to the large guarding windows used in the TDMA round, these equations consider a reduction in the available throughput. Besides the simple division by the

number of slots h, we had to account for the actual time available for communications per slot. In our case that means 100ms every 150ms, i.e., a factor of 2/3, leading to a combined reduction of $1/h \times 2/3$ at every hop section ($h > 1$).

3.6 Multi-hop Network Summary

We focused on creating a chain network of UAVs to increase their range of operation. In particular, we characterized the communications of COTS UAVs, namely the AR Drone 2.0, using their native wireless IEEE802.11 interface. We started by analyzing the packet delivery ratio on a UAV-to-UAV link and we reached two main conclusions, namely that 1) our platform is not omnidirectional in the flight plane and 2) the vehicles achieve a maximum direct range of communication of 75m, if they are oriented in parallel to each other and transmitting relatively short packets. Packet delivery ratio is reduced significantly if the link length is any longer. We proposed increasing the range of the network with a TDMA-based multi-hop topology using other UAVs as relays. The performance of such model was studied and the optimal number of relays that provide maximum throughput was deduced. Finally we validated these results with extensive experimental campaigns.

This work is a first step towards setting up an extendable multimedia streaming system for inspection of difficult to access assets, from tall buildings to bridges and process control plants.

Chapter 4

Self-Synchronized Network TDMA

In this chapter, we design and analyze a new overlay Time Division Multiple Access (TDMA) protocol for use over WiFi that self-synchronizes transmitters, and is based on RA-TDMA (Oliveira et al., 2015). This work has been reported preliminary in (Pinto et al., 2017a). The way this TDMA mechanism operates is described as follows.

In a network with n nodes willing to transmit, a unique slot out of n is assigned to each. A slot is characterized by an unique, sequential ID and a time span, also known as slot-length s. A node is allowed to transmit any en-queued packets during this time span, every T units of time. This time is usually named TDMA round period. The main purpose of TDMA is to guarantee that nodes do not suffer from medium access starvation, i.e., 1) all nodes are able to transmit, and 2) these transmissions are free from interference from other nodes. Hence, time slots must not overlap each other, i.e., no simultaneous transmissions are allowed. One by one, divided in time, all nodes access the wireless medium to orderly transmit; looping from node with slot ID 1 to node with slot ID n, the process repeats every round period T.

The main problem implementing such system is the distributed nature of the wireless mobile network. Each node has its own clock, and the reference of time is not absolute. Without proper synchronization, nodes will set overlapping slots and trans-

missions. For this reason, we will now explain our method for self distributed synchronization. This mechanism is to overlay CSMA/CA, and not to replace it. This way, we can cope with alien traffic of other networks in the area and out of order transmissions in our set of UAVs while our system is converging to a synchronized solution.

4.1   Synchronization Method

We follow an adaptive distributed clockless approach similar to that in (Oliveira et al., 2015). Its operation is now explained in detail. Each node has an internal clock, from where current epoch time is extracted (aka POSIX time, i.e., the number of seconds since January 1st, 1970) with nanosecond resolution. Clock time is converted to milliseconds yielding t_{epoch}, and it is used to compute local current round-time t_{rnd} which is given by the modulo operation with the TDMA round period T (in ms). This operation is depicted in Figure 4.1. Since t_{epoch} is a fractional number, we need to refine the classical integer modulo operation, yielding Equation 4.1.

$$t_{rnd} = \left(\lfloor t_{epoch} \rfloor \mod T \right) + \text{frac}(t_{epoch}) \qquad \text{where} \quad \text{frac}(x) = x - \lfloor x \rfloor \in \mathbb{Z}^{0+}, x \in \mathbb{R}^{0+}$$

$$(4.1)$$

In this chapter and the following ones, we assume that round-period is a positive integer, constant and known in advance. Each node is assigned one transmission slot, which is defined by both its (constant) ID and (*shift-able*) boundaries. Slot ID is a unique constant identification, a positive integer, pre-assigned to each node $\in [1, n]$. Slot boundaries are defined by a beginning and ending round-time marks - t_B and t_E. Note that since round-time is cyclic with period T, t_B might be greater than t_E. A transmitter node may send queued packets if and only if its local current round time t_{rnd} is *in-between*
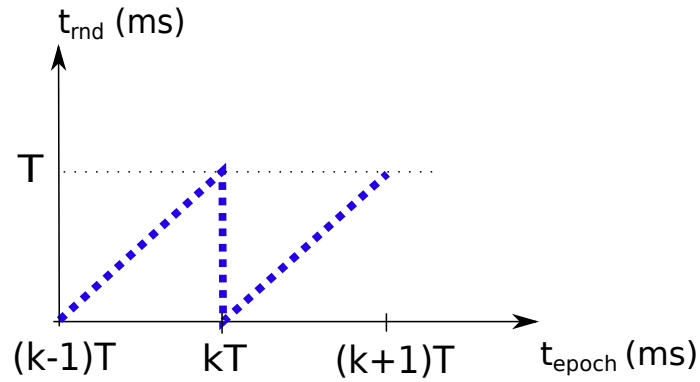
Figure 4.1: Round period time t_{rnd} is obtained from the epoch time t_{epoch} via modulo operation as Equation 4.1 defines.
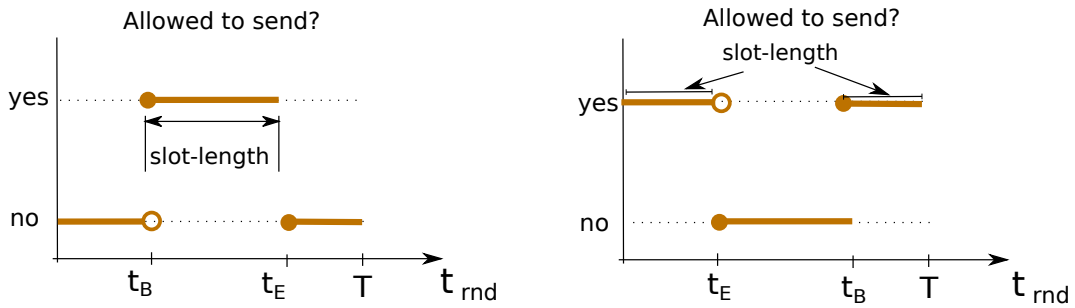
Figure 4.2: Defining a TDMA slot and respective boundaries. Left) Boundary t_B is less than t_E. Right) Boundary t_B is greater than t_E. *Inside* a slot, a node is allowed to transmit packets (cf. Equation 4.2). Slot length is also depicted (cf. Equation 4.3).

these boundaries. Mathematically, this is defined by Equation 4.2, and exemplified in Figure 4.2.

$$\text{ALLOWED TO SEND IFF} = \begin{cases} t_B \leq t_{rnd} < t_E & \text{if } t_E > t_B \\ t_B \leq t_{rnd} \cup t_{rnd} < t_E & \text{if } t_E < t_B \end{cases} \quad t_B, t_E \in [0, T] \quad (4.2)$$

Slot-length s is defined has the time-span a node has available to transmit, and it is depicted in Figure 4.2, too. It is considered constant along this chapter, and defined by

Equation 4.3.

$$
s = \begin{cases} t_E - t_B & \text{if } t_E > t_B \\ (T - t_B) + t_E & \text{if } t_E < t_B \end{cases} \quad t_B, t_E \in [0, T] \tag{4.3}
$$

In order to synchronize slots, we have designed an algorithm where nodes shift their own slot boundaries as needed to avoid overlapping transmissions. A receiver node shifts its own slot boundaries by analyzing the delay of incoming packets (Δ). If in the receiver's perspective packets are arriving earlier than expected, the receiver *pulls back* its own slot, and transmits earlier to erase idle times. If in the receiver's perspective packets are arriving later than expected, the receiver *delays* its own slot, and starts transmitting later to avoid simultaneous transmissions. This works on the premise that all nodes will shift as much as necessary their own slots boundaries until no delay is detected. After this point, no overlapping or minimal overlapping will occur. One of the benefits of this system is that even if alien traffic delays some node's transmission due to underlying CSMA/CA mechanism, the system will adapt accordingly until a new stable point is reached.

We will now describe how to synchronize two nodes, namely node i – the transmitter, and node j – the receiver. First step is to compute packet delay. It is calculated by the difference between current local time of the receiver at the receiving instant $t_{rx}^{(i)}$ and the estimated *a-priori* time of arrival of that same packet $t_{rx}^{\widehat{(i)}}$, such that:

$$
\Delta = t_{rx}^{(j)} - t_{tx}^{\widehat{(j)}} \tag{4.4}
$$

Given the distributed nature of the synchronization, $t_{rx}^{\widehat{(j)}}$ computation is not trivial. The receiver node, with slot ID j and boundaries $t_B^{(j)}$ and $t_E^{(j)}$, needs to acquire two

metrics within the header of incoming packets, namely:

1. transmitter's slot ID – i

2. message position within sender's slot – p

Message position can be viewed as the elapsed time from the beginning of the transmitter's slot until the packet has been sent. Assuming all n slots have the same length s, a receiver with slot ID j considers its transmitting neighbor – node i – has a beginning slot boundary $t_B^{(\hat{i})}$ given by:

$$t_B^{(\hat{i})} = \left(t_B^{(i)} + (j - i)s + T \right) \mod T \qquad \text{where } j, i \in [1, n] \text{ and } s = T/n \qquad (4.5)$$

This estimation process is exemplified on Figure 4.3; the receiver node, with slot ID 3 and slot boundaries $[t_B^{(3)}, t_E^{(3)}]$, estimates the boundaries of slots ID 1 ($t_B^{(\hat{1})}$) and ID 2 ($t_B^{(\hat{2})}$).
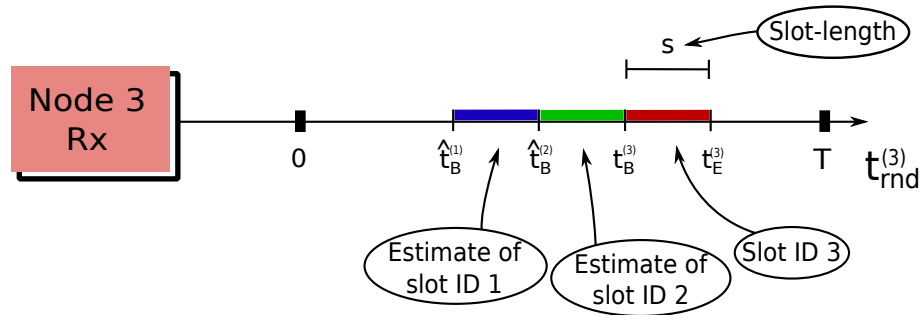
Figure 4.3: Node with slot ID 3 estimates boundaries of slots ID 1 and ID 2, by use of Equation 4.5.

If nodes were synchronized (delay $\Delta = 0$), a receiver i would estimate the time of arrival of a given packet from slot j to be:

$$t_{tx}^{(\hat{i})} = t_B^{(\hat{i})} + p \qquad (4.6)$$

Therefore, returning to Equation 4.4, it comes that delay of any given packet k is estimated by the difference of the actual moment we have received the packet – $t_{rx}^{(i)}$ – and our estimate – $t_{tx}^{\widehat{(i)}}$, yielding Equation 4.7.

$$\Delta_k = t_{rx}^{(i)} - \left(t_B^{\widehat{(i)}} + p \right) \tag{4.7}$$

In order to estimate the delay between these two nodes, for each received packet, delay is measured and used to compute a global average Δ, such that:

$$\Delta = \frac{\sum_k \Delta_k}{k} \tag{4.8}$$

Finally, before the beginning of slot j, the receiver adjusts the phase of its own slot by this same quantity (cf. Equation 4.9).

$$slot' = slot + \Delta \Leftrightarrow \begin{cases} t'_B = t_B + \Delta \\ t'_E = t_E + \Delta \end{cases} \tag{4.9}$$

Figure 4.4 illustrates this whole process using the individual timelines of the transmitter and receiver, as well as a global absolute timeline.

4.2   Experimental Results

This algorithm has been implemented on our AR Drone 2.0 platform. Figure 4.5 exemplifies the synchronization process of a relay node in a multi-hop network, where it is receiving packets from one neighbor, and retransmitting these same packets to another neighbor node. Each line along the x-axis contains events occurred within a round period. The y-axis has the ever-increasing round counter.
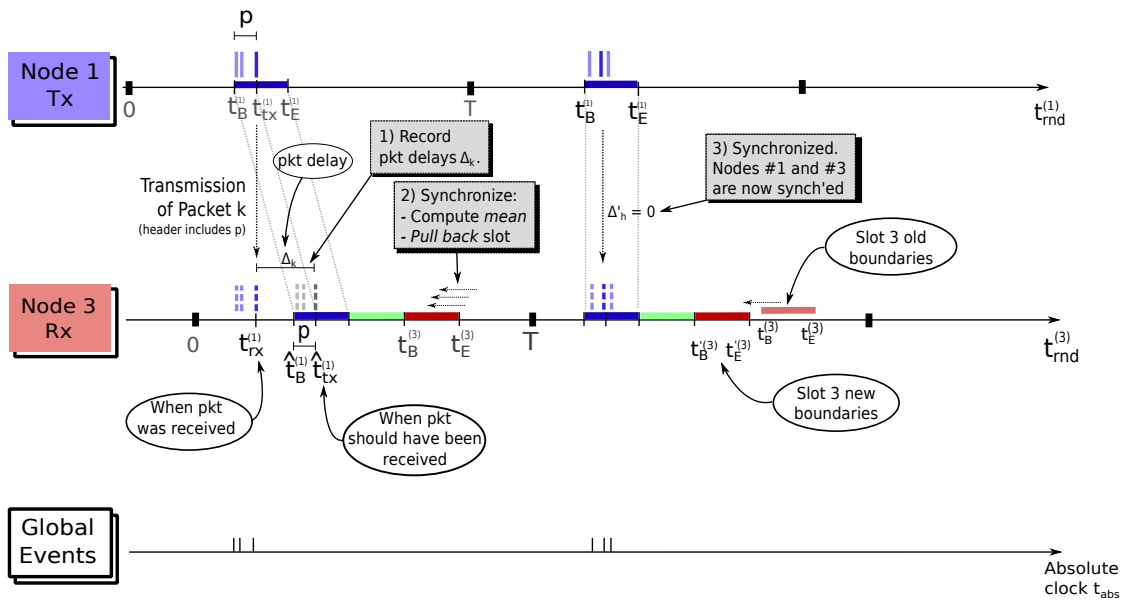
Figure 4.4: Illustration of TDMA self-synchronization mechanism taking place.

Red squares represent received packets; their x-axis position shows the round-time when they were received. Gray squares represent packets transmitted (relayed) by the node. Its current time slot (boundaries) is shown as long thin black rectangles below the gray squares. Figure 4.5 also shows the slot phase adjustment, visible through the slot shifts to the right, caused by delays in the packets received in the previous slot due to retransmissions and interference.

Note that slots are not strictly isolated as typical in TDMA implementations. Residual overlaps can occur and are sorted out with the native WiFi CSMA/CA arbitration. This feature allows our protocol to operate in open networks. Interference caused by other traffic and hidden nodes will appear as delays affecting packets, thus delaying the following slots. When triggered frequently, the slot shifting increases the actual TDMA round period, causing a reduction of the effective channel bandwidth available. The protocol transparently adapts to these cases.
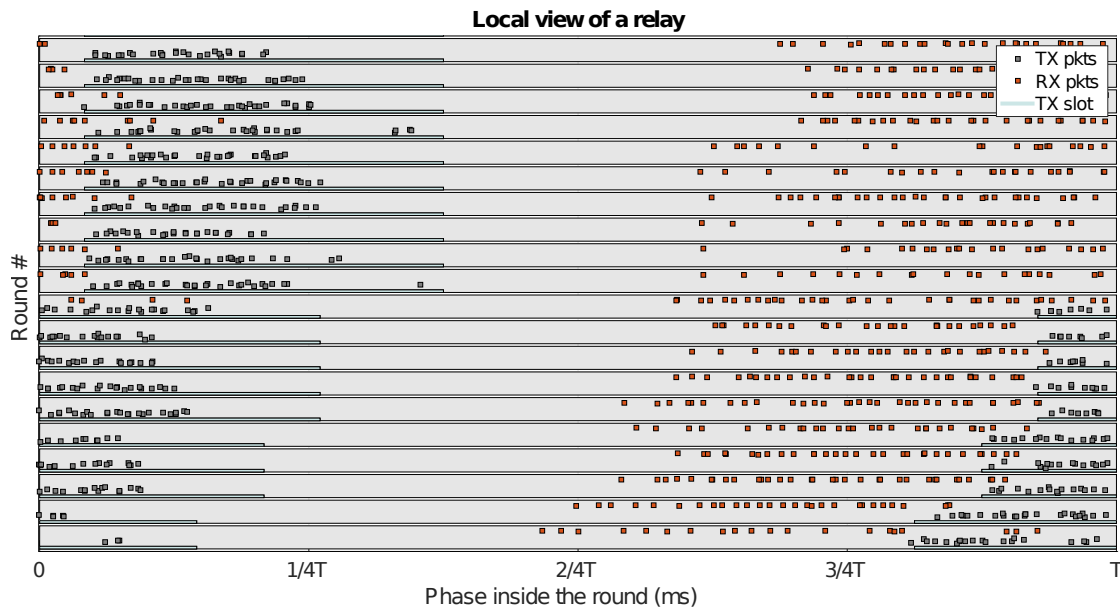
Figure 4.5: Packet reception (red) and transmission (gray) in a relay, using slots 1 and 2 of a TDMA round. Phase misalignment is due to adaptive and clockless synchronization.

4.3   Synchronization Summary

In this chapter we presented the TDMA mechanism where most of the work in this dissertation lies upon. The main idea of the TDMA is to guarantee that all nodes are entitled a slot of time, periodically, to transmit freely of mutual interference. For that, we need to assign different slots to each node, and synchronize their clocks or transmissions. To solve that, we created a distributed method of slot synchronization that relies on the idea that a receiving node can measure delay of each individual packet in regards of the transmitter. Knowing the average packet delay, the receiver node will make an estimation of the transmitter begin and end of its slot, and moves or shifts its own slot accordingly. In the end, all nodes reach a point of no overlapping transmissions. In the next chapter we will see how we can further improve the TDMA scheme by allowing slots to have variable slot size.

Chapter 5

Dynamic Slot-length for TDMA

In this chapter, we design and analyze a new data-link protocol optimized for multi-hop online video streaming applications. Our system provides soft real-time guarantees in terms of delay such that operators can interactively pilot UAV fleets while maximizing reliability to provide reasonable video Quality-of-Service (QoS). This work has been reported preliminary in (Pinto et al., 2017c), and later extended in (Pinto et al., 2017a).

Figure 1.12 shows an example scenario where two UAVs (sensors) are being manually controlled to track desired features in the area of interest using video streams. Meanwhile, other UAVs are relaying the streams across the network to the Ground-Station. We will first show that a naive solution that uses commodity WiFi hardware on commercial multirotor UAVs struggles in terms of both reliability and timeliness. We propose a new protocol, that adapts the length of the TDMA slots in a distributed fashion to minimize in-network queuing. Our protocol works on the assumption that the backlog found towards the middle of the network is the main cause of end-to-end delay. By controlling the length of the TDMA slots according to the status of their associated transmitters, we can mitigate throughput asymmetries among network links and achieve end-to-end throughput equalization. We analytically and experimentally show the advantage of our TDMA protocol on a four-hop network of quadrotor UAVs stream-
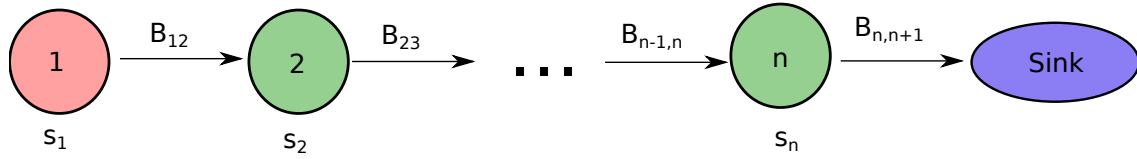
Figure 5.1: Multi-hop Line Network model. Bandwidth of each link is represented by $B_{i,j}$. Variable s_i represents the units of time (time slot) available to each node to transmit periodically every T.

ing video, when compared to a naive approach based on using WiFi directly. Thus, our contributions are:

- DVSP – a new TDMA framework that adapts its slots using a model of actual link bandwidth;

- A proof of DVSP convergence under distributed operation;

- Experimental validation with UAVs.

The chapter is organized as follows. Section 5.1 states the problem we are addressing, followed by the solution we propose in Section 5.2, namely DVSP. Section 5.3 presents the respective protocol used in our implementation. Section 5.6 shows the experimental results that confirm the expected improvements. Section 5.7 concludes the chapter.

5.1   Problem Statement

Consider a multi-hop wireless network architecture with n UAV nodes and a sink, as illustrated in Figure 5.1 where the aim is to deliver real-time message streams, such as live videos, produced by one or more sources to a unique sink, i.e., a ground station, through a line of $n-1$ relays. We have studied before (Pinto et al., 2017d) the delay-range trade-off implied by using UAV relays to connect a live video source to a ground station. Each relay provides additional range but it must use a buffer to hold received packets,

which are forwarded later to the following node, downstream in the line topology, thus adding delay. However, transient reductions of the outgoing packet rate with respect to the incoming rate require further increasing the buffer depth that, in turn, increases the end-to-end network delay. This delay must be below a certain deadline so that an operator in the base station can still interact with the sensor(s) UAV(s) through the live video stream(s) effectively. This corresponds to upper bounding the buffer depth.

For comparison purposes, we establish a baseline case in which the source generates as much data as it can transmit to its immediate neighbor, i.e., the first relay. In turn, relays forward immediately every received packet to the next hop, subsequently closer to the sink. In this case, transmissions are carried out using the native distributed and asynchronous CSMA/CA arbitration of WiFi, without any further control.

As expected, this approach quickly degrades under high load. Transient bandwidth asymmetries between the links of each relay lead to packet buffering, longer delay and eventually to overflow and packet losses. Increasing buffer size is not a solution, as it will increase end-to-end delay. Figure 5.2 illustrates this situation with asymmetric links resulting from either different PHY rates, asymmetric antennas, localized interference generating asymmetric packet loss that leads to different retries at the MAC level, or simply because some node accesses the medium more often under the CSMA/CA random arbitration.

Furthermore, the line topology with concurrent asynchronous network access is prone to hidden nodes, which can contribute to degrade the network performance even more. Both buffer overflow and hidden nodes decrease link PDR and lead to high end-to-end delays. As a consequence the video stream at the sink will be both chopped and lagged.

This is the problem we are tackling in this chapter, i.e., how to manage the traffic in a line multi-hop network, adjusting to variations in instantaneous bandwidth of individual links so to minimize in-network queuing and reduce end-to-end delays.
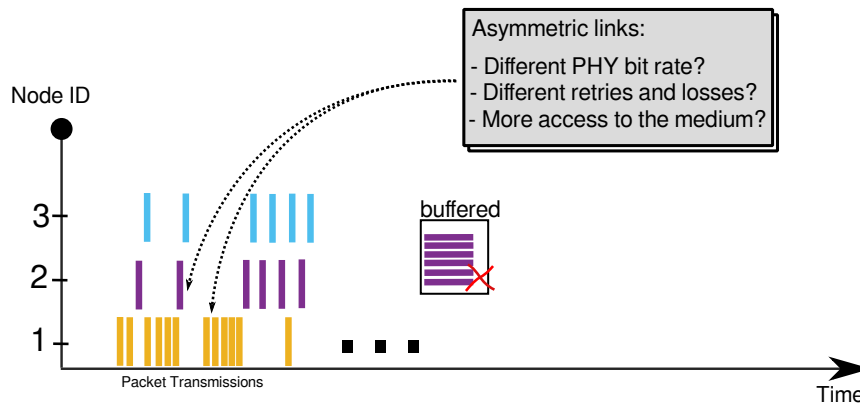
Figure 5.2: Inefficiencies such as buffered packets and wasted bandwidth are created when all nodes are allowed to transmit concurrently and asynchronously, and links have different characteristics such a PHY rate or packet loss. The source, node 1, is transmitting faster than node 2 can cope with.

5.2 A Variable Slot-length TDMA Solution

TDMA schemes typically provide an exclusive (collision-free) slot to every transmitter in the network, granting a fixed length to the slots of all N nodes ($s_1 = s_2 = \cdots = s_N = T/N$) as Figure 5.3 illustrates. Due to bandwidth irregularities across links, we propose a dynamic slot length assignment where each node has an exclusive time slot as Figure 5.4 exemplifies[1].

Time slot length is dynamically set according to the current bandwidth status of the network to mitigate buffer queuing. We define bandwidth $B_{i,j}$ as the average capacity in bytes per second available to transmitter node i to send data to receiver node j (cf. Figure 5.1). Knowing both bandwidth estimates of all links in the line network and (fixed) round period T, we can compute the optimal slot length (s_i) of every node that guarantees no buffered data, and therefore minimum delay. Under our TDMA assumptions, in average a node i receives *rcv* bytes per second from its up stream node $(i-1)$,

---

[1]Channel reuse could eventually improve bandwidth, but not decrease delay which is our major concern.
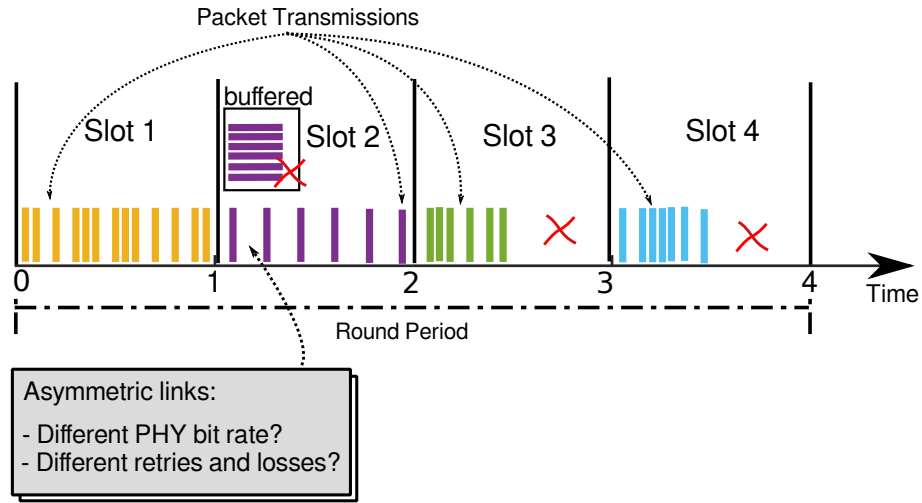
Figure 5.3: Inefficiencies such as buffered packets and wasted transmission time are also created under TDMA when all time slots are of equal length and links are asymmetric.
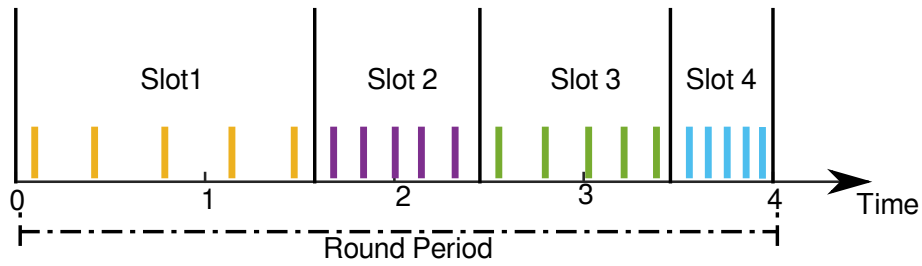
Figure 5.4: Using DVSP, each slot has different length, to guarantee that every node has enough time to transmit all received data from its upstream neighbor. All nodes are sending the same amount of data.

and sends out *snd* bytes of data per second to its down stream node ($i+1$), such that:

$$rcv_{i-1,i} = \frac{s_{i-1}}{T} B_{i-1,i} \qquad\qquad snd_{i,i+1} = \frac{s_i}{T} B_{i,i+1} \qquad\qquad (5.1)$$

To enforce long term stability of the network with limited buffering, we need to

ensure these rates coincide and round period stays constant, thus Equation 5.2.

$$\begin{cases} s_1 B_{1,2} = s_2 B_{2,3} = \cdots = s_n B_{n,n+1} \\ s_1 + s_2 + \cdots + s_n = T \end{cases} \tag{5.2}$$

Solving the system in Equation 5.2 for s_i yields the slot-length solution Equation 5.3.

$$s_i = \frac{(B_{i,i+1})^{-1} T}{\sum_{j=1}^{n} (B_{j,j+1})^{-1}} \tag{5.3}$$

In order to implement this system in a centralized manner, one node (*GS* for instance) would need to collect every link bandwidth estimation and then disseminate the corresponding slot length to every node (cf. (Facchinetti et al., 2004)). We assume that slot order is fixed and chosen to minimize delay from source to sink. This means the slot order in the TDMA round matches the physical order in the link topology from source to sink, to favor propagation of source data. Therefore, collection of link bandwidth estimates would take one round period, and dissemination would take n rounds to complete, where n is the number of nodes excluding the *GS* (same as the number of slots)

There are two main problems with this approach: (1) if the *GS* misses some of the bandwidth estimations or fails to distribute the new slot length to every node, we can get inconsistencies leading to different round periods and potential slots overlapping; and (2) buffers can fill up before the dissemination of slots is completed.

Alternatively, we chose to design a distributed approach where each node sets the best slot length for itself and the node up stream. Since by design, stream data is coming exclusively from neighbor node(s), one node can do flow control and instruct its neighbor to decrease its transmission slot, thus reducing buffering needs. Based on this idea, we created a new protocol for live streaming in multi-hop lines that we call Distributed Variable Slot-length Protocol (DVSP).

5.2.1 Distributed Variable Slot-length Protocol (DVSP)

We propose a distributed variable time slot allocation protocol where the task of time slot adjustment is locally performed by every pair of neighbor nodes. In this approach, initial time slot length values are iteratively redefined until convergence to their optimal values as defined in Equation 5.3. Each node adapts its own slot s_i and up stream node slot s_{i-1} simultaneously such that the sum of the slot lengths is kept constant, thus keeping the round period unchanged. By changing up stream slot time, we can quickly solve buffer problems at the local source, and propagate this effect to the initial data source node. Using an equation system similar to Equation 5.2, and assuming that 1) node i has an accurate estimation of current bandwidth available in the previous and next links, respectively $B_{i-1,i}$ and $B_{i,i+1}$, and 2) bandwidths are constant for a round period, yields Equation 5.4, for iteration k.

$$\begin{cases} s_i^{(k+1)} + s_{i-1}^{(k+1)} = s_i^{(k)} + s_{i-1}^{(k)} \\ s_{i-1}^{(k+1)}.B_{i-1,i} = s_i^{(k+1)}.B_{i,i+1} \end{cases} \tag{5.4}$$

This system of equations result in two recursive functions (Equation 5.5).

$$\begin{aligned} s_i^{(k+1)} &= \zeta_{i-1,i}\left(s_i^{(k)} + s_{i-1}^{(k)}\right) \\ s_{i-1}^{(k+1)} &= \overline{\zeta}_{i-1,i}\left(s_i^{(k)} + s_{i-1}^{(k)}\right) \end{aligned} \tag{5.5}$$

where

$$\zeta_{i-1,i} = \frac{B_{i-1,i}}{B_{i-1,i} + B_{i,i+1}}$$

$$\overline{\zeta}_{i-1,i} = \frac{B_{i,i+1}}{B_{i-1,i} + B_{i,i+1}} = 1 - \zeta_{i-1,i}$$

$$\overline{\zeta}_{i-1,i}, \zeta_{i-1,i} \in\ ]0,1[\quad,\quad i \in \{2,\cdots,n\}$$

5.3   Protocol

Regarding DVSP, we design an handshake protocol to make slot changes consistent and robust to failure. As Figure 5.5 depicts, node i initiates the process computing Equation 5.5. It then sends a request of a new slot length ($s_{i-1}^{(k+1)}$) to node $i-1$, and locks it self to incoming requests from any other node. This guarantees that until the handshake is completed no other handshakes are initiated that could corrupt the round period value (sum of all slot times). In the case this request packet is missed, it is repeated once per round until the handshake is finalized. Upon reception, node $i-1$ sets up its slot length to the new value present in the request ($s_{i-1}^{(k+1)}$). Then, at the beginning of node $i-1$'s slot time, this new length is already used. Every packet contains information about the current transmitter time slot length in its TDMA header to allow slot synchronization. Therefore, as node i receives packets from node $i-1$, the former will know that the new and expected time slot length is being used. Node i changes its own slot time length to new value $s_i^{(k+1)}$. This terminates the handshake.

By design, nodes under handshake lock to incoming requests from other nodes. In a line network, where slots are ascendantly ordered, this means that all nodes with even slot IDs (or odd), can perform handshakes with all upstream odd neighbors (or even), simultaneously. In a following moment, nodes with odd slot IDs (or even) can initiate requests.

5.4   Convergence

To prove the convergence of this method assume a line network with $n+1$ nodes, n of which are transmitters and so n time slots (the sink does not transmit). We name the corresponding time slots length s_1 (source), s_2 (first relay), etc.. We assume every node starts (iteration $k = 0$) with the same time slot length $s_1^{(0)} = \ldots = s_n^{(0)}$. According to
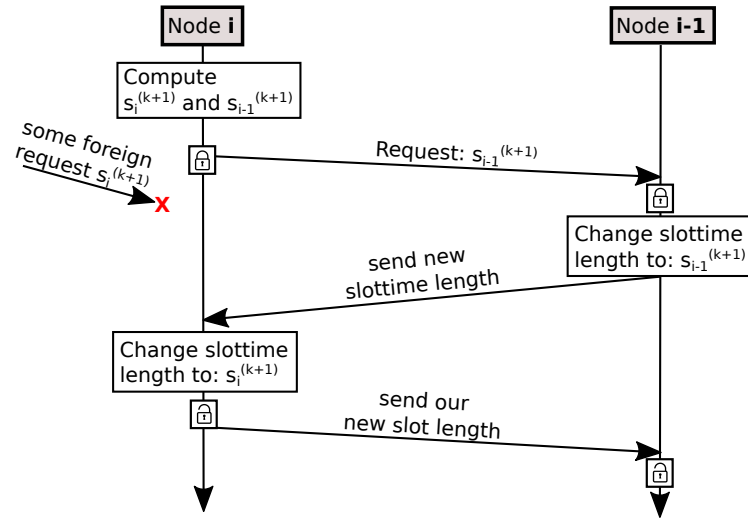
Figure 5.5: Handshake diagram of Distributed Variable Slot-length Protocol (DVSP).

our protocol, in the subsequent iteration ($k = 1$) all nodes with even ids ($i = 2, 4, \ldots$) initiate handshakes with upstream nodes ($i = 1, 3, \ldots$, respectively). For odd number of transmitters, node n remains unchanged. Thus:

$$s_1^{(1)} = \zeta_{1,2}\left(s_1^{(0)} + s_2^{(0)}\right)$$
$$s_2^{(1)} = \overline{\zeta}_{1,2}\left(s_1^{(0)} + s_2^{(0)}\right)$$
$$s_i^{(1)} = \ldots$$
$$s_{i+1}^{(1)} = \ldots$$
$$s_n^{(1)} = s_n^{(0)}$$

$$\text{where } i \in \{3, 5, \ldots\}$$

At the next iteration ($k = 2$), odd nodes ($i = 3, 5, \ldots$) initiate their handshakes with up stream even nodes ($i = 2, 4, \ldots$), and node 1 is unchanged. If n is even, node n is also

unchanged. Thus:

$$s_1^{(2)} = s_1^{(1)}$$

$$s_2^{(2)} = \zeta_{2,3} \left(s_2^{(1)} + s_3^{(1)} \right)$$

$$s_3^{(2)} = \overline{\zeta}_{2,3} \left(s_2^{(1)} + s_3^{(1)} \right)$$

$$s_i^{(2)} = \ldots$$

$$s_{i+1}^{(2)} = \ldots$$

$$s_n^{(2)} = s_n^{(1)}$$

where $i \in \{4, 6, \ldots\}$

We can convert the system into a more compact form using matrix notation, where A and B are $(n \times n)$ matrices, as shown next, and $\mathbf{s}$ the $(n \times 1)$ time slot vector:

$$\mathbf{s}^{(k+1)} = A\mathbf{s}^{(k)} \quad \wedge \quad \mathbf{s}^{(k+2)} = B\mathbf{s}^{(k+1)}$$

$$A_n = \begin{bmatrix} \zeta_{1,2} & \zeta_{1,2} & 0 & \cdots & \cdots & 0 & 0 \\ \overline{\zeta}_{1,2} & \overline{\zeta}_{1,2} & 0 & \cdots & \cdots & 0 & 0 \\ 0 & 0 & \zeta_{3,4} & \zeta_{3,4} & \cdots & 0 & 0 \\ \vdots & \vdots & \overline{\zeta}_{3,4} & \overline{\zeta}_{3,4} & \cdots & 0 & 0 \\ & & & \cdots & & \zeta_{ij} & \zeta_{ij} & 0 \\ & & & \cdots & & \overline{\zeta}_{ij} & \overline{\zeta}_{ij} & 0 \\ 0 & 0 & \cdots & \cdots & \cdots & 0 & 1 \end{bmatrix}$$

$$B_n = \begin{bmatrix} 1 & 0 & \cdots & \cdots & \cdots & \cdots & 0 & 0 \\ 0 & \zeta_{2,3} & \zeta_{2,3} & 0 & \cdots & \cdots & 0 & 0 \\ 0 & \overline{\zeta}_{2,3} & \overline{\zeta}_{2,3} & 0 & \cdots & \cdots & 0 & 0 \\ 0 & 0 & 0 & \zeta_{4,5} & \zeta_{4,5} & \cdots & 0 & 0 \\ \vdots & \vdots & 0 & \overline{\zeta}_{4,5} & \overline{\zeta}_{4,5} & \cdots & 0 & 0 \\ & & \cdots & 0 & 0 & \zeta_{ij} & \zeta_{ij} & 0 \\ & & \cdots & 0 & 0 & \overline{\zeta}_{ij} & \overline{\zeta}_{ij} & 0 \\ 0 & 0 & \cdots & \cdots & \cdots & 0 & 0 & 1 \end{bmatrix}$$

If n is even, last row and column of A_n do not exist. If n is odd, last row and column of B_n do not exist.

Combining two iterations at a time, yields:

$$\mathbf{s}^{(2k)} = (BA)^k \mathbf{s}^{(0)} = C^k \mathbf{s}^{(0)}$$

To prove this system converges, we show that in the limit:

$$\lim_{k \to \infty} (\mathbf{s}^{(2k+2)} - \mathbf{s}^{(2k)}) = \mathbf{0}_n \Leftrightarrow \lim_{k \to \infty} \left(C^{k+1} - C^k \right) = \mathbf{0}_n$$

Performing an eigenvalue decomposition on C, results in $C = VDV^{-1}$, where D is a diagonal matrix with C's eigenvalues. We know that $C^k = (VDV^{-1}) \cdots (VDV^{-1}) = VD^kV^{-1}$, therefore:

$$\lim_{k \to \infty} \left(C^{k+1} - C^k \right) = \mathbf{0}_n \Leftrightarrow$$

$$\lim_{k \to \infty} \left(VD^{k+1}V^{-1} - VD^kV^{-1} \right) = \mathbf{0}_n \Leftrightarrow$$

$$\lim_{k \to \infty} \left(VD^k(D - I_n)V^{-1} \right) = \mathbf{0}_n$$

If in the limit $D^k(D - I_n)$ is zero, then the equation holds and the system converges. Exploring the structure of D, yields:

$$D^k(D - I_n) = \begin{bmatrix} \lambda_1^k(\lambda_1 - 1) & 0 & 0 \\ 0 & \ddots & 0 \\ 0 & 0 & \lambda_n^k(\lambda_n - 1) \end{bmatrix}$$

From the expression above, we see if the modulo of the eigenvalues is less than or equal to 1, then $\lim_{k \to \infty} \lambda_i^k (\lambda_i - 1) = 0$, and the system converges. For the general case, we know that the maximum modulo of the eigenvalues of C, also known as spectral radius $\rho(C)$, is indeed not greater than 1. This comes from Gelfand's formula corollary that states that the spectral radius of the product of two matrices is less or equal to the product of spectral radius of both matrices:

$$\rho(C) = \rho(BA) \leq \rho(B)\rho(A)$$

We can prove that matrices A and B have spectral radius 1. Note that A has n rows, and by design $\lfloor n/2 \rfloor$ pairs of rows are linear dependent, so there are $\lfloor n/2 \rfloor$ zero-valued eigenvalues.

$$\lambda_1 = \ldots = \lambda_{\lfloor n/2 \rfloor} = 0$$

All other $\lceil n/2 \rceil$ eigenvalues are in fact 1. Knowing that the eigenvalues of A^T are the same of A for any matrix, we can trivially find the remaining $\lceil n/2 \rceil$ eigenvectors v_i that make $A^T v_i = 1 v_i$ equation true, because all rows add up to 1. An example is shown below.

$$A^T v_1 = \begin{bmatrix} \zeta_{1,2} & \overline{\zeta}_{1,2} & 0 & \cdots & \cdots & 0 & 0 \\ \zeta_{1,2} & \overline{\zeta}_{1,2} & 0 & \cdots & \cdots & 0 & 0 \\ 0 & 0 & \zeta_{3,4} & \overline{\zeta}_{3,4} & \cdots & 0 & 0 \\ \vdots & \vdots & \zeta_{3,4} & \overline{\zeta}_{3,4} & \cdots & 0 & 0 \\ \vdots & \vdots & \cdots & & \zeta_{ij} & \overline{\zeta}_{ij} & 0 \\ \vdots & \vdots & \cdots & & \zeta_{ij} & \overline{\zeta}_{ij} & 0 \\ 0 & 0 & \cdots & \cdots & \cdots & 0 & 1 \end{bmatrix} \begin{bmatrix} 1 \\ 1 \\ 0 \\ \vdots \\ \vdots \\ \vdots \\ 0 \end{bmatrix} = \begin{bmatrix} 1 \\ 1 \\ 0 \\ \vdots \\ \vdots \\ \vdots \\ 0 \end{bmatrix}$$

It is clear from the example above that the vector v_1

$$v_1 = \begin{bmatrix} 1 & 1 & 0 & \cdots & 0 \end{bmatrix}$$

is an eigenvector. In the same way, it is clear that generically all vectors v_i

$$v_i = \begin{bmatrix} 0 & \cdots & 1_{2i-1} & 1_{2i} & \cdots & 0 \end{bmatrix}^T$$

with exactly $n-2$ zeros and two consecutive ones in an odd and even index are eigenvectors and have the corresponding eigenvalue 1. When n is odd, there is an extra eigenvector $v_{\lceil n/2 \rceil}$ that also has an associated eigenvalue 1, namely:

$$v_{\lceil n/2 \rceil} = \begin{bmatrix} 0 & \cdots & \cdots & 1 \end{bmatrix}^T$$

The rationale used for matrix A can also be used for matrix B, and we have now proved that both matrices have a spectral radius equal to 1 ($\rho_A = \rho_B = 1$), and therefore the whole distributed system converges.
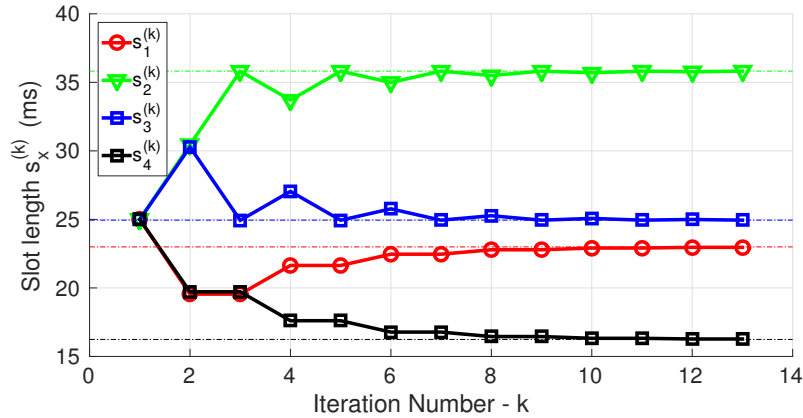
Figure 5.6: Example of slot length convergence in a network with four slots. For any bandwidth values, and for any number of nodes it is proven that the distributed system converges to the global solution.

Figure 5.6 shows a mock example of the distributed algorithm running on four nodes – the source is node 1 ; relays are nodes 2, 3 and 4 and are ordered from source to sink. Bandwidths were randomly selected and the round period set to $T = 100$ms. We can see the slot length of each node (bold lines) changing over thirteen iterations, and converging within 5% of the final value in 6 iterations. That limit is the global solution

given by Equation 5.3, represented by dashed lines. Note how nodes at the tip of the network (1 and 4), only change every other iteration. All other nodes change at every iteration.

Bandwidth changes as UAVs move, due to antenna orientation and path properties, but inspection uses slow velocity and frequent hovering, and bandwidth statistical variations take several seconds. Conversely, our protocol can converge in less than 1s assuming an iteration every round period and a realistic configuration of T=100ms and 3 relays.

To show the speed of convergence we have simulated the convergence process under different conditions and network size. Figure 5.7, Figure 5.8, Figure 5.9 and Figure 5.10 show the result of running the algorithm for 200000 random networks of 4, 6, 10 and 12 hops. Each node is given a random value for bandwidth. The x-axis represents the relative difference of bandwidth among the different nodes. Y-axis shows the number of iterations needed to be within 5% of the steady-state solution. The red dot represents the median. Pink and blue boxes represent 50% and 90% percentiles around the median, respectively.

As we can see, the more different the bandwidths are more iterations are needed to converge as it is expected. Furthermore, the bigger the network more time is taken to converge, too. Nevertheless, we can see that in worst case scenarios (top of the whiskers), convergence is still relatively fast as long as bandwidths are not too different.

5.5   Worst Case Delay

In a line network with n hops, packet end-to-end delay d_{wc} is the sum of the time taken by the packet while being transmitted over the air at all links (d_{tx}), plus the time a packet spends within buffers, waiting to be sent (d_w), yielding:

$$d_{wc} = d_{tx} + d_w \tag{5.6}$$

Time d_{tx} can be considered an affine function of hop count n, since payload size P is fixed and PHY bit-rate R, too. So $d_{tx} = nP/R$.

In Figure 5.4, one can see that every node transmits the same amount of information during its own slot. In this situation, buffer usage does not increase, and in the worst case we can consider that buffers are consistently full. We consider all nodes have the same buffer size U. This way, a new packet entering the system at the source waits till all buffered packets are sent, at each node. At each round T, all links are able to send the same amount of data $k^{(1)} = B_j s_j, \forall j \in [1, n]$, and since there are no concurrent transmissions there is no back-off time to consider. Therefore, the worst case delay is:

$$d_w^{(1)} = n \left\lceil \frac{U}{k^{(1)}} \right\rceil T \tag{5.7}$$

where, using the global solution Equation 5.3,

$$k^{(1)} = \frac{T}{\sum\limits_{i}^{n} B_i^{-1}}$$

The best case is when all buffers are empty ($U = 1$) and as expected, it takes one round to deliver the packet.
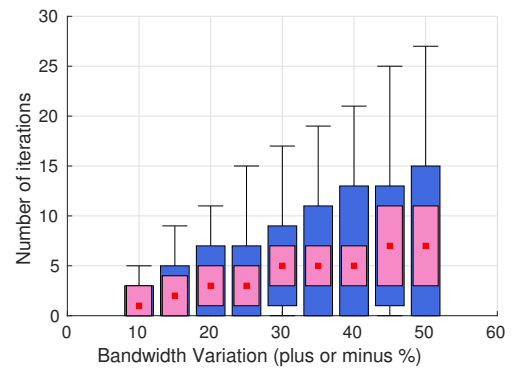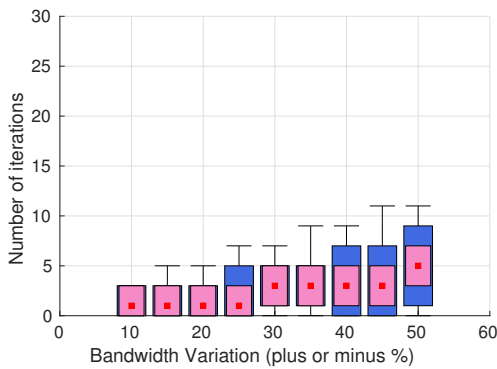
Figure 5.7: DVSP convergence with 4 hops   Figure 5.8: DVSP convergence with 6 hops
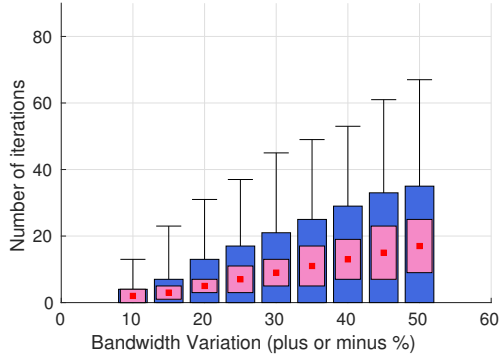
Figure 5.9:   DVSP convergence with 10 hops
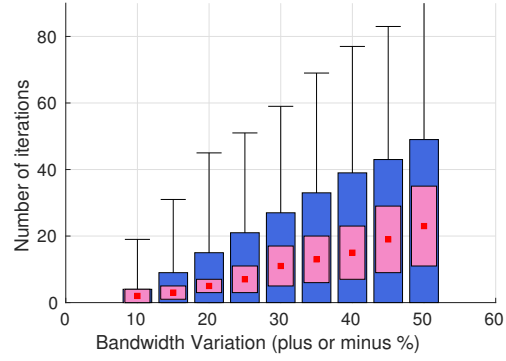
Figure 5.10:   DVSP convergence with 12 hops

Using the same time slot at every node as depicted in Figure 5.3 (*rigid* TDMA case), each node is able to send a different amount of data during its own time slot, and therefore the worst case is when the downstream node has a lower bandwidth than its upstream neighbor, and as such, buffers keep filling or keep full at all times. For such, when a packet reaches its next hop, its buffer is full and has to wait for U packets to be delivered before it proceeds to the next hop. Furthermore, all slots have the same length, but different bandwidths. So, each node can send at most $B_i.s_i$ amount of data per round; they actually send $k^{(2)}$, the minimum of all hops since all sent data comes from the upstream nodes, st.:

$$k^{(2)} = \min_i \left(B_i.s_i \right) \quad , \forall i \in [1, n] \tag{5.8}$$

we have $d_w^{(2)}$ st:

$$d_w^{(2)} = n \left\lceil \frac{U}{k^{(2)}} \right\rceil T \tag{5.9}$$

Under rigid TDMA, delay $d_w^{(2)}$ is guaranteed to be never better than DVSP delay $d_w^{(1)}$, since $k^{(2)}$ is never greater than $k^{(1)}$. We prove this by showing that since under rigid

TDMA all slots have the same size T/n, yields:

$$k^{(1)} = \frac{T}{\sum_i^n B_i^{-1}} \geq \min_i (B_i).\frac{T}{n} = k^{(2)} \tag{5.10}$$

$$\Leftrightarrow \sum_i^n B_i^{-1} \leq n\frac{1}{\min_i (B_i)} \tag{5.11}$$

Furthermore, buffer usage U will be lower in DVSP by design than with rigid TDMA slots.

When using the native WiFi CSMA/CA, the worst case delay for a packet to be delivered is not exactly determined since it depends on the link load and the time taken by the back-off mechanism. Nevertheless, under CSMA there is no guarantees of balanced throughput, leading to strong queuing delays as in rigid TDMA case.

5.6 Evaluation

In this section, we evaluate delay and packet delivery under immediate routing (traditional *CSMA/CA*) and under TDMA with adaptive time slots (*DVSP*). Despite being less important, end-to-end goodput or in other words video frame rate is also measured to guarantee that we compare both methods fairly.

5.6.1 Setup

The experiments were taken inside a laboratory with Parrot (2012) AR.Drone 2.0 UAVs, in fixed locations as Figure 5.11 shows.

One UAV is simultaneously source, using its frontal camera, and sink, to facilitate delay measurements. The video stream is sent through other UAVs in a circular route, returning back to the sink. The number of hops is varied from two to four ($n = 2 \ldots 4$) skipping some relays along the path (Figure 5.11). With DVSP, we chose a round period of $T = 100$ms and the number of slots is updated to match the number of hops. Queues
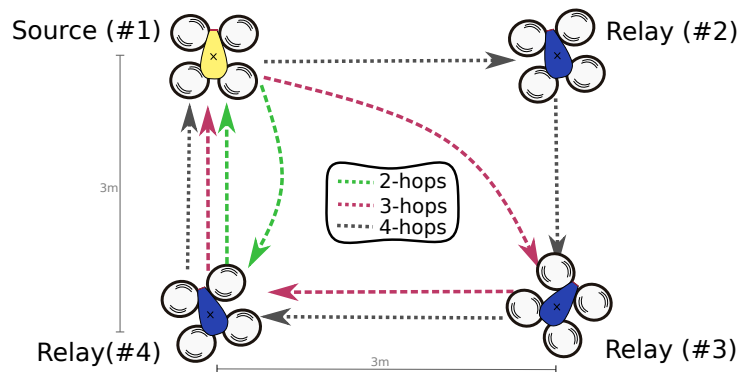
Figure 5.11: Three possible different topologies used during the experiments. Depending on the desired number of hops, traffic is routed through different paths. Under DVSP, the number of slots in use is also updated.

in the relays are limited and, when overflowing, the system will drop oldest packets first.

All nodes were set to operate in the same IEEE 802.11g ad-hoc network at a bit rate of 24Mbit/s. This bit rate guarantees that we can produce data faster than the channel capacity can support, and therefore we are not limited by the processing power of our platform/camera.

Each video stream experiment lasted for roughly 180 consecutive seconds, limited by local log file storage, during which one of the two methods was used. Each frame has 57600 bytes divided in 50 packets that are to be transmitted. Each packet corresponds to one horizontal line of pixels in one image frame. The source is programmed to capture a new frame only if the transmission queue has room for at least 50 packets.

To cause notable asymmetry in the links, the transmitter of the last hop (#4) was set to transmit at 10dBm where all other nodes were set at 15dBm. During a typical video stream scenario, links have different lengths or/and are affected by different attenuation factors due to obstacles or anisotropic antennas, for instance.

5.6.2 Delay

Figure 5.12 shows the histograms of end-to-end delay measurements of successful packets using different number of hops. Red thinner bars show the case of CSMA/CA while blue thicker bars are used for DVSP. We consider end-to-end delay to be the elapsed time between a packet being successfully sent for transmission at the source and being received at the sink. Naturally, the average delay and its variance increase with hop count, but DVSP is consistently better than CSMA/CA. With two-hops, delay increases approximately up to 75% when CSMA/CA is in use. Overlaid dashed lines are Gaussian curves with the same average and variance as the histograms, to merely provide a visual notion of these metrics.

5.6.3 Packet Delivery

Due to buffer overflow, packets are expected to be dropped under heavy load. This translates to a low packet delivery ratio or PDR. Figure 5.13 shows that phenomena when CSMA/CA is in use. The average PDR is far from 100%, specially when more and more relays are added. With CSMA/CA, relays receive packets at a higher rate than they can retransmit. This means that the source is actually sending more data than the network can handle. With DVSP, the source has a periodic slot to transmit data and DVSP shortens its duration whenever the packets are not going through, down in the link, effectively doing a kind of flow control and avoiding network overload. Thus, PDR is close to 100%. With four hops, we obtain gains of 50% in PDR. Figure 5.15 shows a snapshot of the video stream at the sink. With CSMA/CA (right), the low PDR manifests as black lines on the image (missing data). When using DVSP (left), video streaming is visibly improved and frames are generally complete.
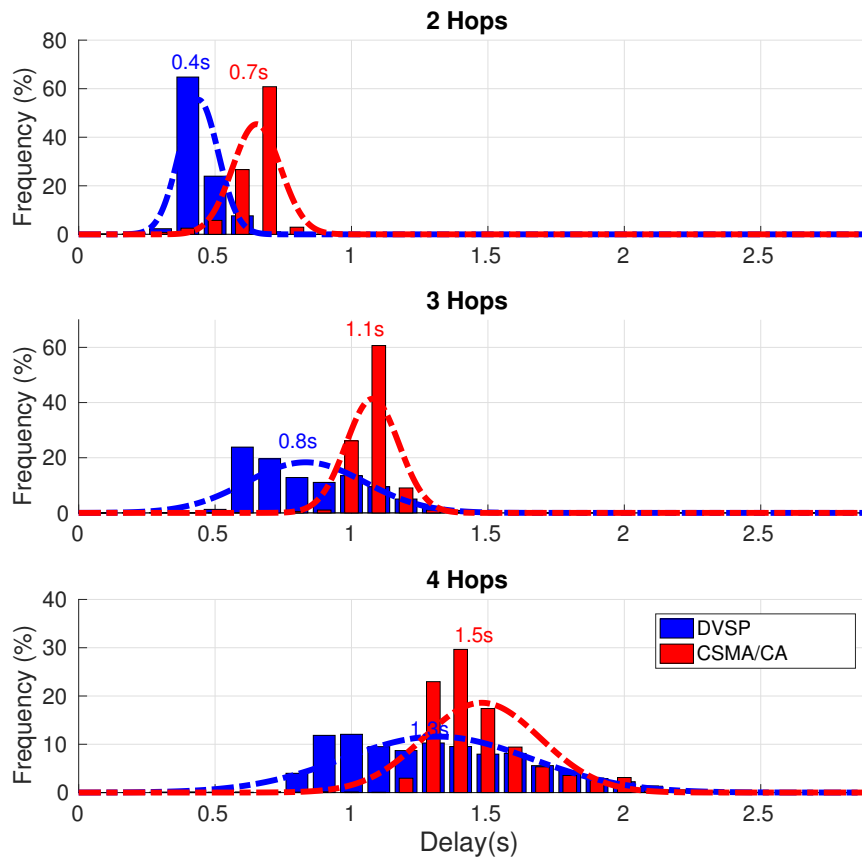
Figure 5.12: Histogram of measured end-to-end delay of each packet with CSMA/CA (red thinner bars) and with DVSP (blue thicker bars), using different number of network hops. It is clear that the average delay increases with hop count, but it is always better when DVSP is in use.
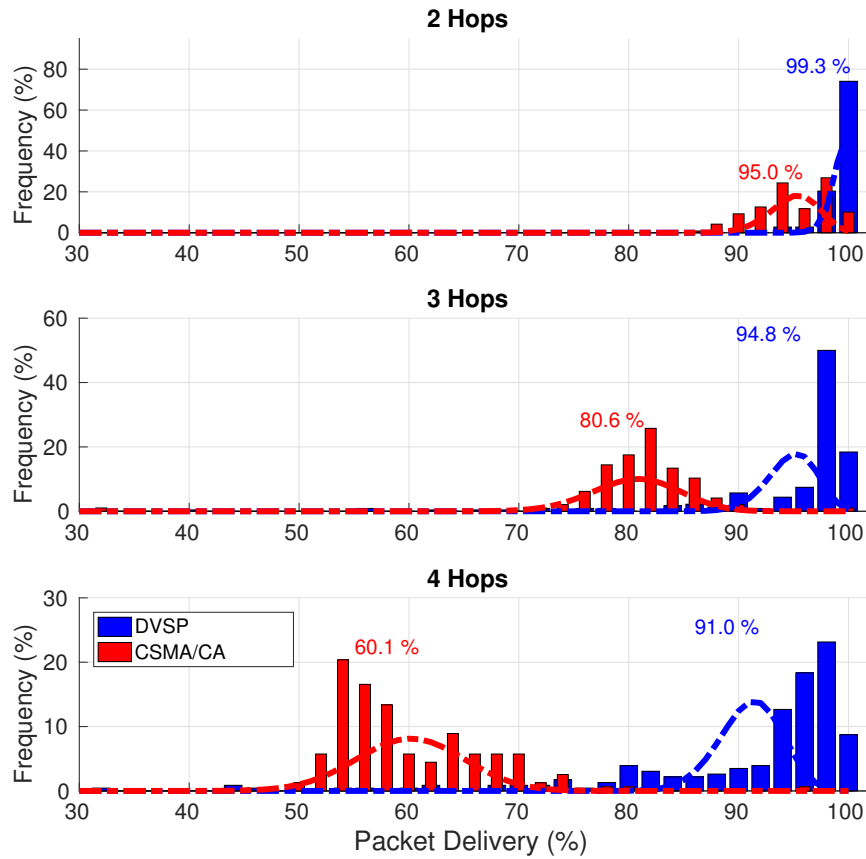
Figure 5.13: Histogram of measured end-to-end packet delivery ratio. There is a noticeable improvement with DVSP, specially when the number of hops increases. Packet loss occurs essentially due to buffer overflow.

5.6.4 Goodput

The last analyzed metric is goodput, which measures application payload data received at the sink per second. As we can see in Figure 5.14, more hops imply less goodput since there are more transmitters sharing the medium, thus end-to-end bandwidth is divided accordingly. Unlike delay and PDR, there is no difference on average goodput between both transmission control methods. This is actually expected since, under heavy load, nodes always have some packets in their buffer (DVSP case) or their buffers are always
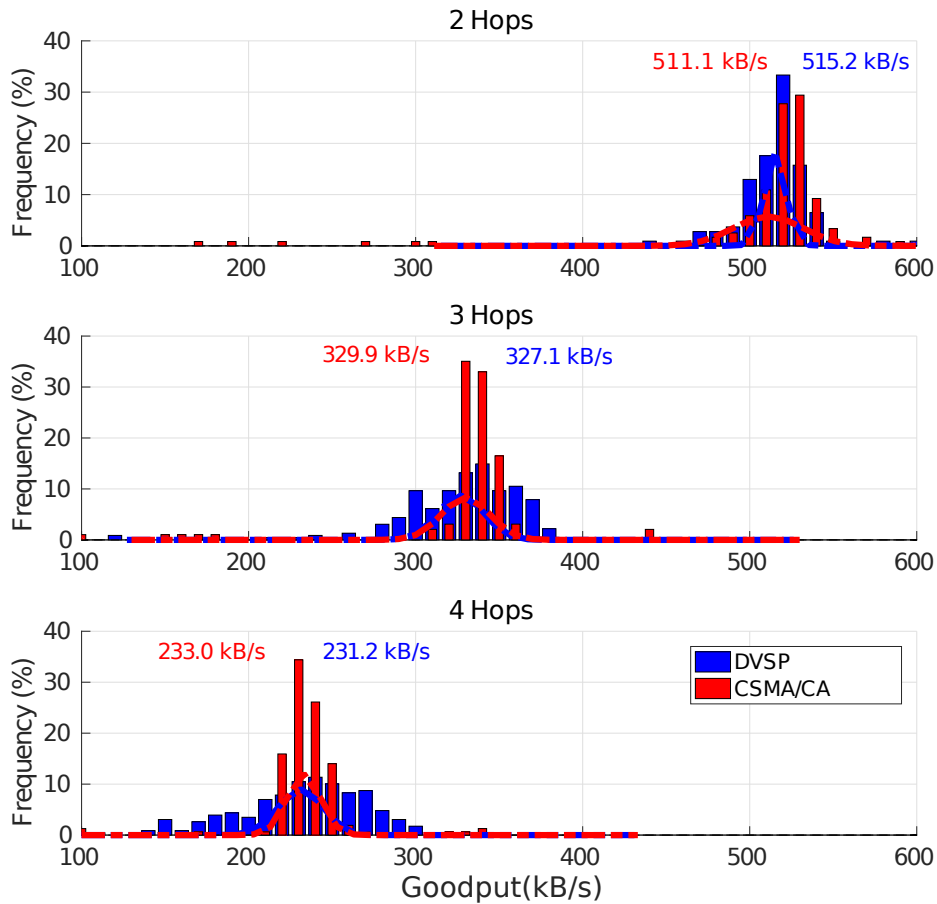
Figure 5.14: Histogram of measured end-to-end goodput, i.e., actual application payload data received at the sink per second. More hops imply less goodput since there are more transmitters sharing the channel. There is no difference, in average, in this metric between both methods.

full (CSMA case), and therefore the medium ends up being used at maximum capacity either way. Therefore, the end-to-end goodput is determined by the slowest link in the network in both methods. The fact that variance is higher with DVSP is explained by the constant adaptation of the time slots, which causes data to arrive at the sink in bursts, unlike the CSMA/CA scenario.

Figure 5.15: Snapshot of the video stream at the sink. With CSMA/CA (on the right), relays cannot handle every received packet, dropping some that appear as black lines in the image. Under DVSP (on the left), video streaming is visibly improved and frames are generally complete.

5.7 Dynamic Slot-length Summary

In this chapter, we showed that due to asymmetry among network radio links, simply relaying packets immediately over the typical CSMA/CA medium access control leads to large queuing delays or high packet drops. To remedy this problem, we propose a novel distributed adaptive TDMA overlay protocol called DVSP, for Distributed Variable Slot-length Protocol, that balances the amount of data each node transmits every round in order to minimize data buffering. We proved that this distributed approach converges to the optimal global solution using only local information. Experimental results show that without loss in goodput, our DVSP protocol outperforms immediate relaying in both network delay and packet delivery ratio. Despite not showing in the chapter, we also carried out some experiments with typical TDMA implementation using fixed equal slots. The results were similar to those of immediate relaying.

Chapter 6

Relay Placement

The potential of using relay drones to increase communication range as been demonstrated in Chapter 4, while in Chapter 5 we proposed an adaptive mechanism to coordinate transmissions to increase PDR and reduce end-to-end latency to mitigate asymmetries in the network links characteristics. This work has been reported in (Pinto et al., 2017b).

In this chapter we follow a complementary approach to mitigate link asymmetries acting on the placing of relays. In particular, we design and analyze a new protocol that adjusts the positions of the relays to improve throughput balancing packet delivery ratio (PDR) in multi-hop online video streaming applications (Figure 1.12). We first show that a naive solution using commodity WiFi hardware on commercial multirotors struggles to stream data at high speeds when links are created based on distance. In fact, obstacles, antennas, local interference, etc, can cause significant asymmetries among links, even with similar length, causing different error rates and throughput, thus negatively impacting the network end-to-end features. Therefore, we propose a protocol to improve the network by balancing the quality of its links, thus their capacity, moving the relay nodes adequately.

Our protocol relies on distributed online PDR measurement in which each node
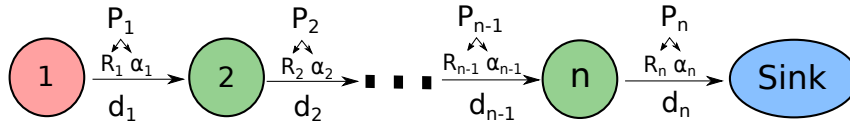
Figure 6.1: Multi-hop line network model. The PDR of link i, between nodes i and $i+1$, is P_i with parameters R_i, α_i, and its length is d_i.

assesses both of its links, in-bound and out-bound directions, and determines where to move to, along the network axis, to balance the respective PDR. We analytically and experimentally show the advantage of our protocol when compared with an equal-link-length approach on a three hop network of real live video streaming drones. Our contributions are:

- a new TDMA overlay protocol named Dynamic Relay Placement (DRP);

- experimental validation in a real scenario streaming video over three hops.

The next section shows the problem statement and the respective related work. Then, Section 6.2 presents the proposed solution. Section 6.4 shows results and Section 6.5 concludes the chapter.

6.1   Problem Statement

Consider a multi-hop wireless network architecture with n UAV nodes and a sink (Figure 6.1) aiming at online video streaming produced by one source (eventually more) to a unique sink i.e. a ground station. Each node buffers received packets and retransmits them in dedicated slots as explained earlier. We assume a buffer size based on the amount of delay that can be tolerated for remote operation.

The work in Chapter 3 considered each link PDR to depend on link-length, orientation and packet size. The operational scenario considered open space, similar packets and aligned UAVs leading to similar link properties. In such case, the general function
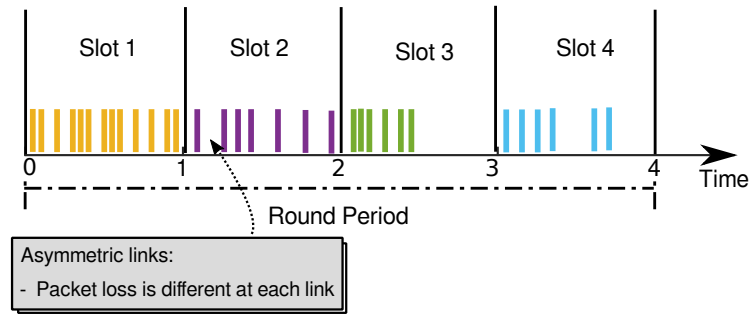
Figure 6.2: TDMA overlay protocol with each node transmitting in its slot. Packets are received and relayed till reaching the base station. Packet loss is distinct at each link.

describing the probability (P) of a packet being delivered on a single link depends on link length (d) as in Equation 6.1, where R is the link-length with a PDR of 50% and α the curve decay.

$$P(d) = e^{-(\ln 2)\left(\frac{d}{R}\right)^{\alpha}} \tag{6.1}$$

In more complex operational scenarios, e.g., with large metallic surfaces or local electromagnetic interference, the individual links are expected to differ, each with its unique PDR function. However, we consider these functions modeled by R and α parameters that remain constant or vary slowly according to our protocol dynamics. To keep the links (nearly) independent we applied an overlay TDMA protocol on top of WiFi CSMA/CA, as described in Chapter 4 (Pinto et al., 2017d), i.e., with fixed slots, which strongly reduces mutual-interference among network nodes. We do not consider DVSP (Chapter 5) here, to avoid potential feature interaction. Figure 6.2 shows how packets are routed through the network. The source (slot 1) transmits during its own slot as many packets as possible to its neighbor. The latter, in its own slot, relays these packets to the next neighbor, and so on until packets reach their final destination (sink). The sink has no dedicated slot. Slot IDs are ordered from source to sink to minimize delay of the video stream. Packets that are lost along the way are not recovered. Figure 6.1 depicts the network and link model. The PDR at each link P_i depends on the link

length d_i and the link parameters R_i and α_i. Assuming links independence, based on the TDMA protocol isolating transmissions of each UAV, the end-to-end network PDR (P_{net}) is given by the probability of a packet being successfully transmitted in every link, i.e., the product of all individual link PDR. Given n hops in a line network with length L, our problem (Equation 6.2) is to find a relay placement (**d**) that maximizes end to end packet delivery (P_{net}).

$$\max_{\mathbf{d}} P_{net} = \prod_{i=1}^{n} P_i(d_i) \qquad \texttt{s.t.} \qquad L = \sum_{i=1}^{n} d_i \qquad (6.2)$$

6.2   Optimal Relay Placement

The maximum of the product of exponentials is hard to derive algebraically, even for two curves. However, for low numbers of nodes, say 5 or less as imposed by the end-to-end bandwidth and delay requirements of interactive video streaming, numerical solutions can be easily found. Figure 6.3 provides an insightful example of the behavior of this function, concerning a network with two links with different PDR functions and $L = 100$m. The relay node is placed at x meters from the source and thus $d_1 = x$ and $d_2 = L - x$. The network PDR $P_{net}(x)$ (black line) is the product of $P_1(x)$ (red line) and $P_2(L - x)$ (blue line) as in Equation 6.3.

$$P_{net}(x) = P_1(x).P_2(L-x) =$$
$$e^{-(\ln 2)\left(\frac{x}{R_1}\right)^{\alpha_1}} e^{-(\ln 2)\left(\frac{L-x}{R_2}\right)^{\alpha_2}} = e^{-(\ln 2)\left(\left(\frac{x}{R_1}\right)^{\alpha_1} + \left(\frac{L-x}{R_2}\right)^{\alpha_2}\right)} = e^{-(\ln 2).f(x)} \qquad (6.3)$$

Maximizing $P_{net}(x)$ is the same as minimizing the variable part of the exponential argument $f(x)$ (Equation 6.4), since the exponential is monotonic.

$$\max_{x} P_{net}(x) = \min_{x} f(x) = \min_{x} \left(\left(\frac{x}{R_1}\right)^{\alpha_1} + \left(\frac{L-x}{R_2}\right)^{\alpha_2}\right) \qquad (6.4)$$
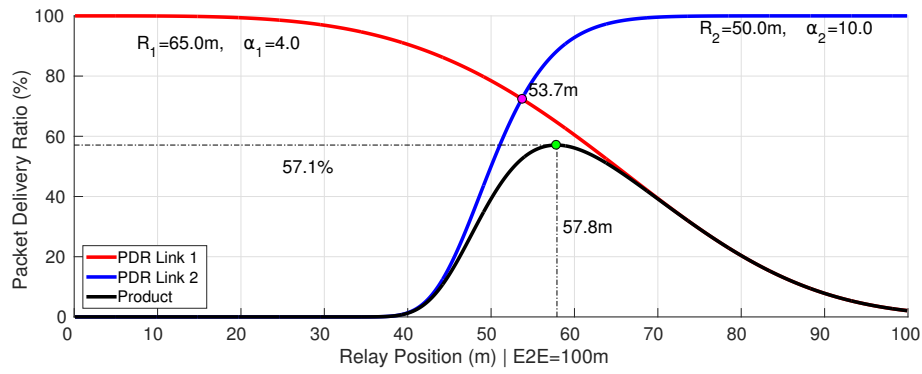
Figure 6.3: Optimal solution (green dot) for the relay position problem in a two-link 100m-length network. Best possible PDR is 57.1%.

This solution is not trivial and it does not correspond to the intersection of the curves (cf. red dot at 53.7m in Figure 6.3), which would be the case with similar links, i.e., $R_1=R_2$ and $\alpha_1=\alpha_2$, leading to $f(x)$ having a minimum at $x = L/2$ (cf. scenarios explored in Chapter 4). In the general case, the derivative of $f(x)$ must be found or an iterative search performed to find the solution of Equation 6.4. In this case, $P_{\texttt{net}}(x)$ is maximum at approximately $x = 57.8$m (green dot).

Figure 6.4 (top) shows the end-to-end PDR of a two-link network as a function of end-to-end network length L, assuming each link is modeled by the curves showed in Figure 6.3. Clearly, the bold line, corresponding to the optimal relay position, dominates the dashed line obtained with the relay placed in the network midpoint. The particular example of a 100m network is highlighted in green. Figure 6.4 (bottom) shows the optimal relay placement (distance from the source) as a fraction of the network length (bold line). This plot shows that as the network length grows, it is more favorable to place the relay closer to the sink than the source. Only in the case of a network of ≈ 70m, it is desirable to have the relay right in the middle. This happens using this particular choice of parameters, where the second link is worse than the first ($P_1(d) > P_2(d)$).
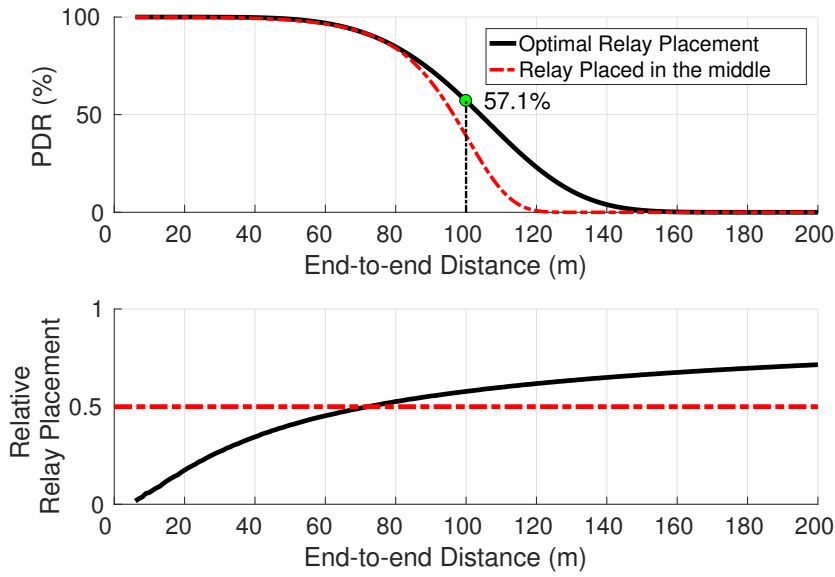
Figure 6.4:   (top) End-to-end PDR on a two-link network as a function of end-to-end network length L (links modeled as in Figure 6.3). (bottom) Optimal position of the relay as fraction of L (bold curve).

6.3   Dynamic Relay Placement (DRP) Protocol

To maximize end-to-end PDR, each relay runs a distributed protocol to track its best placement, which we named Dynamic Relay Placement (DRP). The protocol main idea is that every UAV constantly estimates the PDR of its incoming link and shares this value, together with its GPS position, with the node before in the line topology. This allows each node to acquire the PDR and length estimates of both its incoming and outgoing links and, after collecting multiple estimates, perform a function regression and infer the links R and α parameters (cf.Equation 6.1). Then it computes its optimal relative position between its neighbors and adjusts its position accordingly. Differential GPS units are to be used to minimize link length errors. As visible in Figure 6.3, an error of 5m, typical in standard GPS, leads to a deterioration of near 10% from optimal PDR.

When a relay enters the network to extend its range, it starts estimating the PDR and collecting samples regarding the links to both its neighbors, in runtime. In Figures 6.5,

6.6, 6.7 and 6.8, we can see four iterations of a simulation run of DRP algorithm. In this simulation, we have set a Source node at 100m from the BS. The relay is able to obtain PDR samples with an error of $\pm 5\%$ regarding its link to the BS and to the Source. Such samples are represented by black dots in the figure. In bold red we see the estimated link model for the BS, and in green the one to the Source. The bold black line shows the estimated model for the product of both PDR models. Underlying dash lines, represent the ground truth.

At the beginning, the estimated models are far from the ground truth as only one sample per model as been collected. However, as the relay moves away from the BS, and closer to the Source, more samples are collected, and models are improved. In the last iteration shown, we can see the estimated optimal point for the relay is not far off from the actual optimal (around 57.8m).

–·–·–	Product - Ground Truth
——	Product - Estimated
–·–·–	Link 1 - Ground Truth
——	Link 1 - Estimated
●	Link 1 - Collected Samples
–·–·–	Link 2 - Ground Truth
——	Link 2 - Estimated
●	Link 2 - Collected Samples
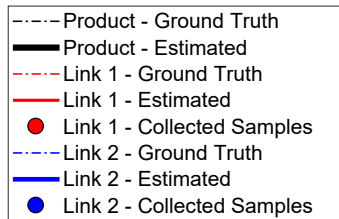
To facilitate PDR sample computation, node i adds a unique sequence number (sq_i) to the packet's header, whose first 4 digits regard the source and destination of the packet. This way, receiving node $i+1$ can determine which packets were lost. An array of the last M sequence numbers of received packets (from every node) is kept updated (in our experiments, we have used $M = 200$). The DRP protocol periodically sweeps this array verifying differences between consecutively registered sequence numbers, determining how many packets from node i to node $i+1$ were lost. The estimated PDR ($P_{[i,i-i]}$) is the number of missing packets divided by the window size M. The TDMA layer of node $i+1$ then sends a *PDR* packet upstream, i.e. to node i, containing the PDR estimate of link $[i, i-i]$. This way, every node is able to estimate the quality of its incoming link (source side) directly, and its outgoing link (sink side) indirectly by means
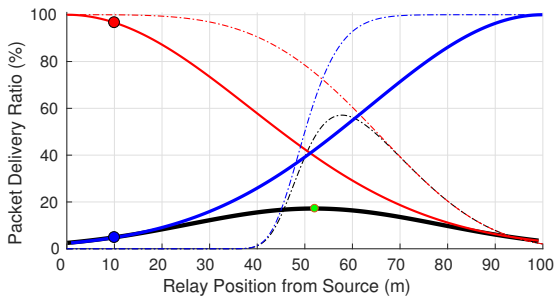
Figure 6.5: DRP initial state. Relay is 10m away from BS.
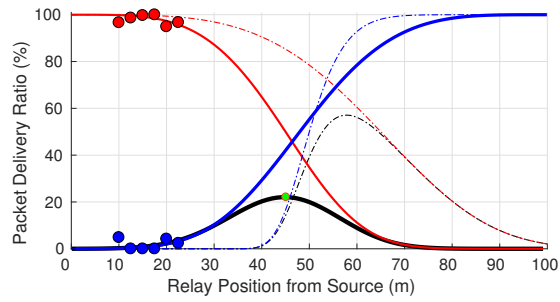
Figure 6.6: DRP state when relay is 23m away from BS.
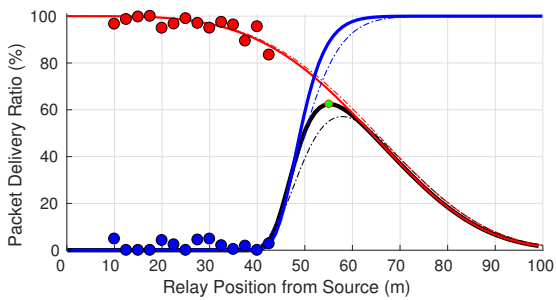
[DRP state when relay is 43m away from BS.]

Figure 6.7: DRP state when relay is 43m away from BS. Estimation matches ground truth.
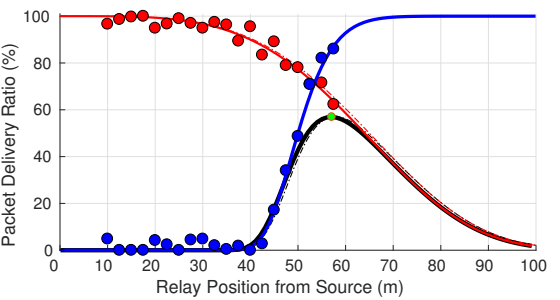
Figure 6.8: DRP final state. Relay estimated the optimal location at 57.8m from the Source.

of the feedback *PDR* packet.

6.4   Experimental results

This section confirms the capability of the proposed DRP protocol to assess the PDR of each link at each relay node, and how the PDR of the links and end-to-end network vary with the relative position of the relay in the line topology. We also show the end-to-end throughput, i.e., video frame rate, to guarantee that we do not improve PDR at the expense of throughput.
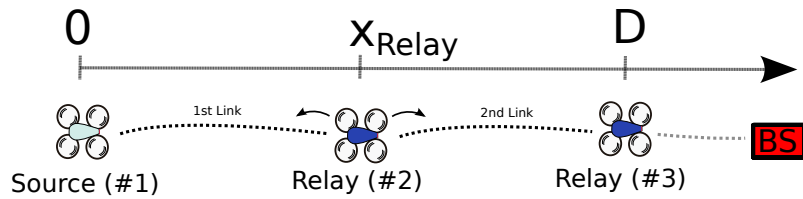
Figure 6.9: Experiment layout (top view) of the UAVs and computer base station. All nodes are fixed except the first relay (node 2). End-to-end length set to $D = 18$m.

6.4.1 Setup

Figure 6.9 shows the top view of the experimental setup where we have a single source UAV that streams images through a line network of two other UAVs that eventually deliver them to the base station. We used AR.Drone 2.0 as the UAV platform. The experiment was carried out indoors and distances between nodes taken from a tape measure. We chose a TDMA round period of $T = 100$ms, and dedicated one equal slot to each transmitting UAV. The network hop count is 3 ($n = 3$), and routing tables are hard-coded accordingly, namely a UAV-source, two UAV-relays and a computer base station. The distance between source and second relay (node 3) is fixed to $D = 18$m, and the first relay (node 2) is the only moving node (Figure 6.9). Thus, for the purpose of analyzing network performance, we will focus on the first three nodes and respective links, only, considering relay node 3 as the effective sink. Queues in the relays are limited, thus the system will drop oldest packets first if new incoming packets find a queue full.

All nodes were set to operate on the same IEEE 802.11g ad-hoc network channel at 24Mbit/s fixed bit rate. At this speed, we guarantee that we can produce data fast enough to saturate the channel, thus not being limited by the processing power of our platform. The transmission power was equally set among the UAVs (10dBm) as well as the maximum number of Wifi MAC retries (2, the minimum the platform allows). Each video streaming experiment lasted for roughly 100 consecutive seconds due to limited local log file storage. Each image frame, in raw format, has 57600 bytes and is divided

into 50 packets. Each packet corresponds to one horizontal line of pixels in an image frame. The source is programmed to capture a new frame only if the transmission queue has room for at least 50 packets.

6.4.2 Packet Delivery Ratio

Figure 6.10 shows the effect of relative distance of a relay to its upstream (source side) and downstream (base station side) nodes on the PDR of the respective links. As the relay moves farther from the source, and closer to its upstream neighbor, PDR from the first link (red) oscillates around 95%, and the one from the second link (blue) improves dramatically. The best end-to-end condition is when this product is maximum. If one of the two links has low PDR, this translates to a low end-to-end PDR since packets have to be successfully transported at every hop to reach the sink. As discussed in Section 6.2, the asymmetric links lead to a best end-to-end scenario with the relay node away from the middle distance between its upstream and downstream nodes. In that midpoint the network PDR is $90\% \times 79\% \approx 72\%$. Figure 6.11a) shows a snapshot of the video stream received at the sink when the relay is placed exactly in the midpoint between its two neighbors. When the relay moves away from the source, the network PDR eventually increases to $\approx 100\%$, i.e., a 40% improvement. Figure 6.11b) shows a snapshot of the video stream with the relay close to the optimal position, revealing less losses as expected. Moving the relay farther away again deteriorates the network performance since the first link worsens significantly.

6.4.3 Throughput

The second metric we analyzed is throughput, measuring the data received at the sink per second, corresponding to the throughput of the second link, since all data that the relay transmits is originally generated at the source. Figure 6.12 shows that placing the relay at $x = 13$m, i.e., $\approx 72\%$ of the source to sink distance, maximizes throughput.
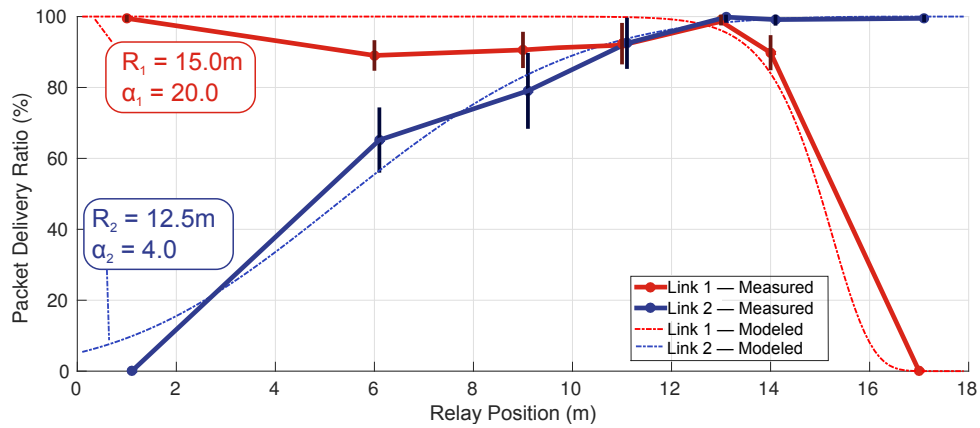
Figure 6.10: Experimentally measured packet delivery ratio at the first (red) and second (blue) links, with respective standard deviation, at different static relay positions. Best scenario when relay is closer to sink ($x = 13$m) leading to end-to-end PDR $\approx 100\%$. Dashed lines are superimposed regressions of Equation 6.1 on experimental data.
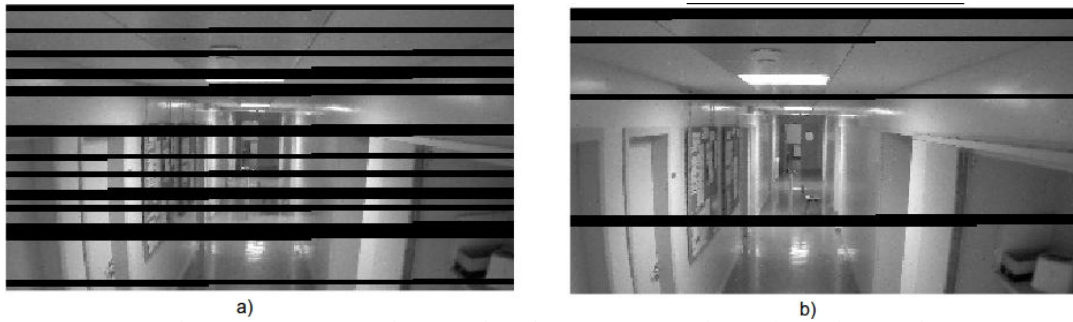
Figure 6.11: Video stream snapshot with relay positioned at: a) midpoint between source and sink, showing plenty of packet losses (black lines); and b) 0.6 of the distance between source and sink ($x = 13$m), leading to balanced links and fewer packet losses.

Interestingly, the achieved throughput is near three times higher than at the mid-point $x = 9$m.

Overall, the experimental results validate our initial assumption that end-to-end network performance in a line topology with asymmetric links is maximized moving the relay nodes to balance the PDR of the respective links.
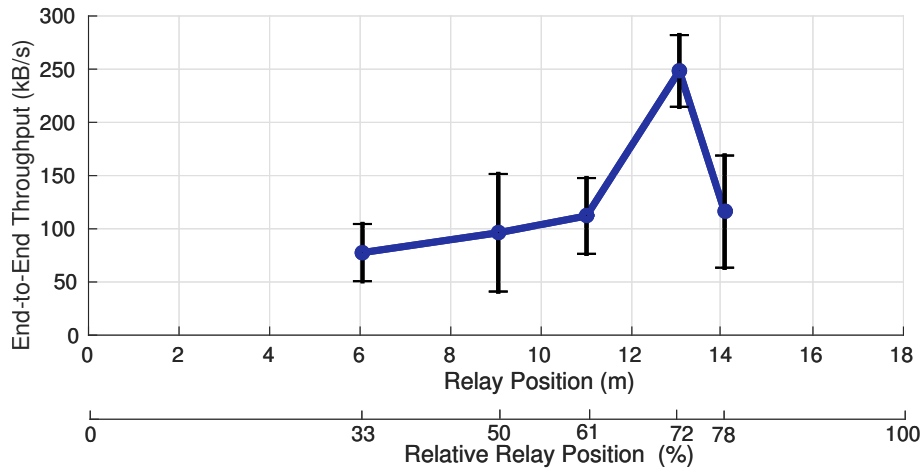
Figure 6.12: Measured end-to-end throughput. Placing the relay at midpoint (x=9m) is not optimal, again. At x=13m, throughput is three times higher.

6.5   Relay Placement Summary

Relay positioning has a significant impact on the end-to-end network performance, particularly PDR and throughput. We showed that in the presence of asymmetries in the links, adjusting UAV positions balancing the links PDR maximizes network performance. Experimental results, at different static positions and with a two-link line network, showed a PDR increase of 40% and 3-fold increase in throughput when compared with placing the relay node in the network mid-point. We also described and implemented an online PDR estimation protocol that will be able to guide the relays dynamically to their best positions. Addressing the solution of the general case of positioning n relays and proving convergence of the protocol when operating iteratively, as well as determining the optimal number of relays in asymmetrical conditions are still an open problem.

Chapter 7

Aerial Monitoring

In this chapter, we design and evaluate a new persistent monitoring application, considering multiple vehicles and communication constraints. This work has been reported in (Pinto et al., 2016b). We envision defining an Area of Interest (AoI) to be surveyed, that might be larger than the field of view (FoV) of a single UAV. Therefore, in order to overcome the FoV limitations, the vehicle can move around in a pattern that periodically visits different sections of the AoI. In many cases such as tracking a target in the AoI, a minimum *global frame-rate* (i.e, the number of times the vehicle visits the whole AoI per unit of time) is a fundamental design parameter. If the AoI is quite large, one UAV might take too long to cover it. As an improvement, we can have not one, but a team of vehicles covering the AoI. Such solution increases the total cost of the system, and the bandwidth available to transmit data is greatly reduced, i.e., using more vehicles does not imply more frames arriving at the operator. However, the total cost and bandwidth per UAV can be controlled by using a limited number of vehicles and coordinating their movement to cover the AoI.

The main contribution of this chapter is a framework that enables on-line monitoring of AoI larger than a single aerial vehicle FoV, and maximizes the global frame rate using a limited number of vehicles. For this purpose, we analyze the single vehicle solution,

taking into account both the motion control and the path planning. Then, we extend it to multiple vehicles using a novel formation control scheme that distributes vehicles uniformly throughout a cyclic route using information from the local neighborhood, only. Note that since we aim at on-line monitoring, we include the impact of limited wireless bandwidth. Simulation results show that this formation control scheme provides up to 7-fold improvement in the global frame-rate in the presence of external interference such as wind gusts.

The organization of this chapter is as follows. In Section 7.1, we define assumptions and the problem of maintaining the performance of a multi UAV matrix-camera. Section 7.2 explains the respective proposed solution. Section 7.4 shows the obtained simulation results. Finally, Section 7.5 provides conclusions.

7.1   System description

In this work, we aim at creating a virtual camera that is capable of surveying an AoI larger than a single camera FoV. We use a team of multirotors that move in a certain pattern and capture images from different points of that AoI periodically, and send them through a wireless medium to a Ground Station (GS) where they will be presented to an operator. Our goal is to minimize the time required to capture and deliver the whole AoI to the GS, or equivalently, maximize the frame-rate of our virtual camera. In this section, we present the different parts of our problem, namely, the sensing model, the UAV motion model and the network model.

7.1.1   Sensing Model

We assume a square AoI of size $W \times W$, divided into $M \times M$ smaller square cells of size $L \times L$, where L is a function of the UAV field of view, and $M = \lceil W/L \rceil$ (cf. Figure 7.2). Each cell is named $c_{i,j}$, where $i, j = \{1 \dots M\}$ are the row and column number within
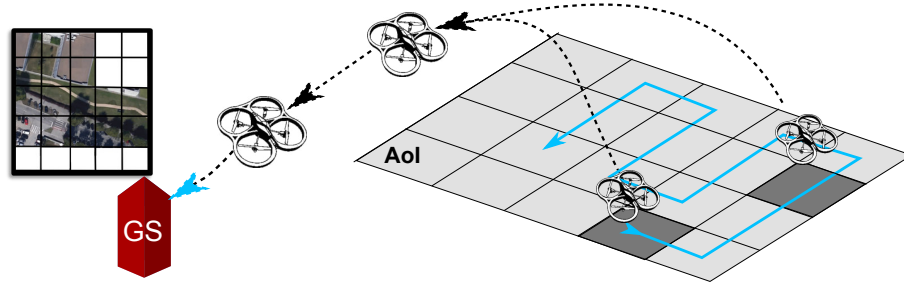
Figure 7.1: Overview of the monitoring system, that performs sweep coverage on a periodic basis, while streaming data live to a Ground Station (GS).

the AoI, respectively. The position of a cell $c_{i,j}$ is $\vec{P}_{i,j}$.

In order to capture an image from $c_{i,j}$, we require the robot to be no farther than ζ from the centre of that cell, defined to guarantee complete coverage of a cell in the presence of localization errors, and at a speed no higher than v_{sense}, defined to avoid blurred images. Consequently, $L \leqslant L_{\text{UAV}} - 2\zeta$, where L_{UAV} is the width of the true FOV of the UAV for a desired resolution. Note that in order to keep the field of view constant we assume the vehicles travel at a constant altitude.

A single image captured by a vehicle over a given cell is called a *frame*, and it contains b bits of data. Similarly, the set of frames of all cells is called a *global frame*.

7.1.2 UAV Motion Model

Concerning the motion model, we represent each UAV as a point in a two-dimensional space, travelling at constant altitude. UAVs are modelled as a third degree dynamic objects, with a state of acceleration, velocity and position ($\vec{a}, \vec{v}, \vec{p} \in \mathbb{R}^2$). Acceleration results from the sum of all forces acting on the vehicle $\vec{F}$, namely air drag $\vec{F}_{\text{drag}}$ and thrust $\vec{F}_u$, divided by the object's mass m.

Thrust $\vec{F}_u$ is a inner force created by the blades of the multirotor. It is represented by a vector that can have any direction in the horizontal plane ($\mathbb{R}^2$), but limited in magnitude to U, i.e. $||\vec{F}_u||_2 \leq U \in \mathbb{R}_{++}$.
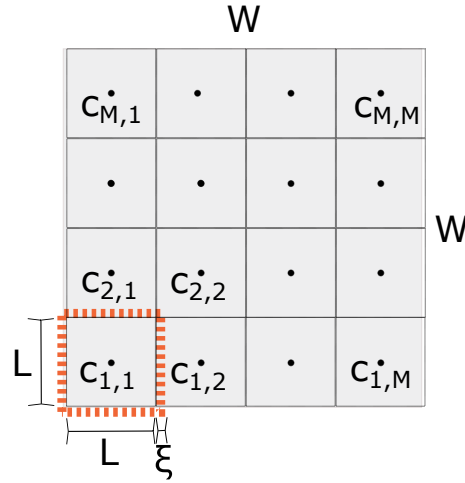
Figure 7.2: Square Area of Interest (side $W \times W$, and respective division into $M \times M$ square cells. L is chosen such that if a vehicle is at the centre of a cell (c_{ij}), with a maximum error of ξ in any direction, then the cell is fully contained in the field of view of a UAV.

Air drag represents the air resistance to the motion of the vehicle, and its magnitude depends quadratically on the relative velocity of the air with respect to the vehicle ($\vec{v}_{air}$). Particularly, considering a certain wind velocity at the UAVs location ($\vec{v}_{wind}$), and vehicle ground speed ($\vec{v}_{ground}$), we have: $\vec{v}_{air} = \vec{v}_{ground} - \vec{v}_{wind}$. Thus, drag force can be computed with Equation 7.1.

$$\vec{F}_{drag} = k_{drag}||\vec{v}_{air}||^2 \hat{v}_{air} \quad ^1 \tag{7.1}$$

The total force applied to the UAV is $\vec{F} = \vec{F}_u + \vec{F}_{drag}$. To model the dynamics of the vehicle we use the corresponding dynamic equations for speed (Equation 7.2) and acceleration (Equation 7.3).

$$\vec{v}_{ground}(t) = \frac{d\vec{x}(t)}{dt} \tag{7.2}$$

$$\vec{a}(t) = \frac{\vec{F}(t)}{m} \tag{7.3}$$

---

[1]where $\hat{x} \equiv \frac{\vec{x}}{||\vec{x}||}$

Given this model, we can compute the time needed to travel a given distance d in a straight line, starting and finishing from a resting position. Without wind ($\vec{v}_{\text{wind}} = 0 \Leftrightarrow \vec{v}_{\text{ground}} = \vec{v}_{\text{air}}$), and at maximum thrust ($\|\vec{F}_u(t)\|_2 = U$), the vehicle will move in a straight line, whose direction is the same as the thrust vector. Thus, we limit calculations to vector magnitude. We can decompose this motion into three stages, namely acceleration, cruising speed and braking.

When accelerating, the vehicle goes from $v = 0$ to cruising speed given by Equation 7.4, achieved when $F_{\text{drag}} = F_u$.

$$v_{\text{max}} = \sqrt{\frac{U}{k_{\text{drag}}}} \tag{7.4}$$

The actual velocity during the acceleration period can be deduced from the system dynamics stated in the differential equation Equation 7.5.

$$\frac{dv}{dt}(t) = a = (F_u - F_{drag})/m = \frac{U}{m}\left(1 - \left(\frac{v(t)}{v_{\text{max}}}\right)^2\right) \tag{7.5}$$

Solving this equation and considering that the UAV starts with $v(0) = 0$, then the actual velocity is given by Equation 7.6. Integrating this equation, and also considering that $x(0) = 0$, we get the position function along that part of the path as in Equation 7.7.

$$v(t) = v_{\text{max}} \tanh\left(\frac{U}{v_{\text{max}}m}t\right) \tag{7.6}$$

$$x(t) = v_{\text{max}}^2 \frac{m}{U} \ln\left(\cosh\left(\frac{U}{v_{\text{max}}m}t\right)\right) \tag{7.7}$$

Note that the acceleration phase lasts until t_a when $v(t_a) \approx v_{\text{max}}$, implying that $\tanh\left(\frac{U}{v_{\text{max}}m}t_a\right) \approx 1$. Since $\tanh^{-1}(1) \approx 2$ (error $< 4\%$) then we will consider $U/(v_{max}m)t_a = 2$ and consequently $t_a = 2mv_{\text{max}}/U$.

During deceleration, the vehicle should come to a halt more rapidly than it takes to accelerate since both drag and thrust act with the same direction now. Solving a similar differential equation to Equation 7.5, and assuming $v(0) = v_{\text{max}}$, we get $v(t)$ for this

Table 7.1: Summary of UAV motion equations

Stage	Distance	Time
Acceleration	$v_{\max}^2 \frac{m}{U} \ln\left(\cosh\left(2\right)\right)$	$\frac{2mv_{\max}}{U}$
Cruising Speed	$v_{\max} t_c$	t_c
Braking	$v_{\max}^2 \frac{m}{U} \ln\left(\sqrt{2}\right)$	$\frac{\pi m v_{\max}}{4U}$
Total	$\gamma v_{\max}^2 \frac{m}{U} + v_{\max} t_c$ $\gamma \equiv \ln\left(\cosh\left(2\right)\sqrt{2}\right)$	$\frac{\eta v_{\max} m}{U} + t_c$ $\eta \equiv 2 + \pi/4$

part of the path (Equation 7.8) and integrating again we obtain the respective position equation (Equation 7.9).

$$v(t) = v_{\max} \tan\left(\pi/4 - \frac{Ut}{mv_{\max}}\right) \tag{7.8}$$

$$x(t) = x_0 + v_{\max}^2 \frac{m}{U} \ln\left(\cos\left(\pi/4 - \frac{Ut}{mv_{\max}}\right)\right) \tag{7.9}$$

The time for braking (t_b) is, thus, the time to go from $v_{\max}$ at $t = 0$ to $v(t_b) = 0$. According to Equation 7.8, this implies that $\pi/4 - \frac{Ut_b}{mv_{\max}} = 0$ which allows deducing t_b as in Equation 7.10.

$$t_b = \frac{\pi m v_{\max}}{4U} \tag{7.10}$$

The distance travelled in this interval $d_b = x(t_b) - x(0)$ is given by Equation 7.11.

$$\begin{aligned} d_b &= v_{\max}^2 \frac{m}{U} \ln\left(\cos\left(0\right)\right) - v_{\max}^2 \frac{m}{U} \ln\left(\cos\left(\pi/4\right)\right) \\ &= v_{\max}^2 \frac{m}{U} \ln\left(\sqrt{2}\right) \end{aligned} \tag{7.11}$$

In Table 7.1, we summarize the travelled distances and respective time intervals, assuming the vehicle has a cruising speed $v_{\max}$ for t_c time.

7.1.3 Network Model

We assume the given AoI is generally far from the ground station (GS). Thus, we assume that the information gathered by the sensor-UAVs may have to be relayed. Nevertheless,

we also assume the AoI is within one hop of the first relay-UAV as shown in Figure 7.3a). Note that, in general, this first relay-UAV will be hovering near the centre of the AoI, at a slightly higher altitude than the sensor-UAVs.
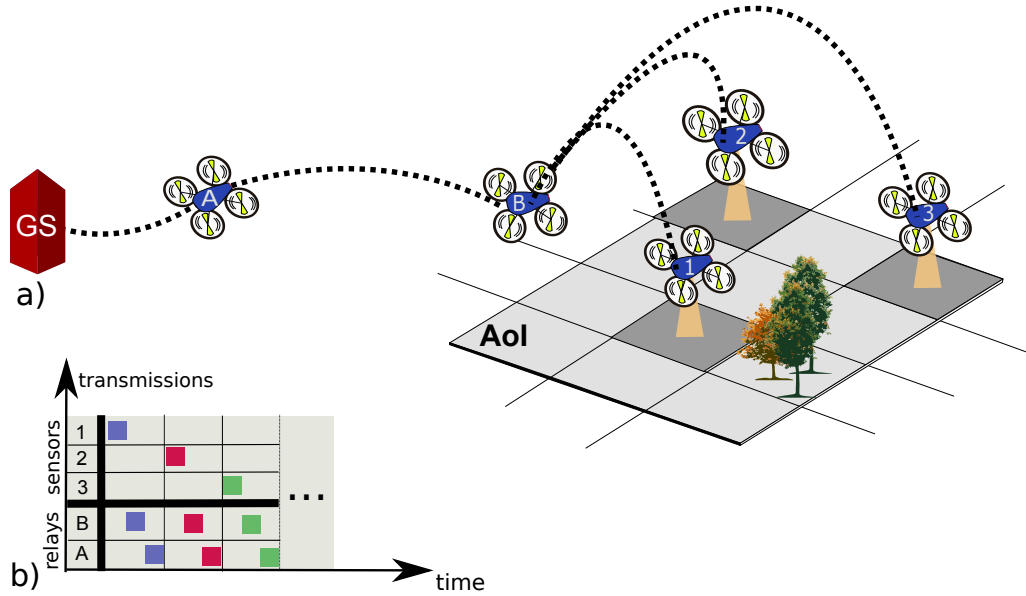
Figure 7.3: The network model encompasses: a) a multi-hop backbone of relay-UAVs that connects the sensor-UAVs (in the AoI)t to the GS; b) a TDMA network access scheme that grants one slot to each sensor-UAV for its exclusive use.

In what concerns the network access management, we use the protocol and forwarding method proposed in Chapter 4 which establish a global TDMA framework that is self-synchronized and offers each sensor-UAV an exclusive fixed slot. In this case, one sensor-UAV at a time transmits in the sensor slot considered in the previous chapters and transmissions are immediately forwarded by the relay-UAVs to the GS (Figure 7.3b) in each TDMA round. The major difference from the original version is that now we considering N sensor-UAVs, and each one gets a sensor slot every N TDMA rounds.

This method grants a fixed bandwidth for each UAV, avoiding collisions at the network access and packet queueing at intermediate nodes. If the network capacity is ζ bit/s, and R the number of relay-UAVs, then each sensor-UAV gets an average capacity

of C_{GS}/N bit/s, where $C_{GS} = \zeta/(R+1)$ represents the total capacity to communicate from the AoI through the relay-UAVs to the GS.

When looking to the global communication pattern (Figure 7.3b) we can see a repetition of N fixed larger slots, each dedicated to one sensor and provided with sufficient length to accommodate the forwarding transmissions through the relay network. Thus, throughout the remainder of this chapter we will refer to this global pattern as a TDMA round with N slots and a period N times that of the inner TDMA round of the relay network.

Finally, we also control the sensor-UAVs so that they acquire a frame in a cell and immediately start transmitting it while moving to the next cell. However, once arrived at the next cell, the new frame is only acquired after the previous one has been fully transmitted. This technique may introduce an extra stop delay but it also avoids queuing (or backlog) in the vehicles network interface.

7.2   Optimal Trajectories and Frame-rate

We now analyze our proposed solution to solve the problem, demonstrating the respective bounds for best and worse cases.

7.2.1   Case with one UAV

When a single UAV is used, we can convert this problem into a variation of the well-known Travelling Salesman Problem (TSP). Given a fully connected undirected graph with a finite number of nodes, the TSP provides the least-cost route that traverses all the nodes and finishes in the starting node. In our context, we need to traverse all the cells minimizing total travel distance or time. Consequently, the TSP, which is a NP-hard problem due to its combinatorial nature, can be solved close-to-optimally using an iterative process with a relatively small number of iterations, as we will show later.

Theorem 7.1. *Given a squared AoI with a total area of $W \times W$ divided in M^2 cells to be visited periodically by one UAV without wind, each cell generating a frame with b bits through a channel with bandwidth C_{GS}, any global frame rate up to $G_0 = 1/D_0$ can be met, where D_0 is given by Equation 7.12 subject to $L \geq \gamma v_{max}^2 m/U$ to allow UAVs to reach cruise speed between cells.*

$$D_0 = M^2 . \max \left(\frac{(\eta - \gamma)m v_{max}}{U} + \frac{L}{v_{max}}, \frac{b}{C_{GS}} \right) \quad (7.12)$$

Proof. This result comes from first finding the shortest route that covers all cells in the AoI (cf. TSP). Ideally, the length of the shortest route ($d_{\min}$) corresponds to traversing all M^2 cells across the shortest path between them (L) and can be easily computed as $d_{\min} = M^2 \times L = M^2 \times (W/M) = MW$.

If the number of cells (M^2) is even, the route with distance d_{min} is feasible. Following the example in Figure 7.4, when starting at the bottom-left corner (cell $c_{1,1}$), the route first goes along the edges of AoI, making an inverted U path until it reaches the bottom-right corner ($c_{1,M}$). Then, it zigzags from right to left, until it reaches cell $c_{1,2}$, and then closes the path.

Conversely, if the number of cells (M^2) is odd, having a diagonal path between two cells is unavoidable, thus the shortest path corresponds to $d = (M^2 - 1 + \sqrt{2}).L$ which is still very close to d_{min} (error is at most 4.6% when $M = 3$). Figure 7.5 exemplifies how this construction is done. Starting at the bottom-left corner (cell $c_{1,1}$), the tour first goes along the edges of AoI, making an inverted U path until it reaches the bottom-right corner ($c_{1,M}$). Then, it zigzags from right to left, until it reaches the fourth column ($c_{M-1,4}$). To sweep the last 2 columns ($2^{nd}, 3^{rd}$), we include a diagonal path from cell $c_{M-2,3}$ to $c_{M-1,2}$. Then, we finish the coverage by zigzagging from top to bottom reaching cell ($c_{1,2}$).

As previously mentioned, a frame can only be captured if the vehicle is passing the cell with a speed below v_{sense}. In this work, we consider this speed to be 0, thus, the vehicles need to stop at each cell. From motion equations (Table 7.1), we know that any
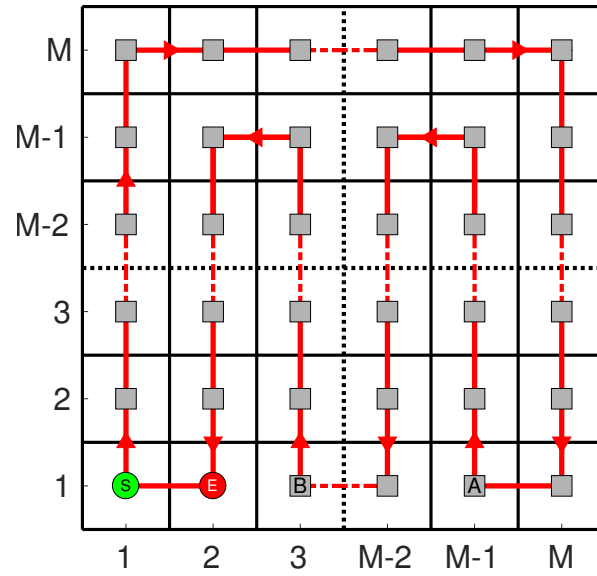
Figure 7.4: Square AoI with even number of cells to visit (M^2). Side size is W. Red path describes the shortest tour, and it starts at "S", it ends at "E", and restarts at "S" again. Tour length d is optimal and equal to $d_{\min}$.
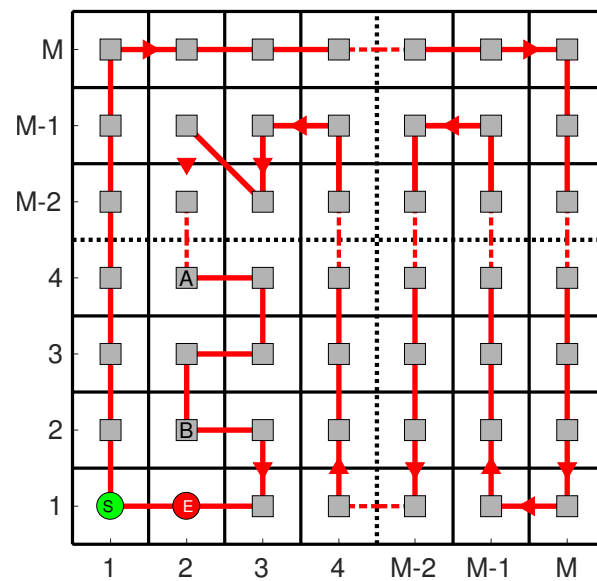
Figure 7.5: Square AoI with odd number of cells (M^2) to visit. Side size is W. Red path describes the shortest tour, and it starts at "S", it ends in "E", and restarts at "S" again. It includes one diagonal edge, so tour length $d \approx d_{\min}$.

distance $d \geq \gamma v_{\max}^2 \frac{m}{U}$ takes $t(d)$ (Equation 7.13) to be travelled.

$$t(d) \approx \frac{\eta m v_{\max}}{U} + \frac{(d - \gamma v_{\max}^2 \frac{m}{U})}{v_{\max}} \tag{7.13}$$

Consequently, ignoring one possible diagonal connection, the minimum time required to fly between two adjacent cells is also given by Equation 7.13 with $d = L$.

On the other hand, each frame takes a minimum of b/C_{GS} seconds to be transmitted to the GS. Moreover, our model considers that a frame transmission is carried out while moving to the next cell, but a new frame can only be captured once the previous frame is completely transmitted to the GS. Thus, Equation 7.14 gives us the time required to move between two adjacent cells (t_{cell}), considering both motion dynamics and data transmission.

$$t_{cell} \approx \max\left(\frac{\eta m v_{\max}}{U} + \frac{L - \gamma v_{\max}^2 \frac{m}{U}}{v_{\max}}, \frac{b}{C_{GS}} \right) \tag{7.14}$$

Finally, Equation 7.15 gives us the total time to sweep the whole area and return to the initial point ($t_{trajectory}$) whilst transmitting all collected data.

$$t_{trajectory} \approx M^2.t_{cell} = D_0 \tag{7.15}$$

Thus, we get a feasible trajectory Γ_1 (Equation 7.16) for our problem, where $\vec{p}_{i,j}$ are the coordinates of cell $c_{i,j}$, and any global frame rate up to $G_0 = 1/D_0$ can be met.

$$\Gamma_1 = \begin{bmatrix} (\vec{p}_{1,1}, 0, 0) \\ (\vec{p}_{2,1}, 0, t_{cell}) \\ \ldots \\ (\vec{p}_{1,2}, 0, (M^2-1)t_{cell}) \\ (\vec{p}_{1,1}, 0, D_0) \end{bmatrix} \tag{7.16}$$

$\square$

7.2.2   Case with multiple UAVs

Theorem 7.2. *If one UAV can meet a global frame-rate of $G_0 = 1/D_0$, then N UAVs can meet at best a frame rate between N/D_0 and $C_{GS}/(M^2 b)$.*

Proof. With N vehicles, we follow a strategy of using the same optimal route computed in the previous case and share it among all UAVs, with the same direction of rotation. This way, every cell will be visited N times within D_0 seconds.

Despite that, if N UAVs travel all together in a tight formation, then, all the N global frames will be delivered to the GS at approximately the same time, and containing roughly the same information. This has marginal advantage when compared with the single vehicle case, therefore we propose another vehicle formation that improves the virtual global camera frame-rate by equally distributing the UAVs along the route, i.e., keeping them at a $d_{\min}/N$ distance apart. This way, each cell will be visited exactly once every $D_N = D_0/N$, resulting in a proportional N-fold decrease of the minimum global frame deadline.

However, if the timing limitation arises from the communications, increasing the number of UAVs will not improve the refresh rate. In fact, the time to transmit all the information contained in the AoI is still $(M^2 b)/C_{GS}$ since each one of the N UAVs has $1/N$ of the available bandwidth C_{GS}.

Thus, Equation 7.17 gives us the minimum global frame deadline D_N that can be achieved with N UAVs. The corresponding maximum global frame rate ($G_N = 1/D_N$) is obtained from the minimum of the inverse of the two terms in D_N, concluding the proof.

$$D_N \approx \max \left(\frac{D_0}{N}, \frac{M^2 b}{C_{GS}} \right) \tag{7.17}$$

$\square$

7.3 Distributed Formation Control

As we have seen, the global frame rate is maximized if the UAVs are equally spaced along their trajectory. This guarantees that cells are visited once every D_0/N. Conversely, if all UAVs follow each other in adjacent cells, these cells are visited at a high rate while the remaining cells will exhibit a long interval between visits, close to D_0, thus cancelling the benefits of our multi-UAV strategy.

To enforce the desired separation between the vehicles, we created a distributed and online algorithm based on the current vehicle state and the state of its two neighbours on the trajectory in a circular way, namely the one that follows ahead of it (*next-neighbour*) and the one immediately behind (*previous-neighbour*). The formation control algorithm is represented in the pseudo-code of Algorithm 1.

It starts by analyzing the current distance to the next and previous neighbours. If a UAV is closer to the *next-neighbour* than to the *previous-neighbour*, it means that it is moving too fast and must slow down. If the UAV is really close to the *next-neighbour*, slowing down would take too long to separate them apart to obtain the desired distance. Thus, it actually moves backward in the trajectory trying to quickly get to the desired separation from the *next-neighbour*. This is particularly useful when the nodes are initiating the sweeping process, or if a UAV is added/removed online.

If a UAV is closer to its *previous-neighbour* than to its *next-neighbour*, it means that it should move faster. However, since ideally the UAV is already moving as fast as possible, its correction will be small and it will be the *next-neighbour* that will slow down.

Algorithm 1 Formation Control Algorithm for UAV i:

Require: route = $\{\vec{P}_1, \ldots, \vec{P}_h, \ldots, \vec{P}_{M^2}, \vec{P}_1\}$

  UAV i: target ID and coordinates $(h, \vec{P}_h)$; position $\vec{p}_i$

  Next UAV: target ID and coordinates $(a, \vec{P}_a)$; position $\vec{p}_{\text{next}}$

  Prev UAV: target ID and coordinates $(b, \vec{P}_b)$; position $\vec{p}_{\text{prev}}$

  if $a > h$ **then**

    $d_{\text{next}} \Leftarrow (a - h)L + ||\vec{P}_h - \vec{p}_i||_2 - ||\vec{P}_a - \vec{p}_{\text{next}}||_2$

  else

    $d_{\text{next}} \Leftarrow (M^2 - h + a)L + ||\vec{P}_h - \vec{p}_i||_2 - ||\vec{P}_a - \vec{p}_{\text{next}}||_2$

  end if

  if $b < h$ **then**

    $d_{\text{prev}} \Leftarrow (h - b)L - ||\vec{P}_h - \vec{p}_i||_2 + ||\vec{P}_b - \vec{p}_{\text{prev}}||_2$

  else

    $d_{\text{prev}} \Leftarrow (M^2 + h - b)L - ||\vec{P}_h - \vec{p}_i||_2 + ||\vec{P}_b - \vec{p}_{\text{prev}}||_2$

  end if

  if $d_{\text{prev}} >> d_{\text{next}}$ **then**

    if $a > M^2/N$ **then**

      new target$_i \Leftarrow \vec{P}_q : q = \lceil a - M^2/N \rceil$

    else

      new target$_i \Leftarrow \vec{P}_q : q = \lceil M^2 + a - (M^2/N) \rceil$

    end if

  else if $(d_{\text{prev}} > d_{\text{next}}) \wedge (\hat{F}_u = \hat{v})$ **then**

    $\vec{F}_u \Leftarrow \vec{F}_u - c(d_{\text{prev}} - d_{\text{next}})\hat{F}_u$

    if $||\vec{F}_u||_2 > U$ **then**

      $\vec{F}_u = U.\hat{F}_u$

    end if

  end if

7.4 Simulation Results

7.4.1 Setup

To validate our framework we simulate different fleets of sensor-UAVs using Matlab, with the continuous motion equations discretized with an adequate time step. This step was set to 1 ms and, when no messages were present in any of the queues, to accelerate the simulation run time, the step was momentarily increased to 2ms. The UAVs settings used are described in Table 7.2.

Table 7.2: Simulation Setup for the Video-monitoring application.

	Variables	Value
m	**Robot Mass**	0.5 kg
ξ	**Max. Location error**	1 m
v_{sense}	**Max. Sensing Speed**	0 m/s
U	**Maximum Thrust**	10 N
k_{drag}	**Air Drag**	0.1 kg.m^{-1}
$\vec{v}_{\text{wind}}$	**Wind Velocity**	0 m/s
	Proportional	1.6
PID gains	**Integral**	0.08
	Derivative	0.8
b	**Frame size**	100kbit
C_{GS}	**Total Capacity to GS**	$100 - 700$kbit/s

Concerning the communications, we set a gobal sensors TDMA round of 100ms, leading to transmission slots of $(100/N)$ms assigned to each UAV. In their slots, the UAVs broadcast their current state, namely position and cell target in a total of 1kbit, every 500ms. The trajectory along the AoI is computed by the UAVs before the mission and they assign themselves a different starting cell at i/N^{th} from the start of the trajectory, where i is their own ID and N the number of vehicles.

Once the mission starts, the UAVs motion is controlled by a PID controller that automatically provides thrust based on the position error (cf. Table 7.2). As UAVs reach their targets, they check if they can already collect a new frame, or whether they have to wait to finish transmitting the previous frame. Moreover, if one vehicle is delayed due to external disturbances, e.g. wind, it will affect the other vehicles speed. This is caused by the formation controller that keeps a constant distance between neighbouring vehicles, which we will now describe.
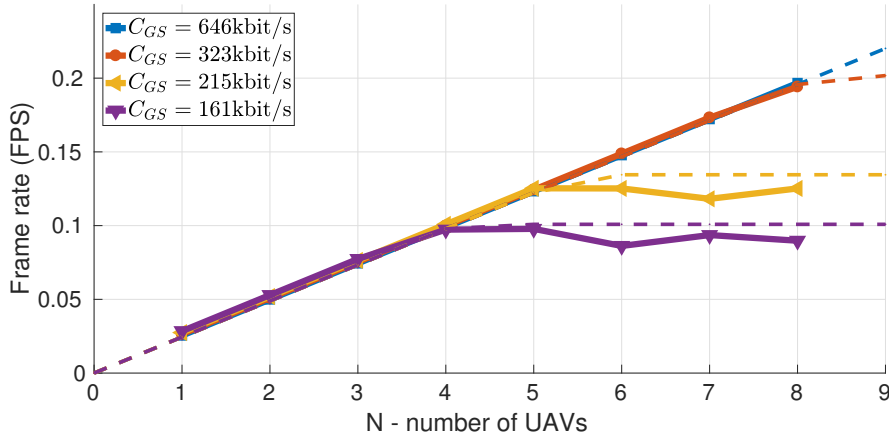
Figure 7.6: Maximum global frame rate versus number of UAVs sweeping the AoI, under different channel bandwidths. AoI: $L = 20$m, $M = 4$.

We tested the performance of our fleet of UAVs in terms of maximum global frame rate achieved under different bandwidth and cell width assuming no external disturbances, and later with disturbances.

7.4.2 Frame-rate as function of bandwidth

We started by evaluating the effect of bandwidth on the system. In Figure 7.6 we see the global frame rate attainable by the system using different number of UAVs, and setting different bandwidth to the GS (C_{GS}). The dashed line shows the theoretic bound while the solid line shows the simulation result. As expected, when the number of UAVs and available bandwidth increases, the overall performance improves. However, we also see that this improvement is capped by the network available bandwidth when the number of UAVs increases beyond a certain value. This effect is naturally more visible when the channel bandwidth is lower. In this situation, the maximum global frame rate is limited not by the flight time, but by the time taken to transmit all the information contained in AoI. Consequently, the global frame rate cannot be improved adding vehicles but only increasing the available bandwidth.
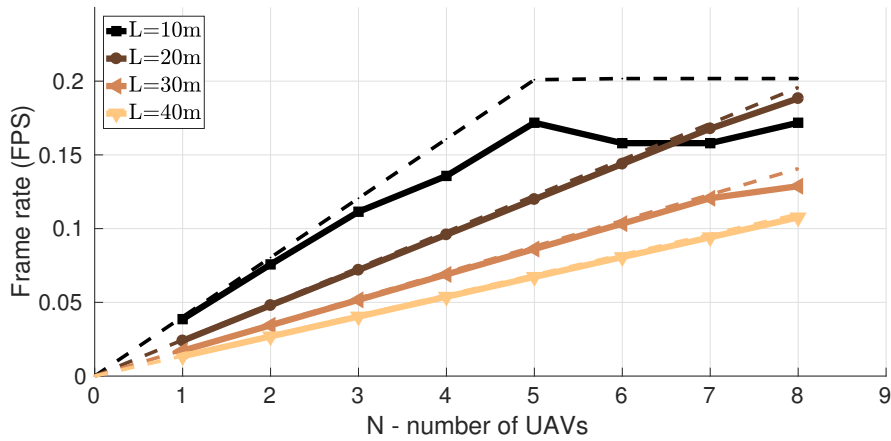
Figure 7.7: Maximum global frame rate versus number of UAVs sweeping the AoI, with different cell sizes L. $C_{GS} = 323\text{kbit/s}$. AoI: $M = 4$.

7.4.3 Frame-rate as function of cell width

In Figure 7.7, we can see the effect of changing the cell width, but keeping the total number of cells fixed as well as the total bandwidth. Wider cells imply longer flights, so in order to keep the frame rate constant, the system needs more UAVs as the AoI increases. Since the flight-time is not a linear function of distance, we can see that the minimum number of UAVs needed to reach a given frame-rate is not an affine function of cell width.

Another note is that the simulation results are slightly below theoretic ones. This is mainly due to errors estimating the flight time, since the simulated vehicles use a PID controller to move and not an on-off controller (full positive / full negative thrust) as considered in the analysis. A PID controller such as the one used in the simulation is more useful in a practical scenario since it adapts thrust dynamically, even when affected by unknown external disturbances such as position error, wind, model estimation error, etc.

7.4.4 Frame-rate with external disturbances

To validate the efficacy of the formation control, we added to the simulation a disturbance, periodic wind gusts (unknown to the UAVs), pointing north, up to 6m/s ($|\vec{v}_{\text{wind}}| = 3 + 3\sin\left(\frac{2\pi t}{30}\right)$ m/s, and direction $\arg\left(\vec{v}_{\text{wind}}\right) = \pi/2 + 0.1\sin\left(\frac{2\pi t}{30}\right)$ rad). Then, we measured the global frame-rate with and without the formation control under wind conditions.

As we see from the results in Figure 7.8, even with control, the frame rate is severely affected by wind – roughly 50% lower than the expected without it (blue line) This is due to an increased flight time. When gusts are at their maximum, UAVs have a hard
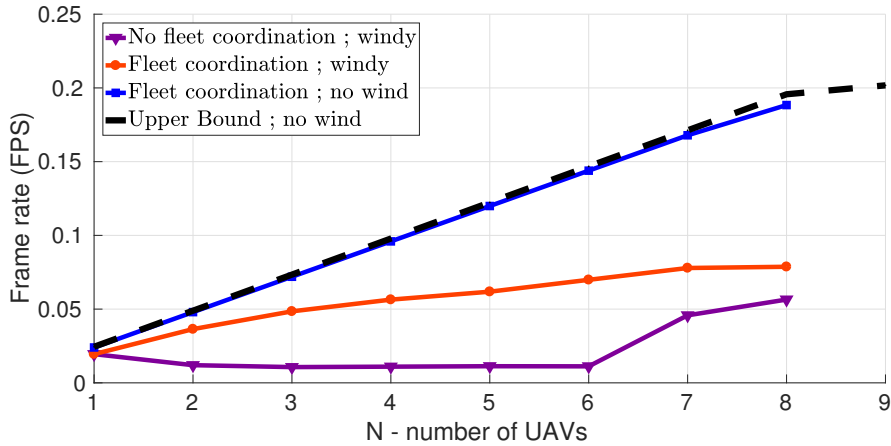
Figure 7.8: Maximum global frame rate to sweep the AoI, with wind gusts pointing north at 6m/s with and without our formation algorithm in place. AoI: $L = 20$m, $M = 4$, $C_{\text{GS}} = 323$kbit/s

time to achieve their targets and slow down in order to keep the formation. Even if the UAVs are well spaced in the beginning, without the formation control, the global frame-rate is up to 7 times worse. This occurs because, due to wind, some UAVs tend to gather while others become farther from their neighbours. This leads to some cells being visited multiple times over the course of a period, while others are not visited at all. In other words, the swarm stops meeting stricter deadlines, so best frame rate

decreases. We note that our control is particularly useful when the number of UAVs is low. In the limit of one UAV per cell, this formation control is not even needed.

7.5 Monitoring Summary

In this chapter, we proposed the use of UAVs to build an extendable camera, to provide an operator a wider image from an AoI than the field of view of a single vehicle without degrading the image resolution. We showed how the refresh rate of the AoI global frame is improved by incrementing the number of UAVs in use with adequate controls, as well as the speed of the wireless links. Furthermore, we showed how a formation control greatly improves the performance of the system when under external disturbances.

Chapter 8

Drones Software Architecture

The drones we used in our work are inexpensive commercial platforms, namely AR Drone 2.0 from Parrot (Parrot, 2012). However, in order to support the controls and communications we put forward in this dissertation, we had to develop a full software stack with appropriate API at which we called Drone-RK. Despite the name, the vast majority of the modules run both on drones and on the computer basestation. Except navigation and actuator modules, and the ones that depend on these two, all other can run on both computers and drones. Figure 8.1 lies down the list of modules that create Drone-RK, and their direct dependencies. This chapter describes this software architecture, focusing on the WiFi communications stack.

8.1 Navigation Data, Actuator and Flight Control

The drone platform runs an auto-pilot independent an closed-source process in background. This process is responsible to measure and interpret navigation data from the physical sensors and also to move the drone and apply changes in the motors. Our software stack communicates with this process by means of two TCP sockets, one to transmit commands and another to receive new navigation data.
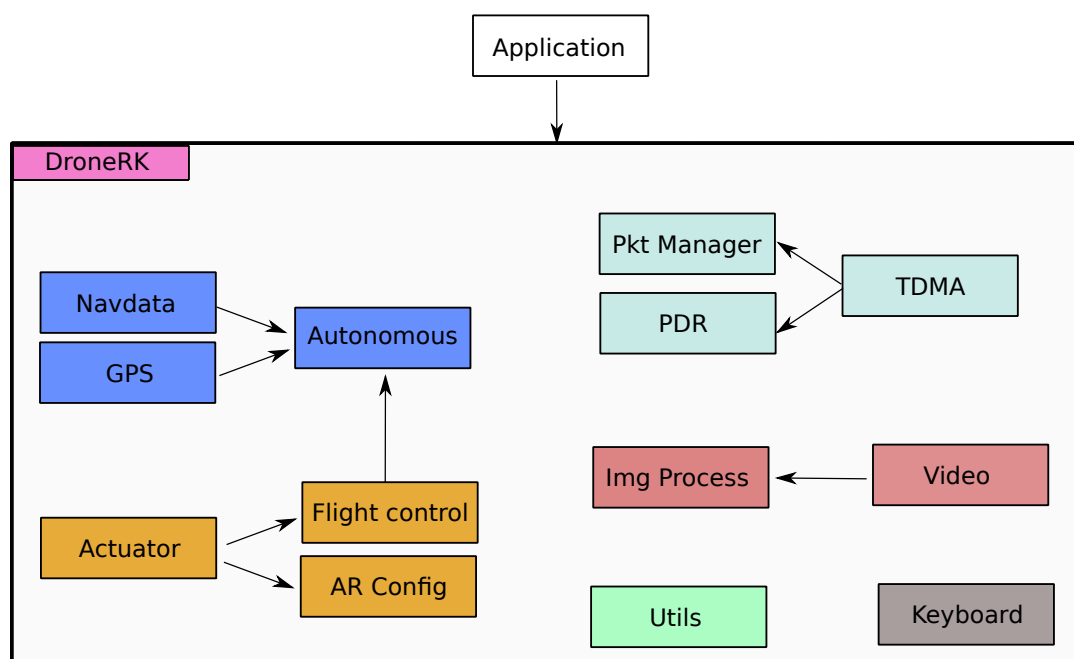
Figure 8.1: Drone-RK software is comprised of several modules, spanning from actuation and sensing to communications.

Therefore, Drone-RK has two modules named Navdata and Actuator. Navdata is the module in charge of collecting internal navigation data periodically from the AR.Drone autopilot and save it into a structure. This includes 3-axis accelerometer data, barometric altitude, ultras-sound height, 3-axis magnetometer data and a gyroscope. A dedicated thread constantly reads data from the autopilot and feeds a public structure that other modules can retrieve from. This structure is protected by a mutex.

Actuator module in conjunction with Flight Control are able to receive and apply motion commands from any other module such as moving forward/backwards, spinning clockwise or anti-clockwise, going up/down, moving left/right. This also includes sending emergency shutoff commands, changing the minimum/maximum altitude of flight, minimum/maximum speed for each direction, and setting the color of the motor LED lights. A dedicated thread periodically sends the command structure data to the autopilot. This structure is also protected by a mutex, since multiple modules can

provide simultaneous commands.

8.2   GPS and Autonomous Flight

GPS is the module that receives data from the GPS unit via serial port, and translate such information into a meaningful location data, such as absolute position and relative to base position. It is also able to save targets aka GPS waypoints given by the user or other modules. These waypoints are characterized by latitude, longitude, altitude, tolerated error (to be considered target-reached) and also maximum speed of flight. The GPS in use is a differential, lowcost, RTK GPS named Piksi (Switfnav, 2017). It relies on the use of a fixed GPS (Figure 8.2), from where mobile GPS units (Figure 8.3) receive extra GPS information to improve their own (differential location). It improves accuracy by collecting extra information such as the phase of the incoming GPS signals and the relative difference at two different receivers. These utilize dedicated radios and respective antennas on the 915Mhz frequency to share such information (visible in both images). These mobile units are able to retrieve differential GPS data in a NED coordinate system – north, east, down – measuring the distance in millimeters to the fixed GPS in these three axis. This system is able to work if and only if there are six or more satellites in view in common, between fixed and mobile units. In case this is not achieved, they also provide absolute location – latitude, longitude and altitude. Merging both metrics above we can obtain a higher quality absolute GPS position assuming the location of the BS is known with high accuracy.

Autonomous flight module feeds from GPS module and navigation data such as north-heading to analyze which motion commands are to be given to Actuator module in order to move the UAV to the current target location. It internally implements a PID controller.

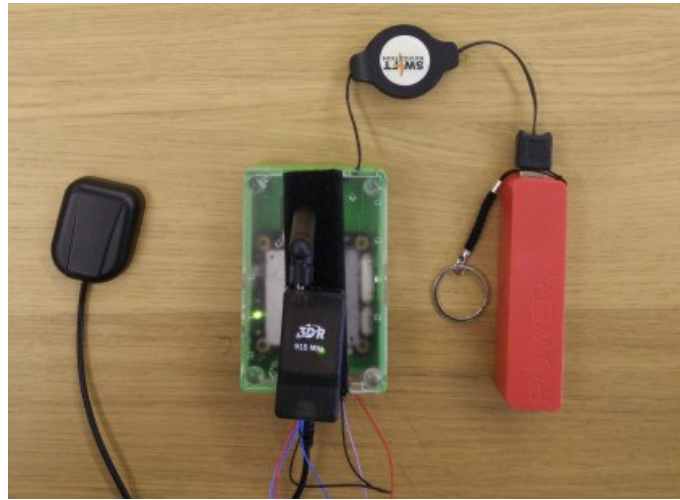Figure 8.2: Piksi GPS Basestation – This unit is placed at a fixed location before drones take off. This unit has dedicated power source (red power bank, on the right), a dedicated radio and antenna (on the middle), and an external GPS antenna, too (on the left).
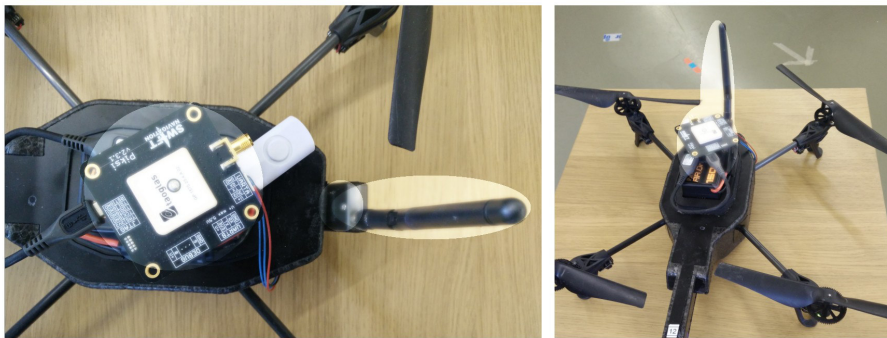
Figure 8.3: Piksi GPS on a drone – This unit is mobile and receives data from the fixed GPS unit via dedicated radio, which can be seen in Figure 8.2.

8.3 Keyboard

For faster development, drones initiate their code via telnet remote terminal. This way, a local computer can get access to the remote standard output/input. For this reason, a keyboard module has been created to allow the user to interact with the running Drone-RK process at each individual drone. This module is able to read key inputs and provide hardcoded features such as manual flight *w+a+s+d* (alike videogame common motion shortcuts), using *up/down* arrow to takeoff/land, calibrate sensors, pause/resume (*p+r*) autonomous flight, set current position as the current waypoint (*0*).

This module also allows setting up at new actions dynamically, by giving the user the option to chose the pair *key* and *function* to be called when the key is pressed. The basestation application also explores this feature to give commands to any drone in the network.

8.4 Communications

Our communication architecture is a three-tiered design with an Application layer (AL) on top, a Packet Manager (PM) and our TDMA layer at the bottom.

8.4.1 Application Layer – Video capture and collection

The AL is only accessed at the source and sink devices since these are the only nodes that are responsible for generating or consuming data. The AL in the source runs the camera application, dedicated to grabbing video frames directly from the camera device using the Video and Image Processing modules for that. The frames are fragmented to fit WiFi packets that are then sent to the PM layer. Each fragment takes attached a corresponding header for proper identification and later re-assembly of frames at the sink. The left side of Figure 8.4 shows the activity diagram of the AL on the source node.
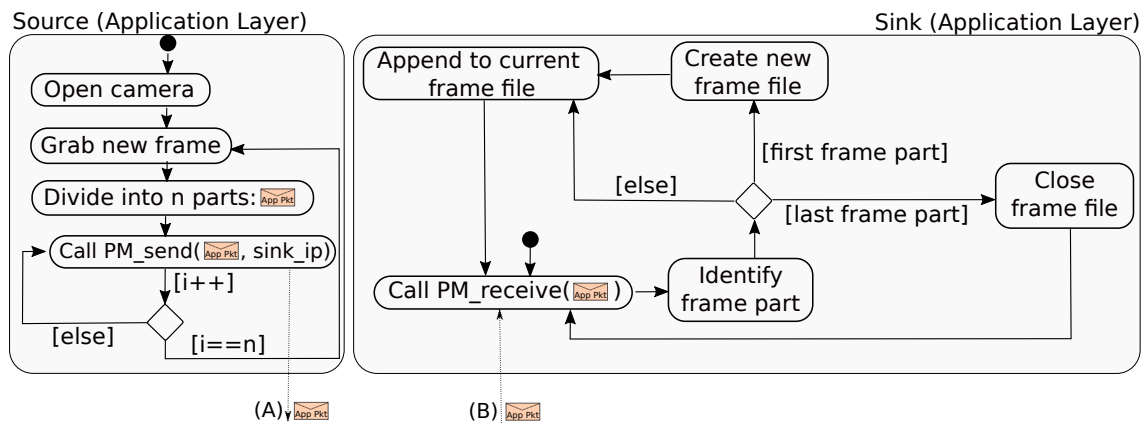
Figure 8.4: Behavior diagrams for the Application Layer running at the Source and Sink. In the Source, the AL is responsible for grabbing camera frames, fragmenting them and sending fragments to the PM layer. In the Sink, the AL does the frame re-assembly. The AL communicates with the PM layer using `PM_send()` and `PM_receive()` functions.

The AL on the sink side just collects frame packets, re-assembles the frames into image files and hands them to the operator application, for display and/or further processing. The respective behavior is outlined in the right side of Figure 8.4.

8.4.2 Packet Manager (PM) Layer – Routing

The PM layer (Figure 8.5) is in charge of finding the next hop of an incoming packet, whether it comes from the upper AL layer or from other node through the lower TDMA layer. Then, the PM either forwards packets to the TDMA layer to proceed their way along the network or, for packets meeting their final destination (the Sink in this case), the PM saves them to an internal queue, for later delivery to the AL.

8.4.3 TDMA Layer – Transmission Shaper

The TDMA layer does the shaping of the outgoing communications to the respective node TDMA slot and its behavior is explained in detail in Figure 8.6. Basically, whenever the TDMA slot of a node comes, and during its duration, that node enqueues pending
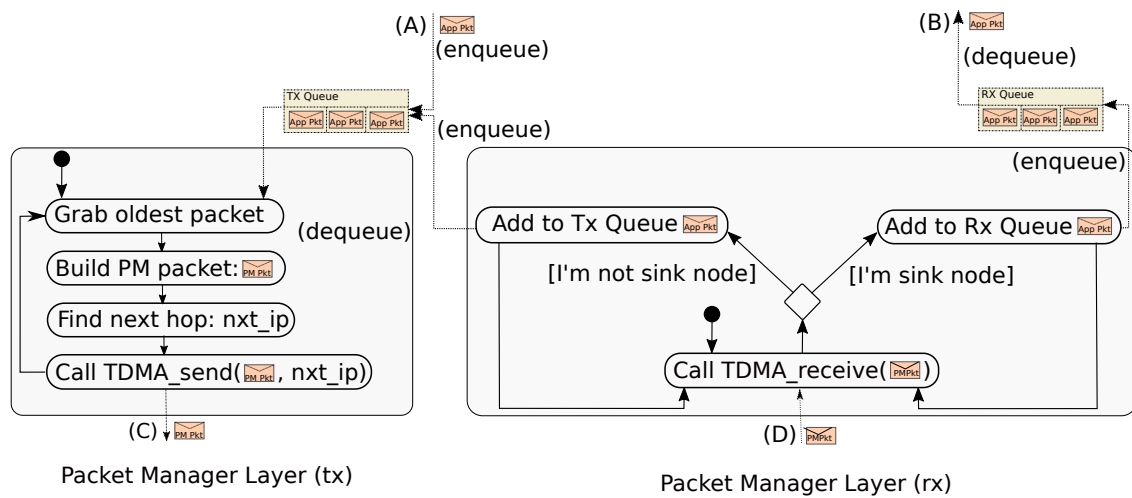
Figure 8.5: Packet Manager (PM) layer, routes packets to the next hop, or holds them for the AL if packets have reached their final destination (Sink). Communicates both with AL (above) and TDMA layers (below).

packets in the wireless card for transmission over the air. Note, however, that a new packet is only sent to the wireless card when the card informs the TDMA module that the previous packet has been sent.

Finally, the TDMA layer is also assessing the bandwidth of both upstream and downstream links and the PDR of its incoming and outgoing links, to run DVSP or DRP when desired. Its requests and replies are periodically sent as TDMA packets and filtered at this layer, being transparent for the layers above.

8.4.4 Encapsulation

Our protocol stack, from the AL to the TDMA layer, is shown in Figure 8.7, which highlights the logical packets (protocol data units – PDUs) of each layer with their specific header information. The header of each layer is only relevant for that layer and accessed and modified at that layer, only, following good layering practices. Thus, each layer can be independently modified, or swapped among different implementation options,
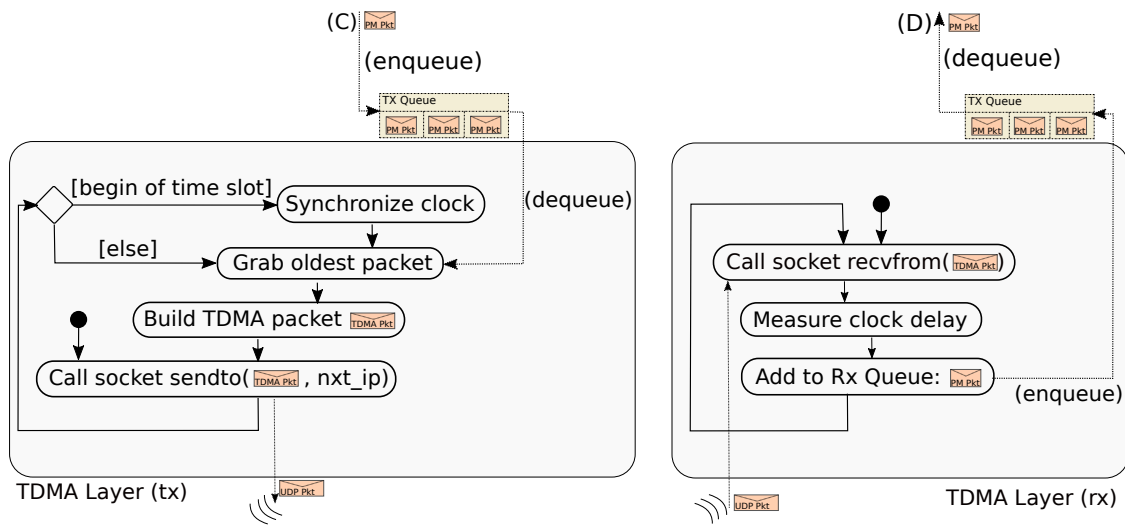
Figure 8.6: TDMA layer is responsible for measuring network delays affecting the incoming packets. The receiver node adjusts the phase of its own TDMA slot according to any such delays, to keep slots sequential and reduce overlap. Queued packets are only transmitted over the air during the TDMA time slot.

without any impact on the remainder of the stack, i.e., in a transparent way. Overall, the three layers impose an extra 26 byte overhead, which we consider negligible compared to the payload of 1kB that we are using.

Finally, the TDMA packets are encapsulated into UDP/IP packets. We opted for UDP instead of TCP to keep better control of the timings of packet transmissions over the network. We also decided not to do cross-layer optimization, despite some potential performance improvement that they could bring. The reason was also to strictly enforce layering, facilitating debugging and future extensions.

UDP Packet

TDMA Packet (14B)

u8 type; u32 seq_num ; u16 timestamp ; u32 slot_limits ; u8 slot_id ; u16 req_slot

PM Packet (7B)

u8 type ; u32 seq_num ; u8 src ; u8 sink

Aplication Packet (5B)

u8 type; u16 frame_id ; u8 part_id ; u8 part_total

Pixels
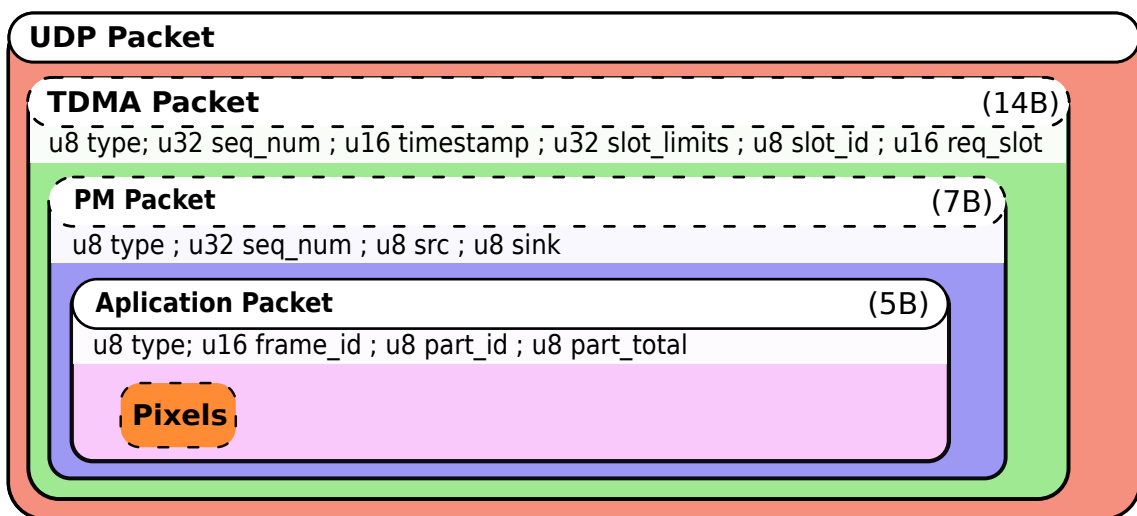
Figure 8.7: Our protocol stack, fully respecting the layering principle, with an independent protocol at each layer using own protocol data units, and final encapsulation in a UDP/IP packet for transport.

Chapter 9

Conclusion

UAVs have never been so ubiquitous as today, and they are enabling a vast set of new applications such as live-stream inspection and monitoring of large-scale infrastructures. But the realization of this promising idea lies dependent on the development of mechanism that can efficiently harness the UAV capabilities. Throughout a series of six chapters (Chapter 3 through Chapter 7), we made several contributions and drew several conclusions that support our claims. Here we wrap the main ideas behind our thesis and its validation.

9.1 Thesis Validation

In the beginning of our dissertation, we claimed that **joint coordination of network protocol and topology (placement of nodes) will improve user-interactive control of UAVs for streaming applications in terms of throughput, delay and reliability**. To show the validity of this, we identified the benefits of using multiple UAVs to extend the reach of the aerial sensor network. We concluded that understanding the UAV-to-UAV link is the first step to decide the optimal number of relays on a multi-hop network of UAVs. Then we were able to identify the two major issues of utilizing such networks.

1. First, the need to synchronize the various transmitters to overcome mutual inter-
   ference.

2. Second, we found there are asymmetries in link quality of the network and that
   these created buffer overflows under heavy utilization.

For the first problem, we proposed a novel and fully distributed self-synchronizing
TDMA protocol (Chapters 3 and 4). For the second one, we offered two different com-
plementary approaches: DVSP (Chapter 5) and DRP (Chapter 6). While the former relies
on adjusting the rate of transmission of the nodes and equalizes links throughput, mini-
mizing end-to-end delay and packet losses, the second second adjusts the position of the
relay nodes to mitigate link asymmetries equalizing the packet losses (the symmetrical
of the PDR) and maximizing end-to-end throughput.

Finally, we showed how to perform vertical monitoring of a given AoI that can be
larger than a single UAV can cover, on top of the relay network studied and developed
in the previous chapters (Chapter 7). We showed how to control a single UAV for that
task and proposed a flexible mechanism to increase area coverage or global frame rate
adding more sensor UAVs.

Along with all this work, we have presented our implementation effort to support all
the previous contributions. This implementation led to the development of Drone-RK,
a software library that allows applications to stream data over multiple relays seam-
lessly (Chapter 8) structured in three main layers, Application, Packet Manager and
TDMA. This library runs on top of Linux and is available at: `http://wise.ece.cmu.`
`edu/redmine/projects/drone-rk/wiki`. It includes modules to retrieve navigation data
and control drone motion, as well.

9.2 Future Work

There are multiple lines of future work that go across all the areas covered in this dissertation.

- TDMA – In this work and to simplify TDMA slot assignment, each node has a dedicated time slot, that is not concurrent with any other. In the future, we expect to relax this condition and allow some slot re-utilization at the expenditure of a more complex/dynamic TDMA scheme but with a possible increase in throughput. Our self-synchronization method is distributed. In the next steps we will take advantage of the GPS receivers to achieve more precise clock synchronization to achieve the desired high network utilization. We are already able to measure PDR in runtime. We intend to use forward error control mechanisms to enhance reliability.

- DVSP – we expect to extend this protocol to work with multiples sources. These will demand the common relay of the sources to negotiate with them in order to balance the load of each.

- DRP – regarding dynamic relay placement, we are currently addressing the solution of the general case of positioning n relays and proving convergence when operating iteratively. Moreover, determining the optimal number of relays in asymmetrical conditions is still an open problem. We also intend to expand our line-topology to other topologies such as mesh, with multiple sources and multiple sinks.

- DVSP+DRP – in this work, we have studied both protocols in separate; it will be interesting to study the major benefits of using both simultaneously. It is expected that DVSP will be able to cope with link asymmetries at the network level, on

a fast timescale. DRP will be able to remove these asymmetries at the origin by moving relays, on a slower timescale.

- Experimental validation of the extendable camera is to be studied in the future. Performing continuous sweeping of a given area has intrinsic value, but it will be interesting to study how GPS errors, communication latency and errors, and camera settings will affect the global frame rate at the basestation in regards to the theoretic one. Finally, we will also explore a smart role assignment policy that switches UAVs between sensors and relays, providing a compromise between area of coverage or frame rate and distance from the ground station.

- Another field to be studied is the portability of the Drone-RK to other drone platforms and other robotic platforms. In special, the communications modules were designed to work in any machine as long as they have WiFi cards; it would be interesting to investigate its multi-hop streaming features on other platforms. We are currently migrating the code to a network of smart-bicycles. We intend to build a digital multi-hop broadcasting system to transmit audio between neighboring cyclists.

Globally, it will be interesting to achieve full vertical integration of all the aspects covered in this dissertation. In this endeavour, we will seek focus on high level of reliability. Robotic systems in general, and drones in particular are inherently sensitive to flaws. As personally experienced during most experiments and flights, failures during mission time are generally catastrophic and result in a crash, and broken hardware. Reliability guarantees will be worked in the future.

Another generic future line of work regards evaluation of our system by other engineering teams, such as civil engineers. We have already initiated communication with other research groups to perform a visual inspection of a bridge, in particular its pillars

and the sensors installed on these. We would like to be reviewed in qualitative terms, on the quality of our system.

Bibliography

Ahmed, N., Kanhere, S. S., and Jha, S. (2013). Utilizing link characterization for improving the performance of aerial wireless sensor networks. *IEEE Journal on Selected Areas in Communications*, 31(8):1639–1649. 19

Asadpour, M., den Bergh, B. V., Giustiniano, D., Hummel, K. A., Pollin, S., and Plattner, B. (2014). Micro aerial vehicle networks: an experimental analysis of challenges and opportunities. *IEEE Communications Magazine*, 52(7):141–149. 20

Asadpour, M., Giustiniano, D., Hummel, K. A., Heimlicher, S., and Egli, S. (2013). Now or later?: Delaying Data Transfer in Time-critical Aerial Communication. In *Proc. Ninth ACM Conf. Emerg. Netw. Exp. Technol. (CoNEXT)*, pages 127–132, Santa Barbara, CA, USA. ACM Press. 20

Banggood (2017). Eachine E013. `banggood.com/Eachine-E013-Micro-FPV-Racing-Quadcopter-With-5_8G-1000TVL-40CH-Camera-VR006-VR-006-3-Inch-Goggles-p-1182628.html`. Accessed: 01-01-2018. 3

Basagni, S., Petrioli, C., Petroccia, R., and Stojanovic, M. (2010). Choosing the packet size in multi-hop underwater networks. In *OCEANS 2010 IEEE - Sydney*, pages 1–9. IEEE. 18

Bohm, A., Lidstrom, K., Jonsson, M., and Larsson, T. (2010). Evaluating CALM M5-based vehicle-to-vehicle communication in various road settings through field trials. In *Proc. IEEE Local Comput. Netw. Conf. (LCN)*, pages 613–620, Denver, CO. IEEE. 19, 25

Cheng, W., Li, M., Liu, K., Liu, Y., Li, X., and Liao, X. (2008). Sweep coverage with mobile sensors. In *Parallel and Distributed Processing, 2008. IPDPS 2008. IEEE International Symposium on*, pages 1–9. 26, 27

CNN (2015). India to use Drones for Crowd Control. `https://edition.cnn.com/2015/04/09/asia/india-police-drones/index.html`. Accessed: 01-01-2018. 5

DJI (2017). DJI Mavic Pro. `https://www.dji.com/mavic`. Accessed: 01-01-2018. 2

Facchinetti, T., Almeida, L., Buttazzo, G. C., and Marchini, C. (2004). Real-time resource reservation protocol for wireless mobile ad hoc networks. In *25th IEEE International Real-Time Systems Symposium*, pages 382–391. 64

Flushing, E. F., Kudelski, M., Gambardella, L. M., and Di Caro, G. A. (2014). Spatial prediction of wireless links and its application to the path control of mobile robots. In *Proc. IEEE Int. Symp. Ind. Embed. Syst. (SIES)*, pages 218–227, Pisa, Italy. IEEE. 24

Forster, C., Lynen, S., Kneip, L., and Scaramuzza, D. (2013). Collaborative monocular slam with multiple micro aerial vehicles. In *2013 IEEE/RSJ International Conference on Intelligent Robots and Systems*, pages 3962–3970. 16

Fortune (2017). Drone captures images after California wildfire. `http://fortune.com/2017/10/13/drones-california-fires-footage/`. Accessed: 01-01-2018. 5

Franco, C. D. and Buttazzo, G. (2015). Energy-aware coverage path planning of uavs. In *Autonomous Robot Systems and Competitions (ICARSC), 2015 IEEE International Conference on*, pages 111–117. 26, 27

Goddemeier, N., Daniel, K., and Wietfeld, C. (2012). Role-based connectivity management with realistic air-to-ground channels for cooperative uavs. *IEEE Journal on Selected Areas in Communications*, 30(5):951–963. 17, 25

Gorain, B. and Mandal, P. S. (2013). Point and area sweep coverage in wireless sensor networks. In *Modeling Optimization in Mobile, Ad Hoc Wireless Networks (WiOpt), 2013 11th International Symposium on*, pages 140–145. 26, 27

Gorain, B. and Mandal, P. S. (2014). Approximation algorithms for sweep coverage in wireless sensor networks. *Journal of Parallel and Distributed Computing*, 74(8):2699 – 2707. 27

Henkel, D. and Brown, T. X. (2008). Delay-tolerant communication using mobile robotic helper nodes. In *Proc. Int. Symp. Model. Optim. Mobile, Ad Hoc, Wirel. Networks Work. (WiOPT)*, pages 657–666, Berlin, Germany. IEEE. 24

Huang, W. H. (2001). Optimal line-sweep-based decompositions for coverage algorithms. In *Robotics and Automation, 2001. Proceedings 2001 ICRA. IEEE International Conference on*, volume 1, pages 27–32 vol.1. 26, 28

Intel (2017). Intel Aero Drone. `https://click.intel.com/intel-aero-ready-to-fly-drone.html`. Accessed: 01-01-2018. 3, 4

Jia, F., Shi, Q., Zhou, G.-m., and Mo, L.-f. (2010). Packet Delivery Performance in Dense Wireless Sensor Networks. In *Proc. Int. Conf. Multimed. Technol. (ICMT)*, pages 1–4, Ningbo, China. IEEE. 18, 25

Li, J., c. Wang, R., p. Huang, H., and j. Sun, L. (2009). Voronoi based area coverage optimization for directional sensor networks. In *Electronic Commerce and Security, 2009. ISECS '09. Second International Symposium on*, volume 1, pages 488–493. 27

Lindhe, M. and Johansson, K. (2009). Using robot mobility to exploit multipath fading. *IEEE Wirel. Commun.*, 16(1):30–37. 24

MATLAB (2016). MATLAB Curve Fitting Toolbox. `https://www.mathworks.com/products/curvefitting.html`. Accessed: 01-01-2018. 38

Muzaffar, R., Vukadinovic, V., and Cavallaro, A. (2016). Rate-adaptive multicast video streaming from teams of micro aerial vehicles. In *2016 IEEE International Conference on Robotics and Automation (ICRA)*, pages 1194–1201. 20

Nigam, N., Bieniawski, S., Kroo, I., and Vian, J. (2012). Control of multiple uavs for persistent surveillance: Algorithm and flight test results. *IEEE Transactions on Control Systems Technology*, 20(5):1236–1251. 26, 28

Oliveira, L., Almeida, L., and Lima, P. (2015). Multi-hop routing within tdma slots for teams of cooperating robots. In *2015 IEEE World Conference on Factory Communication Systems (WFCS)*, pages 1–8. 51, 52

Parrot (2012). Parrot AR Drone 2.0. `http://ardrone2.parrot.com`. Accessed: 01-01-2018. 2, 33, 75, 115

Pinto, L., Moreira, A., Almeida, L., and Rowe, A. (2016a). Aerial multi-hop network characterisation using cots multi-rotors. In *2016 IEEE World Conference on Factory Communication Systems (WFCS)*, pages 1–4. 13, 32

Pinto, L. R., Almeida, L., Alizadeh, H., and Rowe, A. (2017a). Aerial video stream over multi-hop using adaptive tdma slots. In *2017 IEEE Real-Time Systems Symposium (RTSS)*, pages 157–166. 13, 51, 59

Pinto, L. R., Almeida, L., and Rowe, A. (2017b). *Balancing Packet Delivery to Improve End-to-End Multi-hop Aerial Video Streaming*, pages 807–819. Springer International Publishing. 13, 83

Pinto, L. R., Almeida, L., and Rowe, A. (2017c). Demo abstract: Video streaming in multi-hop aerial networks. In *2017 16th ACM/IEEE International Conference on Information Processing in Sensor Networks (IPSN)*, pages 283–284. 13, 59

Pinto, L. R., Moreira, A., Almeida, L., and Rowe, A. (2017d). Characterizing multi-hop aerial networks of cots multirotors. *IEEE Transactions on Industrial Informatics*, 13(2):898–906. 13, 32, 60, 85

Pinto, L. R., Oliveira, L., Almeida, L., and Rowe, A. (2016b). Extendable matrix camera using aerial networks. In *2016 International Conference on Autonomous Robot Systems and Competitions (ICARSC)*, pages 181–187. 13, 95

SIC (2017). Pedrogao aftermatch. `sicnoticias.sapo.pt/`. Accessed: 01-01-2018. 5

Suzuki, K. A., Kemper Filho, P., and Morrison, J. R. (2012). Automatic battery replacement system for uavs: Analysis and design. *Journal of Intelligent & Robotic Systems*, 65(1-4):563–586. 27

Switfnav (2017). Piksi RTK GPS. `https://www.swiftnav.com/piksi-multi`. Accessed: 01-01-2018. 117

Tech, L. (2017). LeddarOne. `www.leddartech.com`. Accessed: 01-01-2018. 4

Toksoz, T., Redding, J., Michini, M., Michini, B., How, J. P., Vavrina, M., and Vian, J. (2011). Automated battery swap and recharge to enable persistent uav missions. In *AIAA Infotech@ Aerospace Conference*. 27

Tuna, G., Mumcu, T. V., and Gulez, K. (2012). Design strategies of unmanned aerial vehicle-aided communication for disaster recovery. In *High Capacity Optical Networks and Enabling Technologies (HONET), 2012 9th International Conference on*, pages 115–119. 27, 28

Wandeler, E. and Thiele, L. (2006). Optimal tdma time slot and cycle length allocation for hard real-time systems. In *Proceedings of the 2006 Asia and South Pacific Design Automation Conference*, ASP-DAC '06, pages 479–484, Piscataway, NJ, USA. IEEE Press. 22

Wang, Q., Jaffrès-Runser, K., Xu, Y., Scharbarg, J. L., An, Z., and Fraboul, C. (2017). Tdma versus csma/ca for wireless multihop communications: A stochastic worst-case delay analysis. *IEEE Transactions on Industrial Informatics*, 13(2):877–887. 23

Wireshark (2016). Wireshark. `https://www.wireshark.org`. Accessed: 01-01-2018. xix, 47, 48

Yang, M., Kim, D., Li, D., Chen, W., Du, H., and Tokuta, A. O. (2013). Sweep-coverage with energy-restricted mobile wireless sensor nodes. In *Wireless Algorithms, Systems, and Applications*, pages 486–497. Springer. 27

Yanmaz, E. (2012). Connectivity versus area coverage in unmanned aerial vehicle networks. In *Communications (ICC), 2012 IEEE International Conference on*, pages 719–723. 26

Zhao, J. and Govindan, R. (2003). Understanding packet delivery performance in dense wireless sensor networks. In *Proc. First Int. Conf. Embed. Networked Sens. Syst. (SenSys)*, page 1, Los Angeles, CA, USA. ACM Press. 18, 25

Chapter A

Channel Assessment Model

Proof of Equation 3.17

The $\zeta_{max}(d)$ function, described in Equation 3.17 can be derived from the intrinsic properties of $\zeta_h(d)$, namely: Equation 3.14, Equation 3.15 and Equation 3.16. By using Equation 3.16b and Equation 3.15, we show that if the network uses x-hops, throughput is greater than using any higher number of hops ($x+n$), as long as distance is lower than $d_{x,x+1}$:

$$\begin{cases} \zeta_x(d) > \zeta_{x+1}(d) & \text{if } d \in [0, d_{x,x+1}) \\ \zeta_x(d) > \zeta_{x+n}(d) & \text{if } d \in [0, d_{x,x+n}) \\ d_{x,x+1} < d_{x,x+n} & \forall n \in \mathbb{N}_{>x} \end{cases} \tag{A.1}$$

By using Equation 3.16c and Equation 3.15, we show that if the network uses x-hops, throughput is greater than using any lower number of hops ($x-m$), as long as distance

is higher than $d_{x,x-1}$:

$$
\begin{cases}
\zeta_x(d) > \zeta_{x-1}(d) & \text{if } d \in (d_{x-1,x}, +\infty) \\[2mm]
\zeta_x(d) > \zeta_{x-m}(d) & \text{if } d \in (d_{x-m,x}, +\infty) \\[2mm]
d_{x-m,x} < d_{x-1,x} & \forall m \in \mathbb{N}_{<x}
\end{cases}
\tag{A.2}
$$

According to Equation 3.15, $d_{x,x+1}$ is greater than $d_{x,x-1}$. So:

$$
\text{From Equation A.1: } \zeta_x(d) > \zeta_{x+n}(d) \quad \text{if } d \in [0, d_{x,x+1}) \Rightarrow
$$

$$
\zeta_x(d) > \zeta_{x+n}(d) \quad \text{if } d \in (d_{x,x-1}, d_{x,x+1})
$$

$$
\text{From Equation A.2: } \zeta_x(d) > \zeta_{x-m}(d) \quad \text{if } d \in (d_{x-1,x}, +\infty) \Rightarrow
\tag{A.3}
$$

$$
\zeta_x(d) > \zeta_{x-m}(d) \quad \text{if } d \in (d_{x,x-1}, d_{x,x+1})
$$

$$
\text{Yielding: } \zeta_x(d) > \zeta_y(d) \quad \text{if } d \in (d_{x-1,x}, d_{x,x+1})
$$

$$
\forall x, y \in \mathbb{N}, x \neq y
$$

We proved that $\zeta_x(d)$ is optimal in the interval $(d_{x-1,x}, d_{x,x+1})$ regarding any other number of hops in use.

Proof of Equation 3.16a and Equation 3.18

There is a unique intersection point $\{D, \Theta\} \in \mathbb{R}^2$, where $\Theta = \zeta_x(D) = \zeta_y(D)$.

$$
\zeta_x(D) = \zeta_y(D)
$$

$$
\frac{B}{x} e^{\left(\beta\left(\frac{D}{x}\right)^\alpha x\right)} = \frac{B}{y} e^{\left(\beta\left(\frac{D}{y}\right)^\alpha y\right)}
$$

$$
\frac{e^{\beta\left(\frac{D}{x}\right)^\alpha x}}{e^{\beta\left(\frac{D}{y}\right)^\alpha y}} = \frac{x}{y}
\tag{A.4}
$$

$$
D^\alpha = \frac{\ln\left(\frac{x}{y}\right)}{\beta\left(x^{(1-\alpha)} - y^{(1-\alpha)}\right)}
$$

We see now that Equation A.4 has a unique positive real solution. Both numerator and denominator are strictly negative due to $\beta < 0$, $y > x$, and $\alpha > 1$. This shows that inside the domain interval $\mathbb{R}_0^+$, those two functions intersect only once at d_{AB}.

Proof of Equation 3.16b: x-hops leads to higher throughput than y-hops, if $d<d_{xy}$ ($x<y$)

As a consequence of Equation 3.16a, in the domain interval $d \in [0, d_o)$, $\zeta_x(d)$ and $\zeta_y(d)$ never intersect each other (as long $x \neq y$). Since $\zeta_h(d)$ is a continuous function, Bolzano's intermediate value theorem is applicable. So, Equation 3.16b is true iff there is at least one point in that domain where $\zeta_x(d)$ is greater than $\zeta_y(d), \forall x < y$. We know that $\zeta_x(0)$ is greater than $\zeta_y(0)$, so the proof is completed:

$$\zeta_x(0) = \frac{B}{x} > \frac{B}{y} = \zeta_y(0) \tag{A.5}$$

Proof of Equation 3.16c: y-hops leads to higher throughput than x-hops, if $d>d_{xy}$ ($x<y$)

As a consequence of Equation 3.16a, in the interval $d \in (D, +\infty)$, $\zeta_x(d)$ and $\zeta_y(d)$ never intersect each other (as long $x \neq y$). Since $\zeta_h(d)$ is continuous, we can prove Equation 3.16c, showing that the derivative of $\zeta_y(x)$ is lower than $\zeta_x(d)$ at $d = D$, i.e.:

$$\begin{cases} \exists^1 D : \zeta_x(D) = \zeta_y(D) \\ \left.\frac{\partial \zeta_x(d)}{\partial d}\right|_{d=D} < \left.\frac{\partial \zeta_y(d)}{\partial d}\right|_{d=D} \end{cases} \Rightarrow \zeta_x(d) < \zeta_y(d) \tag{A.6}$$

$$\forall d \in (D, +\infty)$$

First, we derive throughput derivative function $\left(\frac{\partial \zeta_h(d)}{\partial d}\right)$:

$$\begin{aligned} \frac{\partial \zeta_h(d)}{\partial d} &= \frac{\partial}{\partial d}\left[\frac{B}{h}e^{\beta\left(\frac{d}{h}\right)^\alpha h}\right] \\ &= \zeta_h(d)\left(\beta\frac{h}{h^\alpha}d^\alpha\right)' \\ &= \zeta_h(d)\left(\beta\frac{h}{h^\alpha}\right)\alpha d^{\alpha-1} \end{aligned} \tag{A.7}$$

Analyzing Equation A.7, we conclude throughput function has a strictly negative derivative since $\beta \in \mathbb{R}^-$ and $\zeta_h(d), d, \alpha, \in \mathbb{R}^+$. So, proving that the inequality of derivatives Equation A.6 is true, is equivalent to show that:

$$\frac{\left(\frac{\partial \zeta_x(d)}{\partial d}\right)}{\left(\frac{\partial \zeta_y(d)}{\partial d}\right)}\Bigg|_{d=D} > 1 \tag{A.8}$$

$$\frac{\left(\frac{\partial \zeta_x(d)}{\partial d}\right)}{\left(\frac{\partial \zeta_y(d)}{\partial d}\right)}\Bigg|_{d=D} = \frac{\zeta_x(D)\left(\frac{\beta x \alpha}{x^\alpha}\right) D^{\alpha-1}}{\zeta_y(D)\left(\frac{\beta y \alpha}{y^\alpha}\right) D^{\alpha-1}} = \left(\frac{y}{x}\right)^{\alpha-1} > 1 \tag{A.9}$$

Proof of Equation 3.15: $\zeta_x(d)$ intersects $\zeta_y(d)$ at a lower distance than $\zeta_x(d)$ intersects $\zeta_z(d)$, if $x < y < z$

To prove that $d_{xy} < d_{xz}$ if $y < z$, we can show that $d_{xy} < d_{x\mathbf{w}}, \forall \mathbf{w} > y$, i.e.. we convert solution d_{xw}, from Equation 3.18, into a function of w, and prove that d_{xw} is a strictly increasing function of $w \in \mathbb{N}_{>x}$, i.e:

$$\frac{\partial(d_{x\mathbf{w}})}{\partial \mathbf{w}} = \left(\frac{\ln\left(\frac{w}{x}\right)}{\beta\left(x^{(1-\alpha)} - w^{(1-\alpha)}\right)}\right)'$$

$$= \frac{k \cdot w^k \cdot \ln\left(x/w\right) + (w^k - x^k)}{\beta w(x^k - w^k)^2} \quad , (k = 1 - \alpha) \tag{A.10}$$

Since $kw^k \ln\left(x/w\right)$, $(w^k - x^k)$ and $\beta w(w^k - x^k)^2$ are all negative, the proof is complete.

Chapter B

Drone-RK API

We present here the list of functions available by each one of the Drone-RK modules.

B.1   Navdata

```
int      drk_sensor_data_init(void);
int      drk_sensor_data_close(void);
/** obtain heading relative to north **/
float    drk_heading(void);
vector   drk_drone_speed_get(void);
/** printout all sensor data **/
void     dump_sensors(void);
double   drk_ultrasound_raw(void);
/** Ultrasound altitude reading compensated for tilt **/
double   drk_ultrasound_altitude(void);
/** barometric altitude **/
double   drk_abs_altitude(void);
/** barometric altitude minus a known groundzero altitude **/
double   drk_rel_altitude(void);
/** set groundzero barometric altitude **/
void     drk_zero_altitude( uint16_t dft ) ;
```

```
/** Prints and shows a graph of the battery **/
void    drk_print_battery(void);
/** return percentage of bat left **/
int     drk_get_battery(void);
```

B.2   GPS

GPS module has dozens of functions. We present here wrappers for the main ones:

```
/* return lastest gps sample data received */
llh_t   drk_gps_data( void );
/* Check for a GPS fix */
int drk_gps_myfix( void );
/* Get number of visible sats */
int     drk_gps_get_numsats( void );
/* Calculate the distance between : */
/* two LLH structs */
double  drk_gps_distance_between( llh_t gpsA, llh_t gpsB );
/* current position and a coordinate pair */
double  drk_gps_mydistance_to(llh_t target);
/* Get altitude from GPS */
double  gps_get_altitude(void) ;
/* current position and a GPS struct */
double  drk_gps_true_bearing(llh_t target);
/* Returns GPS altitude of drone */
double  drk_gps_altitude_get(void);
/* Returns ground speed of drone */
double  drk_groundSpeed_get(void);
/* Debugging methods */
void    drk_gps_print(void);
```

B.3 Flight Control

It is possible to use a small set of high level wrapper functions to move the drone, as well as set or remove the emergency state. The list below contains some of the main functions we developed in that regard, that end up calling Actuator module's functions.

```c
/** Send a takeoff command, then block for five seconds to wait for
    completion **/
void    drk_takeoff(void);
/** Send a land command, then read sensor data until landed  **/
void    drk_land(void);
/** Trigger an emergency shutoff (kill the motors)  **/
void     drk_emergency(void);
/** Removes the drone from emergency state  **/
int     drk_remove_emergency(void);
/** Puts the drone in hover mode, using the camera to stabilize **/
void    drk_lockdown_hover(int time);
/** Puts the drone in hover mode, using the camera to stabilize **/
void     drk_hover(int time);
/** Combined movement **/
void    drk_translate(float pitch, float roll, float yaw, float gaz, int
    time_ms);
/**Rotate to the left **/
void    drk_spin_left(float rate, int time);
/**Rotate to the right **/
void    drk_spin_right(float rate, int time);
/**Move forward **/
void    drk_move_forward(float rate, int time);
/** Move backward **/
void    drk_move_backward(float rate, int time);
/** Move right **/
void    drk_move_right(float rate, int time);
/** Move left **/
```

```
void    drk_move_left(float rate, int time);
/**Fly upward **/
void    drk_move_up(float rate, int time);
/** Fly downward **/
void    drk_move_down(float rate, int time);
```

B.4   Autonomous Flight

The list of actions available at this module are mainly the following ones:

```
/** initiates autonomous controller **/
error_t         drk_autonomous_init(void);
/** Clean up and close **/
void            drk_autonomous_close(void);
/** Pause movement immediately **/
void            drk_autonomous_pause(void);
/** Resume flight  **/
void            drk_autonomous_resume(void);
/** Returns state of flight: PAUSED- no rotor output; FLYING - flying to
    target **/
enum flight_status drk_autonomous_get_state(void);
/** returns the current waypoint target**/
gps_waypoint_t  drk_autonomous_get_waypoint(void) ;
/** Gives new waypoint to go; overwrites current waypoint **/
void            drk_autonomous_set_waypoint( gps_waypoint_t in_waypoint
    );
/** is drone at target position? (<= distance_tolerance) **/
enum target_status drk_autonomous_target_reached(void);
/** print a small ascii map with cur pos, BS, and cur target **/
void            drk_print_map(void)  ;
/** go to piksi base **/
void            drk_autonomous_goBS(void );
```

```
/** shift current target: north, if dist_m > 0  ; south, if dist_m < 0 *
    */
void drk_autonomous_goNorth( double dist_m );
/** shift current target: east, if dist_m > 0 ; west, if dist_m < 0 **/
void drk_autonomous_goEast( double dist_m );
/** set PID controller parameters: Kp_? - proportional  ; Ki_? -
    integral ; Kd_? - differential ; ?_h - horizontal ; ?_v - vertical *
    */
void drk_autonomous_set_PID( double _kp_h, double _ki_h, double _kd_h,
    double _kp_v);
```

B.5   Packet Manager

```
/** init PM module **/
error_t drk_PM_init( uint8_t my_ip ) ;
/** close the module properly **/
error_t drk_PM_close( void ) ;
/** send a packet to PM **/
error_t PM_send( uint8_t sink_IP, uint16_t pkt_len, const void * const
    pkt_ptr ) ;
/** print current routing table **/
error_t PM_printRoutingSettings( void ) ;
/** read a packet in PM Rx queue. Option to block till reception. **/
error_t PM_receive( pkt_t *pkt, uint8_t blocking ) ;
/** get number of packets in the out-buffer **/
float   PM_getTxBufferUse( void ) ;
/** get number of packets in the in-buffer **/
float   PM_getRxBufferUse( void ) ;
/** set new topology: routing pairs of [sink-IP; next-hop-IP] **/
error_t PM_newTopology( const pair_ips_t const* topology , int entries )
    ;
```

B.6   PDR

```
/** feedback my neighbors with the value of PDR from-everyone-to-me **/
error_t PDR_shareWithNeighbors( void );
/** analyze PDR of a given LINK [OTHER]-->[MYSELF] **/
error_t PDR_estimate( uint32_t s_num, uint8_t other_IP ) ;
/* Reset/Clean up estimates */
error_t PDR_init(void);
/** parsing a rcvd pdr packet **/
error_t PDR_parsePkt( const void * const rx_tdmapkt_ptr, uint16_t
    num_bytes_read, uint8_t other_IP );
/** get value of pdr from other ip to myself **/
float PDR_get_in( uint8_t ip ) ;
/** get value of pdr from myself to other ip **/
float PDR_get_out( uint8_t ip ) ;
```

B.7   TDMA

These are the main functions that TDMA module implements to be used by any other
module or user.

```
/** init module: threads, slots, etc **/
error_t drk_TDMA_init( uint8_t my_id );
/** close and cleanup module **/
error_t drk_TDMA_close( void ) ;
/** change between TDMA modes: CSMA/ rigidTDMA slots / dynamicTDMA slots
     (DVSP) **/
void TDMA_off( void ); /* aka CSMA */
void TDMA_rigid( void );
void TDMA_dynamic( void );
/** Get newly rcvd packets. **/
ssize_t TDMA_receive( void *pkt_ptr , uint8_t *other_ip ) ;
/** send a packet of any chosen type  **/
```

```
error_t TDMA_sendAnyPacket ( uint8_t dest_ip , tdma_type_t type , uint16_t
    pkt_len ,
        const void * const pkt_ptr );
/** send packet of type PM **/
error_t TDMA_send ( uint8_t dest_ip ,uint16_t pkt_len , const void * const
    pkt_ptr ) ;


/** get buffer status **/
int TDMA_isRxBufferFull ( void ) ;
/** Printout current Tx queue content **/
void TDMA_dumpTxQueue ( void );
/** incorporate a new active slot list - BS sends updates **/
error_t TDMA_newSlotList (const uint8_t * const slot_list , const int len
    );
/** return current bandwidth being used in and out **/
bandwidth_t TDMA_getBandwidth ( void ) ;
/** request some slot width to a neighbor - used in DVSP **/
void TDMA_reqSlotWidth ( uint16_t req_ms , uint8_t dst_ip )
```

B.8   Video

This module is in charge to open the video device desired by the user, and allows its
caller to grab a copy of the latest available frame.

```
int drk_video_close ( void ) ;
int drk_video_init ( char cam_id ) ;
int drk_video_front_init ( unsigned int h , unsigned int w ) ;
int drk_video_bottom_init ( unsigned int h , unsigned int w ) ;
int grab_frame ( void *p , uint32_t *len ) ;
```

B.9   Image Processing

This module is responsible to process the raw UYUY image out of the camera and converted it as needed by the user. The main functions in use are the following ones, that allow to extract the black and white component and to sub-sample it into a lower resolution version of itself.

```c
int UYVY_2_Y( const uint8_t * const in_uyvy, unsigned long len, uint8_t
    *out_gray ) ;
int Y_subsample( const uint8_t * const in_y, unsigned long len, uint16_t
    width, uint8_t *out_sub_y, uint8_t factor ) ;
```

B.10   Actuator

```c
error_t drk_actuator_init( void ) ;
error_t drk_actuator_close( void ) ;
/* Send a command to the drone autopilot */
int     drk_send_at_command( const char *send_command , ... );
/* Play an animated sequence on the LEDs */
int     drk_play_LED_animation(enum LED_ANIMATION animation, float
    frequency, int duration);
```

B.11   AR Config

It is possible to configure some settings of the AR Drone. These are the main functions we use.

```c
/** Maximum pitch / roll angle. Must be between 0 and 0.52 radians **/
int drk_ar_change_max_angle( float radians );
/** min Altitude of the drone in millimeters. 50 - max **/
int drk_ar_change_min_altitude( int altitude_mm );
/** Maximum Altitude of the drone in millimeters. 500 - 5000, or 10000 =
    no lim **/
```

```
int drk_ar_change_max_altitude( int altitude_mm );
/** Maximum Vertical Speed, in millimeters per second, 200-2000 **/
int drk_ar_change_max_vertical_speed ( int speed_mm_per_sec);
/** Maximum Yaw Speed, in radians per second, 0.7 - 6.11 **/
int drk_ar_change_max_yaw_speed( float speed_rad_per_sec);
/** to zero inertial sensors **/
int drk_ar_flat_trim(void);
/** make drone spin a 360 deg to calibrate compass **/
void drk_ar_calibrate_magnetometer(void);
int drk_ar_set_outdoor_flight(void);
int drk_ar_set_indoor_flight(void);
int drk_ar_set_outdoor_hull(void);
int drk_ar_set_indoor_hull(void);
```

B.12   Keyboard

```
error_t drk_keyboard_init( void ) ;
error_t drk_keyboard_close( void ) ;
error_t drk_keyboard_setKey( int(*action)(int) , int input , char key );
```

B.13   Utils

```
/** get last part of ip, from a struct sockaddr_in **/
uint8_t getOtherIP( struct sockaddr_in si_other ) ;
/** Get last segment of current IP **/
int16_t getMyIP(void) ;
/** open and return a point to a new file **/
int     open_log_file( const char* const prefix, const char * const
    sufix, FILE **file_p ) ;
/** get struct with current epoch time **/
int     getCurrentTime( struct timespec *temp_time ) ;
/** same, but in fractional single number (seconds) **/
```

```c
double   getEpoch( void ) ;
/** time since Drone-RK as initiated **/
double   drk_elapsedTimeSecs( void ) ;
/** statistics: **/
int32_t computeMax( int32_t *array , int64_t n ) ;
int32_t computeMean( int32_t *array , int64_t n ) ;
int32_t computeStd( int32_t *array , int64_t n , int32_t average ) ;
int32_t computeMin( int32_t *array , int64_t n );
/*** math, trigonometry , etc: ***/
double   wrapTo360( double angle_in_degrees ) ; /* range 0-360deg -
    double */
float    wrapTo360f( float angle_in_degrees ) ; /* range 0-360deg - float
       */
/** convert units **/
double   degrees_to_radians( double degrees );
double   radians_to_degrees( double radians );
/** force creation of semaphore by name **/
int      drk_sem_create( char *sem_name , sem_t **sem_ptr ) ;
/** clean semaphore by name **/
int      drk_sem_cleanup( char *sem_name , sem_t *sem_ptr ) ;
/** signal safe sem_wait() **/
error_t sem_wait_safe( sem_t *semaphore_ptr, volatile int *exit_flag);
/** signal safe sem_timedwait() **/
error_t sem_timedwait_safe( sem_t *semaphore_ptr, volatile int *
    exit_flag, useconds_t t_us );
/** terminal setup **/
void     drk_restore_termios(void) ;
void     drk_setup_termios(void) ;
/** error handling - print human readable msgs **/
void     printError( error_t status ) ;
/** print array in hex form **/
void     dumpData( uint8_t *data, uint16_t len ) ;
/** Signal related **/
```

```
void     unblock_all_signals(void);
void     block_all_signals(void);
void     unblock_one_signal(int sig);
void     block_one_signal(int sig);
/** pair a given function callback to a signal **/
error_t sig_set_action( void(*cb)(int), int sig);
```